

T-3510

**THE PATAGONIAN BATHOLITH AT 48° S LATITUDE, CHILE:
IMPLICATIONS FOR THE PETROLOGICAL AND
GEOCHEMICAL EVOLUTION OF
CALC-ALKALINE BATHOLITHS**

by

Stephen G. Weaver

ProQuest Number: 10796358

All rights reserved

INFORMATION TO ALL USERS

The quality of this reproduction is dependent upon the quality of the copy submitted.

In the unlikely event that the author did not send a complete manuscript and there are missing pages, these will be noted. Also, if material had to be removed, a note will indicate the deletion.



ProQuest 10796358

Published by ProQuest LLC (2019). Copyright of the Dissertation is held by the Author.

All rights reserved.

This work is protected against unauthorized copying under Title 17, United States Code
Microform Edition © ProQuest LLC.

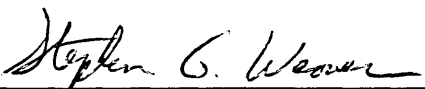
ProQuest LLC.
789 East Eisenhower Parkway
P.O. Box 1346
Ann Arbor, MI 48106 – 1346

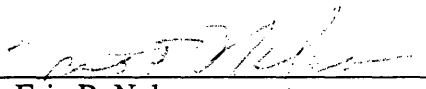
T-3510

A thesis submitted to the Faculty and the Board of Trustees of the Colorado School of Mines in partial fulfillment of the requirements for the degree of Doctor of Philosophy (Geology).

Golden, Colorado

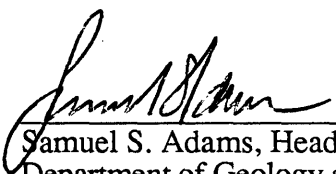
Date: April 4, 1988

Signed: 
Stephen G. Weaver

Approved: 
Dr. Eric P. Nelson
Thesis Advisor

Golden, Colorado

Date: April 4, 1988


Samuel S. Adams, Head
Department of Geology and
Geological Engineering

ABSTRACT

The study of calc-alkaline batholiths at convergent continental margins is important to our understanding of magmatic processes related to the dynamic setting of the subduction environment. The Patagonian batholith, located in southern Chile, is one such calc-alkaline batholith that is the subject of a petrologic and geochemical study presented in this dissertation. The results of this study suggest that the genesis and evolution of the batholith is the product of a complex set of magma sources and petrogenetic processes involving both mantle and crustal components.

The Patagonian batholith at 48° S is composed of numerous plutons of varying lithologies, ranging from gabbro to granite. The age of plutons in this area range from 150 to 48 Ma. Two major rock series have been identified by lithologic and chemical characteristics. The first series is classified as calc-alkaline tonalitic (CAT) and is characterized by low K₂O and other LIL element concentrations and dominantly consists of tonalite and leucotonalite with little or no K-feldspar. The second series is classified as calc-alkaline granodioritic (CAG) and is characterized by higher K₂O and LIL element concentrations and consists of quartz monzodiorite, granodiorite and granite. Both rock series also contain gabbros. The fundamental chemical differences of these two rock series suggest that two distinct parental magma types were involved in the formation of the Patagonian batholith. Geochemical studies from other regions in the batholith confirm the existence of these two primary magma groups, and suggest that they were derived from different mantle sources or different depths in the mantle wedge beneath the magmatic arc. The more evolved granites and leucotonalites found in the batholith are likely partial melts of mafic and intermediate rocks of both magma series induced by a continuing magma flux from the mantle.

Sr and Nd isotope data suggest that crustal contamination has played an important role in the petrologic and chemical evolution of the batholith at 48° S. These data suggest that the batholith is composed of mixtures of mantle-derived magmas and crustal components, and that there was a progressive decrease in crustal involvement during evolution of the batholith. Initial $^{87}\text{Sr}/^{86}\text{Sr}$ ratios range from 0.7036 to 0.7074 ($\epsilon \text{ Sr} = -14$ to 40) and initial $^{143}\text{Nd}/^{144}\text{Nd}$ range from 0.51279 to 0.51217 ($\epsilon \text{ Nd} = 6.7$ to -6). There is a distinct correlation between age and isotopic composition regardless of lithology. The oldest plutons have the highest initial $^{87}\text{Sr}/^{86}\text{Sr}$ ratios and the lowest $\epsilon \text{ Nd}$, and progressively younger plutons exhibit progressively lower initial $^{87}\text{Sr}/^{86}\text{Sr}$ ratios and higher $\epsilon \text{ Nd}$. This relationship is consistent with a decrease in crustal involvement in the evolution of the batholithic complex. Mixing calculations suggest that the oldest, most contaminated plutons can be modeled as mixtures between mantle magmas and partial melts of the basement complex which hosts the batholith. The basement is a forearc accretionary wedge complex composed of a volcanoclastic flysch sequence mixed with minor oceanic crustal material. Younger less contaminated plutons can be modeled as forming by assimilation of basement along with fractional crystallization (AFC).

The apparent decrease in contamination through time that is suggested by the isotope data can be explained by an evolution of the basement accretionary wedge complex whereby it dried out and became more refractory with time. This evolution resulted in decreased potential for chemical interaction between magmas and basement material, and progressively less contaminated younger plutons were produced. Physical isolation of younger plutons from basement by older plutons occupying space previously filled by basement also could have contributed to the decrease in crustal component present in the younger plutons of the Patagonian batholith.

TABLE OF CONTENTS

	<u>Page</u>
ABSTRACT.....	iii
LIST OF FIGURES.....	viii
LIST OF TABLES AND PLATES.....	x
ACKNOWLEDGEMENTS.....	xi
PREFACE.....	1
Chapter 1. PETROLOGY, GEOCHRONOLOGY, AND GEOCHEMISTRY OF THE PATAGONIAN BATHOLITH, 48 ° S, CHILE.....	3
Introduction.....	4
Regional Geologic and Tectonic Setting.....	7
Lithologies of the Patagonian Batholith at 48° S.....	8
Aerial Variations in Lithology.....	12
Lithologies of the Western Zone.....	14
Lithologies of the Central Zone.....	14
Lithologies of the Eastern Zone.....	15
Classification by Rock Series.....	16
Geochronology.....	16
Geochemistry.....	20
Analytical Methods.....	20
Geochemical Classification.....	20
Major and Trace Element Variations.....	23
Chemical Differences between Low K calc-alkaline (CAT) and Normal K (CAG) rocks.....	32
Chemical Characteristics of the 2-Mica Granites.....	34
Chemical Characteristics of the Gabbros.....	34

Geochemical Variations in Space and Time.....	35
Transverse Geochemical Variations Across the Batholith....	35
Temporal Geochemical Variations Within the Batholith.....	35
Discussion.....	38
Summary and Conclusion.....	45
 Chapter 2. SR, ND, AND PB ISOTOPE VARIATIONS IN THE PATAGONIAN BATHOLITH, 48° S, CHILE: IMPLICATIONS FOR THE EVOLUTION OF CRUSTAL CONTRIBUTIONS.....	47
Introduction.....	48
Regional Geologic and Tectonic Setting.....	48
Patagonian Batholith at 48° S.....	51
Isotope Data.....	53
Analytical Methods.....	53
Sr and Nd Isotope Variations.....	54
Isotopic Variations in Time.....	58
Mixing Between Mantle and Crustal Components.....	60
Assimilation with Fractional Crystallization (AFC).....	62
Mixing Between a Mantle Magma and a Partial Melt of Basement.....	66
Pb Isotope Data.....	68
Discussion.....	71
Summary.....	73
 REFERENCES CITED.....	75

Appendix A: SAMPLES AND LOCATIONS.....	82
Appendix B: PETROGRAPHIC DESCRIPTIONS.....	84
Appendix C: ANALYTICAL METHODS.....	95
Appendix D: GEOCHEMICAL DATA.....	101
Appendix E: $^{40}\text{AR}/^{39}\text{AR}$ AGE DATA.....	105

LIST OF FIGURES

<u>Figure</u>	<u>Page</u>
1.1 Location Map for the Southern Patagonian Batholith.....	6
1.2 QAP Diagram.....	9
1.3 Baker Area Lithology Histogram.....	10
1.4 Location Map of Dated Samples.....	13
1.5 Age Histogram for the Patagonian Batholith.....	19
1.6 AFM Diagram.....	21
1.7 Peacock Index Diagram.....	22
1.8 Alkalinity Index vs. Aluminous Index Diagram.....	24
1.9 Harker Diagrams (K ₂ O, Na ₂ O).....	25
1.10 Harker Diagrams (CaO, Al ₂ O ₃).....	26
1.11 Harker Diagrams (FeO*, MgO).....	27
1.12 Harker Diagrams (TiO ₂ , P ₂ O ₅).....	28
1.13 Trace Element Harker Diagrams (Rb, Ba).....	29
1.14 Trace Element Harker Diagrams (Sr, Zr).....	30
1.15 Trace Element Harker Diagrams (Nb, Y).....	31
1.16 Total Alkalies vs. SiO ₂ Diagram.....	36
1.17 ⁸⁷ Sr/ ⁸⁶ Sr Initial Ratio (Sri) vs. Age Diagram.....	37
1.18 Spider Diagrams Comparing CAT and CAG Series Rocks.....	41
1.19 CaO vs. Sr Diagram for the 84 Ma Biotite Granites.....	43
2.1 Patagonian Batholith Location Map.....	49
2.2 Map of Baker Area Isotope Sample Locations.....	52

2.3	ϵ Sri vs. ϵ Nd Diagram.....	57
2.4	Sri vs. Age Diagram.....	59
2.5	Bulk Mixing Models.....	61
2.6	Sr Isotope Assimilation-Fractional Crystallization (AFC) Models.....	64
2.7	Partial Melt Mixing Model.....	67
2.8	$^{207}\text{Pb}/^{204}\text{Pb}$ vs. $^{206}\text{Pb}/^{204}\text{Pb}$ Diagram.....	70

LIST OF TABLES AND PLATES

<u>Table</u>		<u>Page</u>
1.1	Baker Age Data.....	17
1.2	Comparison of CAT and CAG Series Rocks.....	33
2.1	Sr and Nd Isotope Data.....	55
2.2	Sr and Nd Initial Ratios.....	56
2.3	Pb Isotope Data.....	68
A-1	Patagonian Batholith Sample Locations and Descriptions.....	82
B-1	Patagonian Batholith Modal Data.....	93
D-1	Major Element Data.....	101
D-2	Trace Element Data.....	103
<u>Plate</u>		
A-1	Patagonian Batholith Sample Locations.....	in pocket

ACKNOWLEDGEMENTS

The research in this project cannot have taken place without the support and assistance of numerous individuals and organizations. I would first like to thank my advisor Eric Nelson for giving me the opportunity to work on the Patagonian batholith project and for giving constant support and encouragement. I thank Craig Simmons for helping to improve my understanding of geochemistry and Greg Holden for providing constant support and lively petrologic discussions. I also thank Bob Hamilton for his interest and support and for providing access to the XRF at Johns-Manville Corporation when the CSM XRF went down, and I thank committee member Richard Yeats for his interest and patience. Alan Zindler generously allowed complete and generous access to (including living in !) the isotope geochemistry lab at Lamont-Doherty Geological Observatory. A special thanks to Hannes Brueckner for teaching me the practical aspects of isotope geochemistry. My acceptance into the "Lamont isotope research group" is gratefully appreciated. Stan Mertzman of Franklin and Marshall College is gratefully acknowledged for numerous XRF analyses and for being a positive role model and a mentor early in my geologic career. I thank Carl Erickson for getting the CSM XRF in working order and ironing out a lot of the "bugs" in the CSM XRF procedures. Gary Girty of San Diego State University provided several U/Pb zircon dates. Bob Bruce ran numerous Ar/Ar age samples at the University of Maine, Orono. Bob also provided friendship and many stimulating geological discussions throughout my CSM experience. The financial support from CSM in the form of a teaching assistant, a Van Tuyl fellowship, and a Graduate School research grant is gratefully acknowledged. Other financial support for this project was supplied from NSF grants EAR 82-06646 and EAR 83-07064 to Eric Nelson.

Finally, I would like to thank my wife Deb for putting up with this project for four years and for providing constant encouragement and emotional support. Lastly, I would like to thank my parents who cultivated and encouraged my interests in nature and science at an early age. Without their support, I would not be writing this today.

PREFACE

Modern plate tectonic theory has provided igneous petrology with the driving mechanism behind much of the magmatic activity which has occurred on our planet. The study of subduction-related magmatism is a major thrust of contemporary igneous petrology, and the study of calc-alkaline batholiths at convergent continental margins is important to our understanding of magmatic processes related to the dynamic setting of the subduction environment. Major circum-Pacific calc-alkaline batholiths, such as the Peruvian, Sierra Nevada, Peninsular Ranges, and Coast Range batholiths, have been the focus of numerous studies (Pitcher et al., 1986; Bateman, 1983; Gromet & Silver, 1987; etc.) which have contributed to our understanding of the genesis of these major geologic features. In addition to their importance in our understanding of granitoid petrogenesis, the study of calc-alkaline batholiths also plays a major role in the understanding of crustal growth and the processes of orogenesis in Andean-type mountain belts.

One of the largest, yet least studied, circum-Pacific batholiths is the Patagonian batholith in southern South America. Like other batholiths, the Patagonian batholith displays a wide variety of rock types and geochemical attributes which can be related to the overall chemical and petrological evolution of the batholith and its changing interaction with the basement into which it was emplaced. This dissertation presents a petrological and geochemical study of samples from a transect across the Patagonian batholith at 48° S latitude in southern Chile.

The format of this dissertation consists of two major chapters which focus on different aspects of the geology of the Patagonian batholith. Chapter 1 discusses the basic petrology and variations in major and trace element geochemistry of the batholith in the study area.

Chapter 1 also presents geochronological data for the area. Chapter 2 examines variations in the isotopic geochemistry of the batholith and presents a model to explain the observed isotopic trends. As both of these chapters are intended as concise, stand-alone papers for publication, some repetition of material such as introductions, geologic and tectonic setting and other descriptive material is unavoidable. In addition to the two chapters, five appendices provide the basic data from which the discussions and models are drawn. Appendix A provides a list of all samples with their locations keyed to a folded location map (Plate A -1). Appendix B presents petrographic descriptions of the major plutons of the study area and also provides a table of mineral modes. Appendix C describes the analytical procedures used in the study, and Appendix D provides tables of geochemical data. Finally, appendix E presents $^{40}\text{Ar}/^{39}\text{Ar}$ age data.

Chapter 1

**PETROLOGY, GEOCHRONOLOGY, AND GEOCHEMISTRY
OF THE PATAGONIAN BATHOLITH, 48° S, CHILE**

Introduction

The study of major calc-alkaline batholiths provides a better understanding of the processes and rock record of subduction-related magmatism. Such major batholithic complexes as the Sierra Nevada, Peruvian, and Patagonian batholiths are complex features composed of hundreds of plutons of varying rock types and chemical compositions. However, studies have shown that consistent patterns of variation exist within batholiths, an example being the progression of mafic to felsic magmatism with time in the Peruvian Coastal batholith (Pitcher, 1978). Lithological and chemical variations in time and space can be related to the dynamic nature of the subduction process. Plate interactions, such as variations in relative plate motions and change of subduction dip angle can affect the production of magma from the subducted slab or overlying mantle wedge. Changing stress patterns in the upper plate (i.e. compression vs extension) may affect the emplacement of magmas and also may affect the production of magmas by crustal melting. Variations in the continental crust which hosts a batholith can affect its lithological and chemical composition through contamination and by providing a source for magma generation. Thus, studies of the lithological and geochemical variations of major calc-alkaline batholiths are vital to our understanding of granitoid petrogenesis and crustal growth at convergent continental margins. One of the largest, yet least studied of the major circum-pacific batholiths is the Patagonian batholith of the southern Andes. This paper will present petrologic, geochronologic and geochemical data from a suite of samples collected on an east-west transect across the batholith at 48° S latitude.

Previous geologic work in the southern Patagonian batholith has been limited, consisting primarily of early field reconnaissance studies and a few recent petrochemical and geochronologic studies of specific transects or areas. Early works include

observations made during expeditions to the region prior to the middle of the 20th century (Darwin, 1846; Quensel, 1910; Kranck, 1932). Halpern (1973) provided the first geochronological work, and Stern and Stroup (1982) the first modern geochemical study. Other modern studies include Suarez (1977), Bartholomew and Tarney (1984), and Herve et al. (1984)

The Patagonian batholith is the southernmost of the major subduction-related batholithic complexes in South America. It is exposed for 1500 km along the continental margin from about 41° S to 56° S in a continuous curvilinear outcrop belt 50-150 km wide (Fig. 1.1). This report focuses on the batholith at 48° S where it is roughly a 150 km wide, extending from the Pacific ocean at 76° 30' to 74° 30' in the Chilean fjord country. This area will be referred to as the Baker area after Canal Baker, a major east-west trending canal which drains the Rio Baker. The area is extremely remote and almost completely uninhabited. The physiography is dominated by peninsulas, numerous islands and interconnecting fiords and canal systems. Relief ranges from a few meters to about 1500 meters, with thick vegetation extending from high tide line to about 500 meters. Tidewater glaciers emanating from the Southern and Northern Patagonian ice fields are present in the northeastern and southeastern parts of the study area.

Field work was supported by the U.S. National Science Foundation Research Vessel HERO. Two cruises during the austral winters of 1983 and 1984 allowed a reconnaissance sea level examination of much of the batholith in the Baker area. The examination of Baker area is only one part of a larger reconnaissance study of the batholith south of 46° S latitude. The Baker area is one of three areas (Fig. 1.1) where we have carried out detailed petrologic, geochemical, and geochronologic studies.

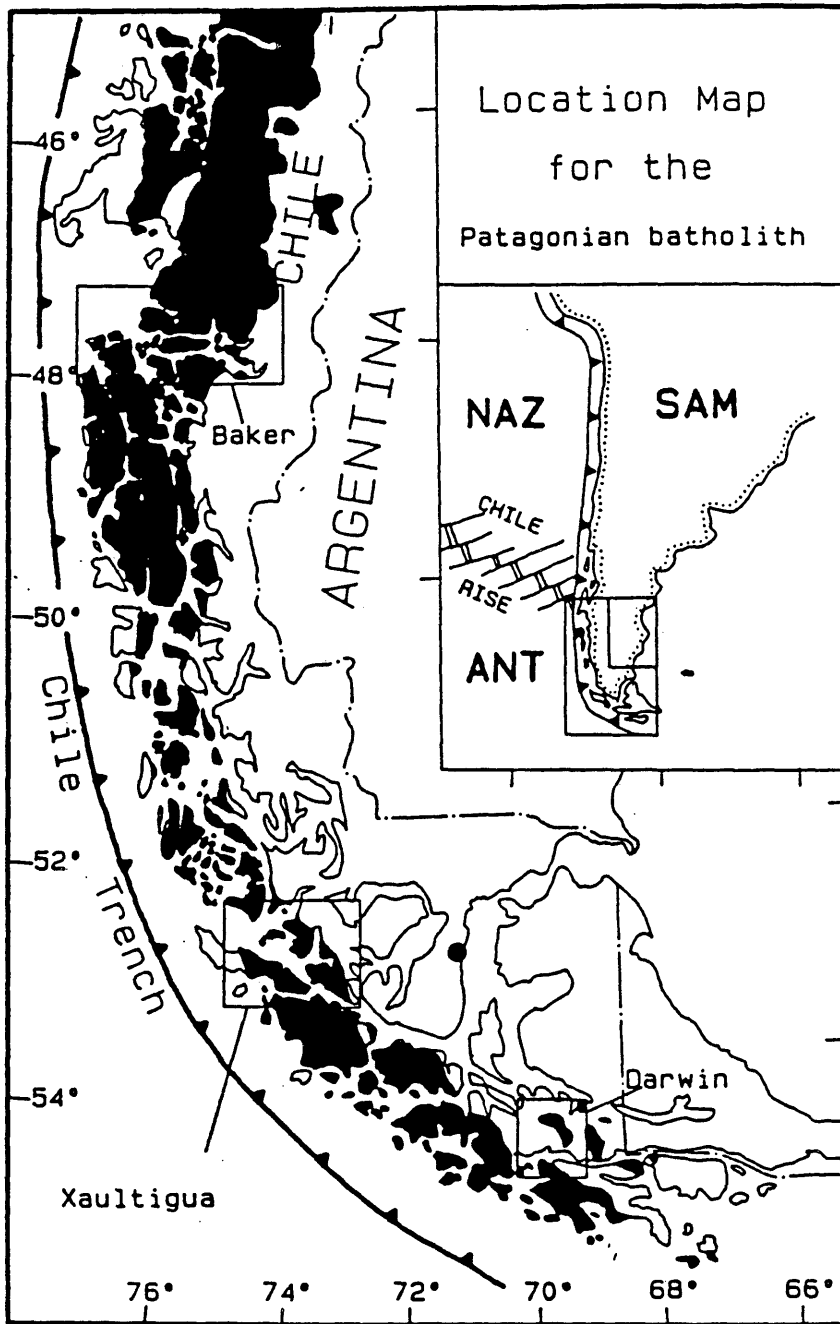


Fig. 1.1 Location Map for the Southern Patagonian Batholith

The batholith is shown in black. The area of this study at 48° S is outlined. The Xaultigua area (53°S) and Darwin area (56° S) are also outlined

In the Baker area approximately 135 stations at 1-5 km spacing were examined. Of the 135 stations, 106 were located in batholithic rocks, with the remainder being in Paleozoic basement, volcanic or Tertiary sedimentary rocks. Because of the reconnaissance nature of the field work, the size and extent of individual plutons could not be delineated and detailed variations within single plutons cannot be addressed. Nevertheless, large scale regional variations have been delineated and such a regional study lays the groundwork for future work on the batholith.

Regional Geologic and Tectonic Setting

The Patagonian batholith is situated along the active continental margin of southern South America where the Nazca and Antarctic plates are being subducted beneath the South America plate. Subduction in this region has probably been active semi-continuously since the Late Paleozoic (Dalziel, 1981; Forsythe, 1982). Paleozoic subduction produced a magmatic arc east of the Patagonian batholith, but by mid-Jurassic time the locus of magmatism had moved west with intrusion of plutons into the Paleozoic forearc sequence and eruption of extension-related bimodal volcanics (Bruhn et al., 1978). The Early Cretaceous marked the formation of the Rocas Verdes marginal basin and associated ophiolitic magmatism in the area presently south of 50° S (Dalziel, 1981). Subsequent arc-continent collision during the Andean orogeny closed this marginal basin by mid-Cretaceous time with compressional tectonics continuing into the Tertiary (Nelson et al., 1980).

The basement sequence, into which much of the Patagonian batholith was intruded, is an accretionary forearc complex of a Late Paleozoic magmatic arc to the east. Basement lithologies include: 1) a volcanoclastic flysch sequence of graywacke and shale,

2) radiolarian ribbon chert, 3) limestone, 4) mafic-ultramafic rocks containing high pressure mineral assemblages, 5) pillow basalt, and 6) quartz-veined phyllite (Mpodozis and Forsythe, 1983; Nelson et al., in press). These lithologic elements suggest that a volcanoclastic flysch sequence and a mixture of oceanic crustal material and allochthonous terranes were accreted to the margin prior to the Late Jurassic (Forsythe, 1982). Other wall rocks, exposed along the eastern contact and within isolated exposures in the batholith, include Late Jurassic silicic volcanic rocks, Early Cretaceous ophiolitic rocks, and Early Cretaceous shale and volcanoclastic flysch (Nelson et al., in press).

Lithologies of the Patagonian Batholith at 48° S

Plutonic lithologies present in the Baker area represent the typical range of rock types found in most major calc-alkaline batholiths. These range from hornblende gabbro, diorite and tonalite, through granodiorite and true granite. A complex of noritic gabbro and several plutons of garnet-bearing 2-mica granite are also exposed. All lithologic nomenclature used in this study is based on the IUGS classification scheme (Streckeisen, 1974).

Modal compositions were determined by point counting 1000 points on thin sections of medium- to fine-grained samples and stained slabs of coarse-grained samples. Of 91 samples, 33% are granite, 22% are granodiorites, 22% are tonalites, and 10% are quartz diorites (Figs. 1.2 and 1.3). Two -mica granites make up 4% of the samples and gabbros 9%. This apparent skew toward more silicic compositions is due to the presence of a large area of biotite granite in the eastern part of the Baker area. Modal data from the rest of the Patagonian batholith suggest that the Baker area may be anomalously silicic in composition (Nelson et al., in press), and show that tonalite is the dominant lithology of the batholith.

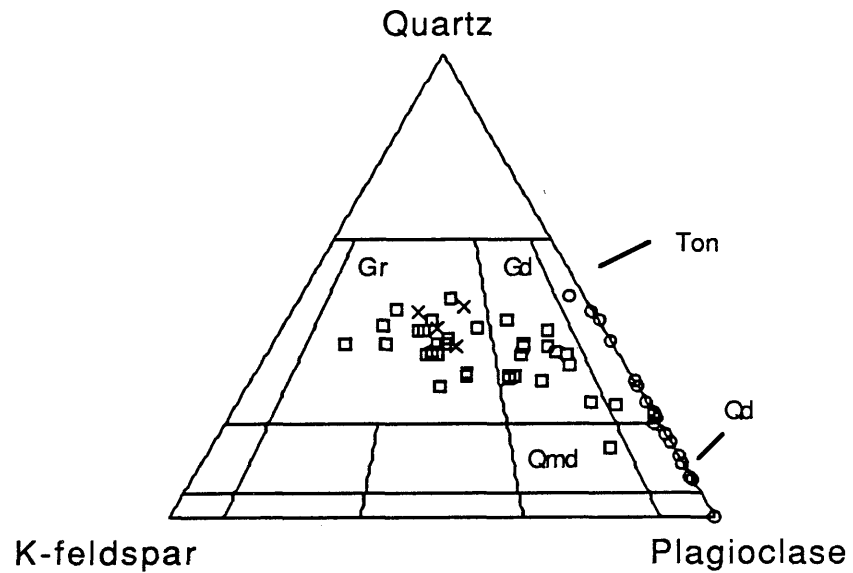


Fig. 1.2 QAP Diagram

Low K calc - alkaline series (CAT) plotted as circles. Normal K calc - alkaline series (CAG) plotted as squares. 2-mica granites plotted as X 's. Series classification from Lameyre and Bowden (1982). Gr = granite, Gd = granodiorite, Ton = tonalite, Qmd = quartz monzodiorite, and Qd = quartz diorite (Streckeisen, 1974).

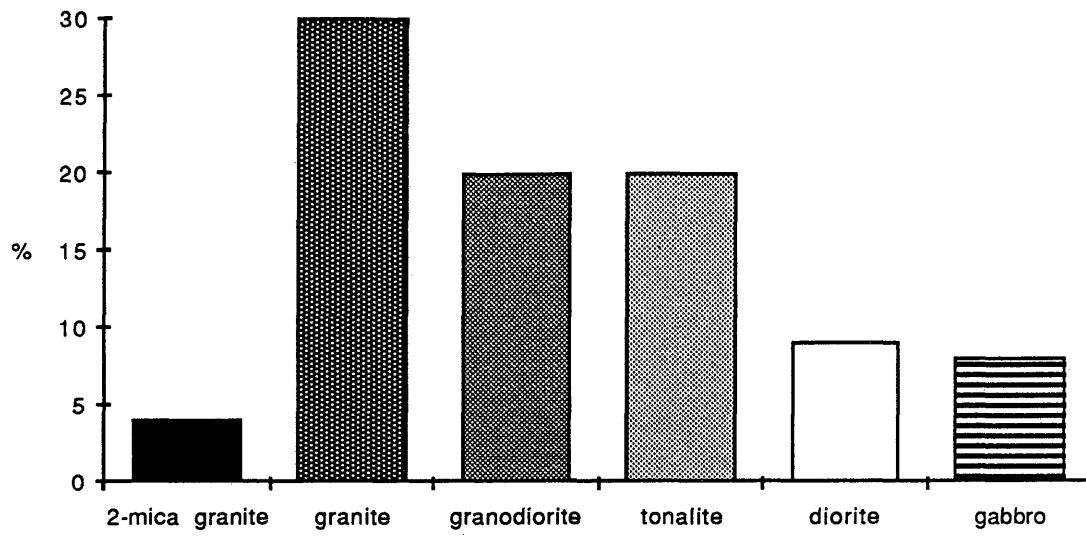


Fig. 1.3 Baker Area Lithology Histogram

Total number of samples = 91.

Mafic, aphanitic to fine-grained dikes are exposed throughout the area. These mafic rocks range in composition from basalt to porphyritic hornblende andesite, and are dominantly post plutonic. They are most likely Late Cretaceous or younger, but at the present time remain undated.

Mineralogical content and variations of the plutons at 48° S are typical of the rest of the Patagonian batholith and other calc-alkaline batholiths. Plagioclase is present in all lithologies and ranges from ~ An 80 to An 15 in composition depending on lithology. Plagioclase grains are usually euhedral to subhedral and exhibit normal zoning. Oscillatory zoning is rare. Some tonalites and granodiorites contain plagioclase grains with calcic cores which show disequilibrium textures, suggesting the cores are restite material (White and Chappell, 1977; Bateman and Nockelberg, 1978). Quartz is present in intermediate to silicic lithologies as subhedral to anhedral grains often as intergranular material. K-feldspar, when present in intermediate rocks, is present as late crystallizing, often intergranular material. Tartan twinning suggest that it is dominantly microcline. K-feldspar present in granites is perthitic, and usually is present as subhedral to anhedral grains coexisting with quartz and plagioclase in a hypidiomorphic texture.

All lithologies present, including the most mafic, contain one or more hydrous minerals. Hornblende is the dominant mafic mineral in gabbro and diorite, often present as reaction rims on pyroxene. Most gabbros contain minor biotite in reaction relation with hornblende. Hornblende and biotite are present together in most tonalite and granodiorite, typically making up to 30% of the mode. Textures suggest that biotite usually followed hornblende in the crystallization sequence. Primary epidote is present in some tonalite and granodiorite. All granites contain biotite, but hornblende is extremely rare. Accessory minerals include apatite, zircon, allanite, Fe-Ti oxides, and rare tourmaline. Sphene is

notably absent in all but a few samples. A minor population of leucocratic peraluminous 2-mica granites contain minor biotite, muscovite and garnet. Trace amounts of dumortierite have been noted in one of these granites.

The plutons in the Baker area are typically characterized by medium- to coarse-grained hypidiomorphic granular textures. Cumulate textures are present in some of the gabbro. These textures, along with a complete absence of fine-grained granite with miarolitic cavities suggest mesozonal emplacement depths. The presence of magmatic epidote in equilibrium with hornblende and biotite in some of the tonalite and granodiorite corroborates this suggestion. This assemblage is interpreted as resulting from crystallization at pressures between 6 and 8 kb, which corresponds to an emplacement depth of 18-24 km (Zen and Hammarstram, 1984)

Aerial Variations in Lithology

In order to study the aerial variations in lithologies of the Patagonian batholith at 48°S, the study area has been divided into three zones parallel to the continental margin (Fig.1.4). This division generally reflects the tectonic segmentation and magmatic zonation of the batholith. A major lineament represented by the north-trending Canal Mesier separates the western zone from the central zone. This tectonic discontinuity probably represents a major shear zone as suggested by the presence of cataclastic textures and the more highly altered nature of the lithologies in outcrops along this zone. Unfortunately the timing of shearing is unknown (Nelson et al., in press). The boundary between the central and eastern zone was chosen as the westernmost exposure of biotite granite which is the

dominant lithology in the eastern zone. This boundary also corresponds with a north-trending lineament defined by the alignment of several fjords.

Lithologies of the Western Zone. The western zone is defined as the area west of Canal Mesier between 74° 45' and 75° 30' and consists of numerous islands including Isla Millar, Isla Juan Stuvan, Isla Wager and Isla Byron (see Plate 1 for location of geographic features). The plutons present are dominated by mafic and intermediate lithologies. The westernmost plutons consist of mafic biotite hornblende quartz diorite and hornblende biotite tonalite. Granite is rare, the only sample being from a highly altered pluton on the southwest coast of Isla Byron. Of particular interest are tonalite and granodiorite which contain primary magmatic epidote in equilibrium with biotite and hornblende. Other lithologies include noritic gabbro, quartz monzo-diorite and 2-mica leucotonalite.

Lithologies of the Central Zone. The central zone is defined as the area between 74° 15' and 74° 45' east of Canal Mesier. The plutons located in this zone along Canal Mesier are commonly highly altered and foliated and show evidence of cataclastic deformation. This deformation fabric, which is strongly suggestive of shearing, is confined to the western 15 km of the central zone. The alteration is characterized by chlorite and epidote replacement of biotite and hornblende and extensive sericitization of plagioclase. The altered plutons range from tonalite to granite, including a 2-mica granite. Unaltered and unfoliated lithologies east of the shear zone are dominantly tonalite but include hornblende gabbro, hornblende quartz diorite, and minor hornblende biotite granodiorite.

Altered mafic and silicic volcanic rocks also crop out at several locations in the western central zone. Altered basalts crop out on several islands at the intersection of Canal Baker

and Canal Mesier including Isla Porcia and Isla Orlebar. These basalts have been intruded by granitoids of the batholith, suggesting that they may be related in time and space to the mid Jurassic back-arc basin volcanics exposed further south in the Sarmiento and Tortuga complexes (Bruhn et al., 1978). Additional evidence to support this correlation is the presence of silicic tuffaceous material similar to the silicic volcanics of the mid Jurassic Tobifera formation. Silicic tuffs are present on Peninsula Sweet just southeast of Isla Orlebar, and several locations south along Canal Mesier. Also, rhyolite porphyry is present near the mouth of Fiordo Pulpo in the northwestern section of the central zone. Unfortunately no age determinations have been made of these silicic volcanics, but limited geochemical data suggest a relationship to the Tobifera formation.

Lithologies of the Eastern Zone. The eastern zone is defined as the area between 74° 15' and 73° 15', and is dominantly composed of Late Cretaceous biotite granite and granodiorite. This large area of biotite granite (~ 1250 km²) is exposed from central Isla Merino Jarpa east into Fiordo Mitchell and north into Fiordo Steffen. Minor variations in modal abundance and textures do exist, however, no major mineralogical or textural zonation has been noted among the samples. Micro-diorite inclusions are often present in these granites and mafic dikes are rare. Hornblende and biotite bearing tonalite and granodiorite, typical of much the Patagonian batholith, makes up most of the remainder of the batholith in the eastern zone. Gabbro in the eastern zone crops out in several scattered locations but volumetrically is minor. Additional lithologies include garnet-bearing 2- mica granite and a biotite leucotonalite.

Classification by Rock Series

The intrusive rocks of the Patagonian batholith can be classified into two major rock series as defined by the method of Lameyre and Bowden (1982) and Bowden et al. (1984) using the modal abundances of quartz, plagioclase, and K-feldspar. These include a low K calc-alkaline tonalitic series (CAT), and a normal K calc-alkaline granodioritic series (CAG). The CAT series has little or no K-feldspar and plots along or adjacent to the QP tie line of the QAP Streckeisen (1974) diagram in the quartz diorite and tonalite fields (Fig. 1.2). In contrast, the CAG series contains substantial K-feldspar and plots in the granite, granodiorite and quartz monzodiorite fields. Both series diverge from gabbroic compositions on the QAP diagram. These two rock series suggest the presence of two distinct magma groups, low potassium magmas which produce evolved rocks low in potassium, and magmas with higher potassium which ultimately produce normal calc-alkaline granodiorites and granites by magma fractionation or partial melting of rocks of the series. Major element geochemistry confirms these two groups, and in the ensuing discussions this division into the two series will be maintained. In addition to these two groups, the 2-mica granites will be considered as a separate group. These rocks fall into the category of crustal granites in the classification of Lameyre and Bowden (1982) and Bowden et al. (1984).

Geochronology

Age data for samples from the Baker area are reported in Table 1.1. Most of the ages were determined by the $^{40}\text{Ar}/^{39}\text{Ar}$ method at the University of Maine, Orono. Two samples from which zircon separates were obtained were analyzed by the U/Pb method at San Diego State University, and three samples were analyzed by the Rb/Sr mineral-whole

Table 1.1

Baker Age Data

sample #	lithology	material dated	method*	age (Ma)
G-58	gabbro	hornblende	$^{40}\text{Ar}/^{39}\text{Ar}$	48.2 ± 2.2
BK-13	granodiorite	biotite	$^{40}\text{Ar}/^{39}\text{Ar}$	82.2 ± 2.2
BK-19	granite	biotite	$^{40}\text{Ar}/^{39}\text{Ar}$	83.0 ± 0.6
RB-98	tonalite	biotite	$^{40}\text{Ar}/^{39}\text{Ar}$	89.8 ± 1.4
		biotite, K-feldspar, WR	Rb/Sr ^a	92 ± 6
OE-4	tonalite	biotite	$^{40}\text{Ar}/^{39}\text{Ar}$	92.1 ± 1.1
PU-8	quartz diorite	hornblende	$^{40}\text{Ar}/^{39}\text{Ar}$	95.8 ± 2.4
RB-104	2-mica granite	plagioclase, K-feldspar muscovite, WR	Rb/Sr ^a	110 ± 3
OE-6A	granodiorite	biotite	$^{40}\text{Ar}/^{39}\text{Ar}$	108.3 ± 1.2
		zircon	U/Pb [^]	113.1 ± 0.7
RB-105	2-mica granite	plagioclase, muscovite, WR	Rb/Sr ^a	124 ± 27
OE-10	tonalite	biotite	$^{40}\text{Ar}/^{39}\text{Ar}$	128.5 ± 1.2
RB-106	granodiorite	biotite	$^{40}\text{Ar}/^{39}\text{Ar}$	146 ± 5.4
		zircon	U/Pb [^]	149.3 ± 0.8

* $^{40}\text{Ar}/^{39}\text{Ar}$ plateau ages, uncertainties are one standard deviation with n-1 weighting

[^] U/Pb concordant zircon ages, uncertainties are at the 2σ level

^a York fit model III age (Ludwig, 1985), uncertainties are at the 2σ level

rock isochron technique at Lamont-Doherty Geological Observatory. The $^{40}\text{Ar}/^{39}\text{Ar}$ ages are at least minimum ages, although the U/P concordant zircon age for one sample (RB-106) lies within the error limits for its $^{40}\text{Ar}/^{39}\text{Ar}$ age on biotite, suggesting that some of the $^{40}\text{Ar}/^{39}\text{Ar}$ ages may represent crystallization ages.

Ages determined for plutons from the Baker area range from 149 Ma to 46 Ma. Previous widely scattered age determinations of the batholith (Halpern, 1973; Herve et al., 1981; Halpern and Fuenzalida, 1978), along with our age determinations from other areas in the batholith (Bruce et al., 1986a), suggest that magmatism occurred semi-continually from about 166 Ma to 12 Ma with a peak occurring between 100 and 70 Ma (Fig.1.5). Age data from individual areas within the batholith such as the Baker area are discontinuous and exhibit a smaller range when compared with data from the entire batholith. This may reflect sampling bias or suggest that plutonism was episodic in different areas of the batholith. However, Bruce et al. (in press) have suggested that the different age spectra present in different areas of the batholith may be an artifact of differential uplift, and that plutonism was indeed semi-continuous throughout the history of the batholith.

The Baker area does not exhibit regular unidirectional migration of plutonism with time (Fig.1.4), as noted in northern Chile by Farrar et al. (1970). The oldest dated plutons in the Baker area are located on the eastern margin of the batholith. The next oldest plutons in the Baker area are concentrated in the western zone (Fig.1.4). Progressively younger plutons show no regular placement, but generally are scattered in the central and eastern zones. This arrangement of older plutons located at the western and eastern margins may indicate that they were emplaced in an extensional regime or that intrusion of younger plutons into the main mass of the batholith pushed older plutons away from the main locus of magmatism producing the age pattern seen today.

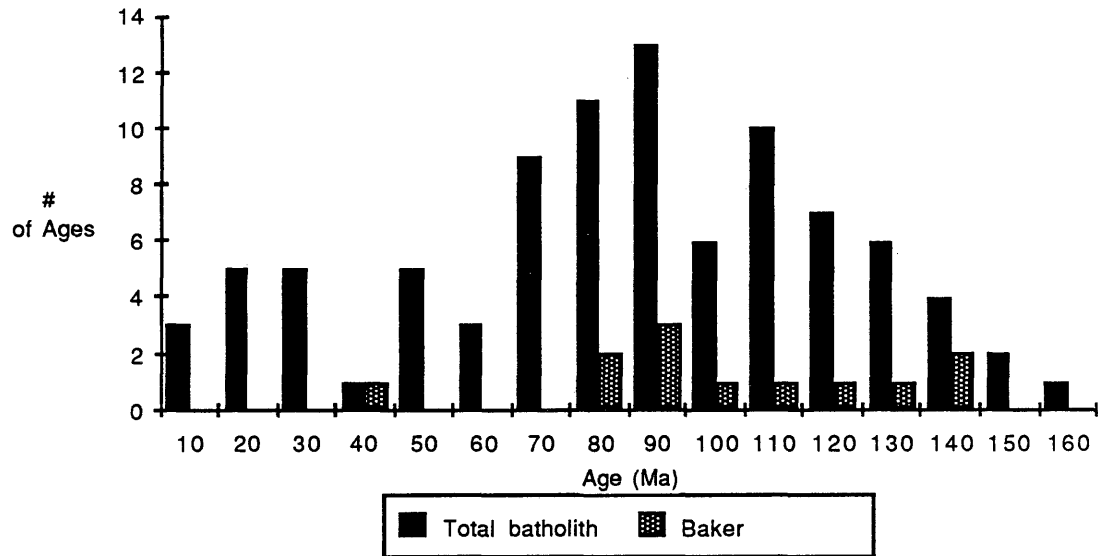


Fig. 1.5 Age Histogram for the Patagonian Batholith.

Geochemistry

Analytical Methods

Whole rock samples (1-2 kg) were crushed and ground and ~ 50g splits were tumbled and mixed for 48 hours to ensure homogeneity. Major elements were determined by XRF analysis at Franklin & Marshall College using fused glass discs fluxed with $\text{Li}_2\text{B}_4\text{O}_7$. Analytical precision is as follows: $\text{SiO}_2 \pm 0.4\%$, $\text{Al}_2\text{O}_3 \pm 0.12\%$, $\text{Fe}_2\text{O}_3 \pm 0.10\%$, $\text{FeO} \pm 0.04\%$, $\text{TiO}_2 \pm 0.02\%$, $\text{MnO} \pm 0.01\%$, $\text{MgO} \pm 0.07\%$, $\text{CaO} \pm 0.03\%$, $\text{Na}_2\text{O} \pm 0.09\%$, $\text{K}_2\text{O} \pm 0.02\%$, and $\text{P}_2\text{O}_5 \pm 0.02\%$. FeO was determined by the wet chemical method of Goldich (1984). Selected trace elements were analyzed by XRF on whole rock powder pellets bound with microcrystalline cellulose. Trace element concentrations were corrected for mass absorption and matrix effects by the method of Hower (1959). Sr and Rb analyses have an uncertainty of $\pm 5\%$ and Ba, Nb, Ni, Y, Zr, and V have an uncertainty of $\pm 10\%$.

Geochemical Classification

Like most subduction-related continental margin batholiths, the Patagonian batholith dominantly exhibits calc-alkaline characteristics. Fig.1.6 is an AFM diagram with the fields for calc-alkaline and tholeiitic rocks displayed (Irvine and Baragar, 1971). Noting the exception of the gabbros, the majority of the Patagonian batholith samples plot in the calc-alkaline field. However, a Peacock diagram recast in the manner of Brown (1982)(Fig.1.7) classifies the low K CAT series rocks as calcic with a Peacock index of ~ 66, and the medium K CAG series plots as calc-alkaline with a Peacock index of ~60. In order to maintain consistency with the petrographic based classification of Lameyre and

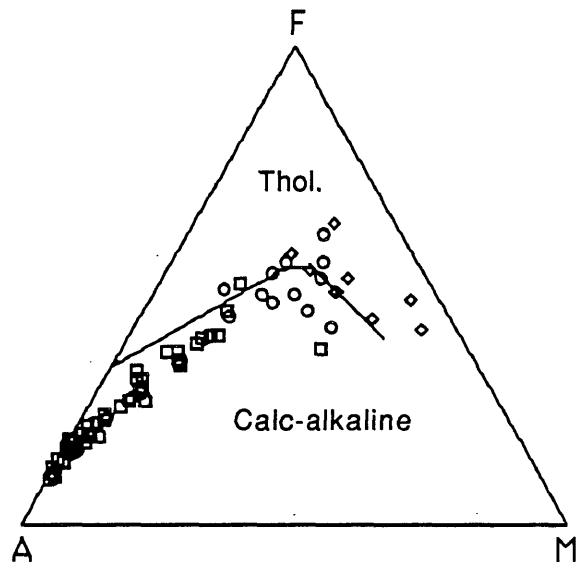


Fig. 1.6 AFM Diagram

Gabbros plotted as diamonds. CAT series plotted as circles. CAG series plotted as squares. Tholeiitic and calc-alkaline fields from Irvine and Baragar (1971).

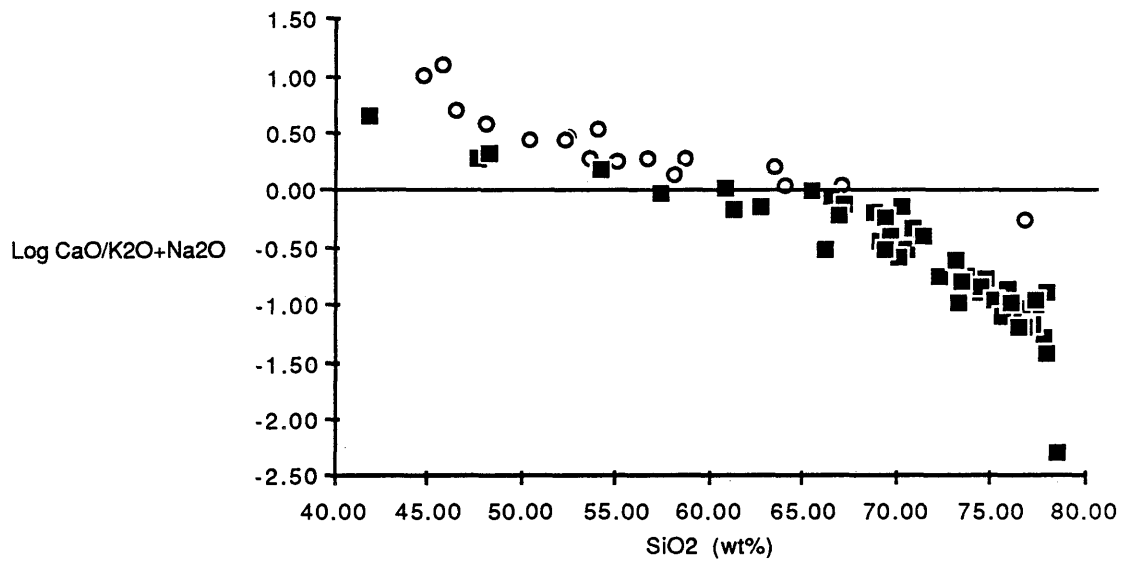


Fig. 1.7 Peacock Index Diagram

Peacock index diagram modified after Brown (1982). CAT series plotted as open circles and CAG series plotted as filled squares. The Peacock index for a particular series is calculated from the point where the series cross the 0 Log (CaO/K₂O+Na₂O) value.

Bowden (1982), the ensuing discussions will maintain the calc-alkaline low K and normal K classification in lieu of a calcic and calc-alkaline series suggested by the Peacock index.

In addition to classification by the alkali-lime index, granitoids can be classified by alumina saturation utilizing the aluminous index (AI) of Shand (1927). Rocks are classified peraluminous when their AI is greater than 1. The AI is defined as the molecular proportion of Al_2O_3 divided by the sum of molecular $(CaO+Na_2O+K_2O)$. Rocks that are peraluminous have corundum in their norm and usually contain one or more aluminous minerals such as muscovite, biotite, garnet, aluminosilicates, corundum, or tourmaline. Rocks that are metaluminous have AI's less than 1, but molecular Al_2O_3 is greater than (Na_2O+K_2O) . Fig. 1.8, a plot of $\text{mol } (K_2O+Na_2O)/Al_2O_3$ vs. $\text{mol } Al_2O_3/(CaO+Na_2O+K_2O)$, indicates that the gabbros and most of the CAT series rocks are metaluminous and the CAG and 2-mica granites are peraluminous. Strongly peraluminous ($AI > 1.1$) 2-mica garnet-bearing granites have been considered to be S-type granites, those granites produced by partial melting of aluminous sedimentary rocks (Chappell and White, 1974). In contrast, granites produced from partial melting of igneous rocks are classed as I-types and generally are metaluminous to weakly peraluminous ($AI < 1.1$). The peraluminous nature of the CAG series suggests that contamination by aluminous sedimentary rocks may have been important in their genesis and evolution.

Major and Trace Element Variations

Major and trace element variations for the CAT and CAG series rocks are illustrated on Harker diagrams (Figs. 1.9 -1.15). In addition to these two major groups, gabbros and the 2-mica granites are also plotted in these figures. In most cases, these four groups of rocks clearly can be distinguished on many of the Harker diagrams.

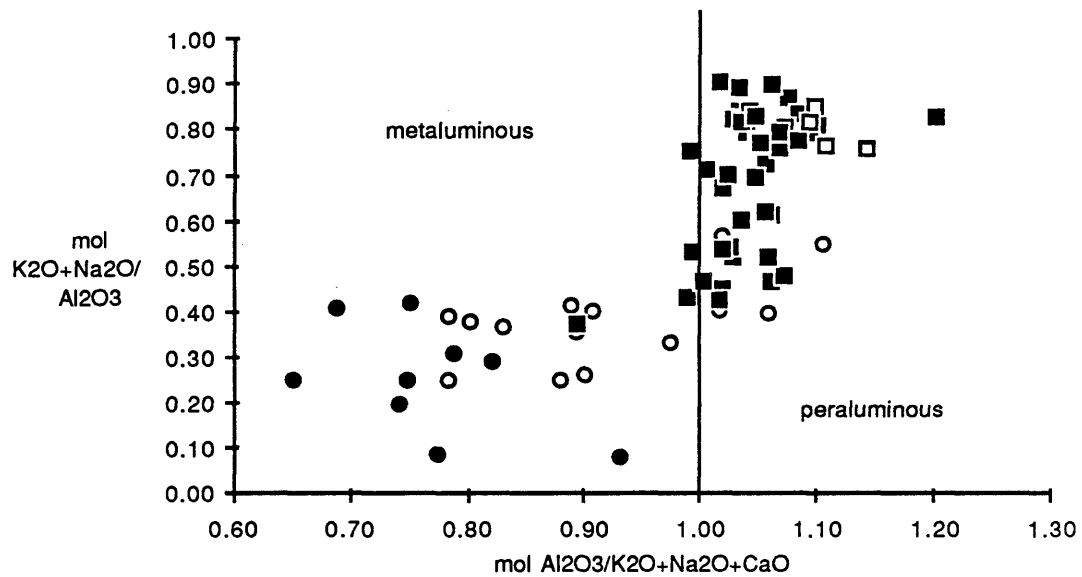


Fig. 1.8 Alkalinity Index vs. Aluminous Index Diagram

Classification from Shand (1927). Gabbros = filled circles. CAT series = open circles. CAG series = filled squares, and 2-mica granites = open squares.

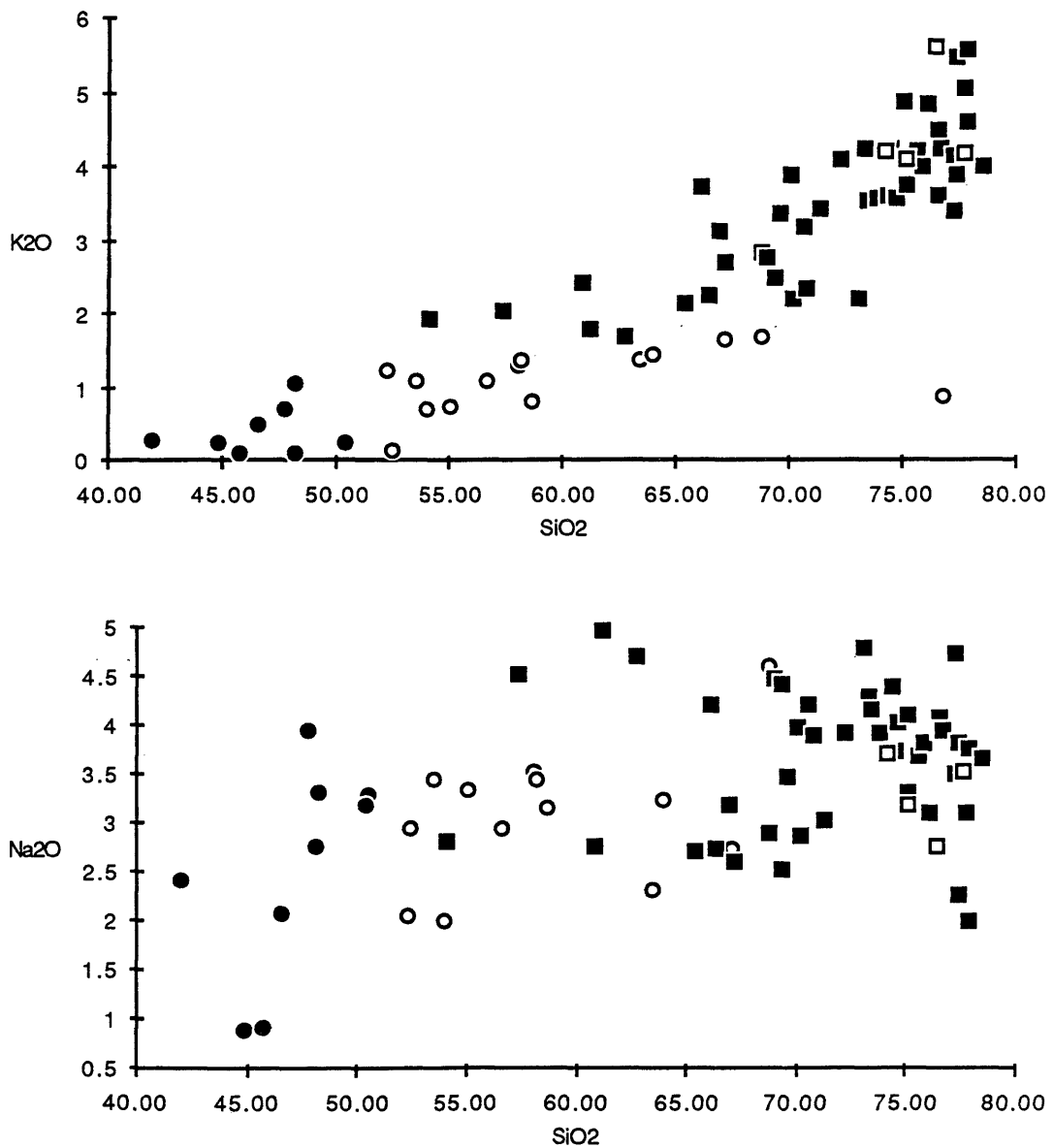


Fig. 1.9 Harker Diagrams (K₂O, Na₂O)

Gabbros = solid circles, CAT series = open circles, CAG series = solid squares, and 2-mica granites = open squares. All data is in weight %.

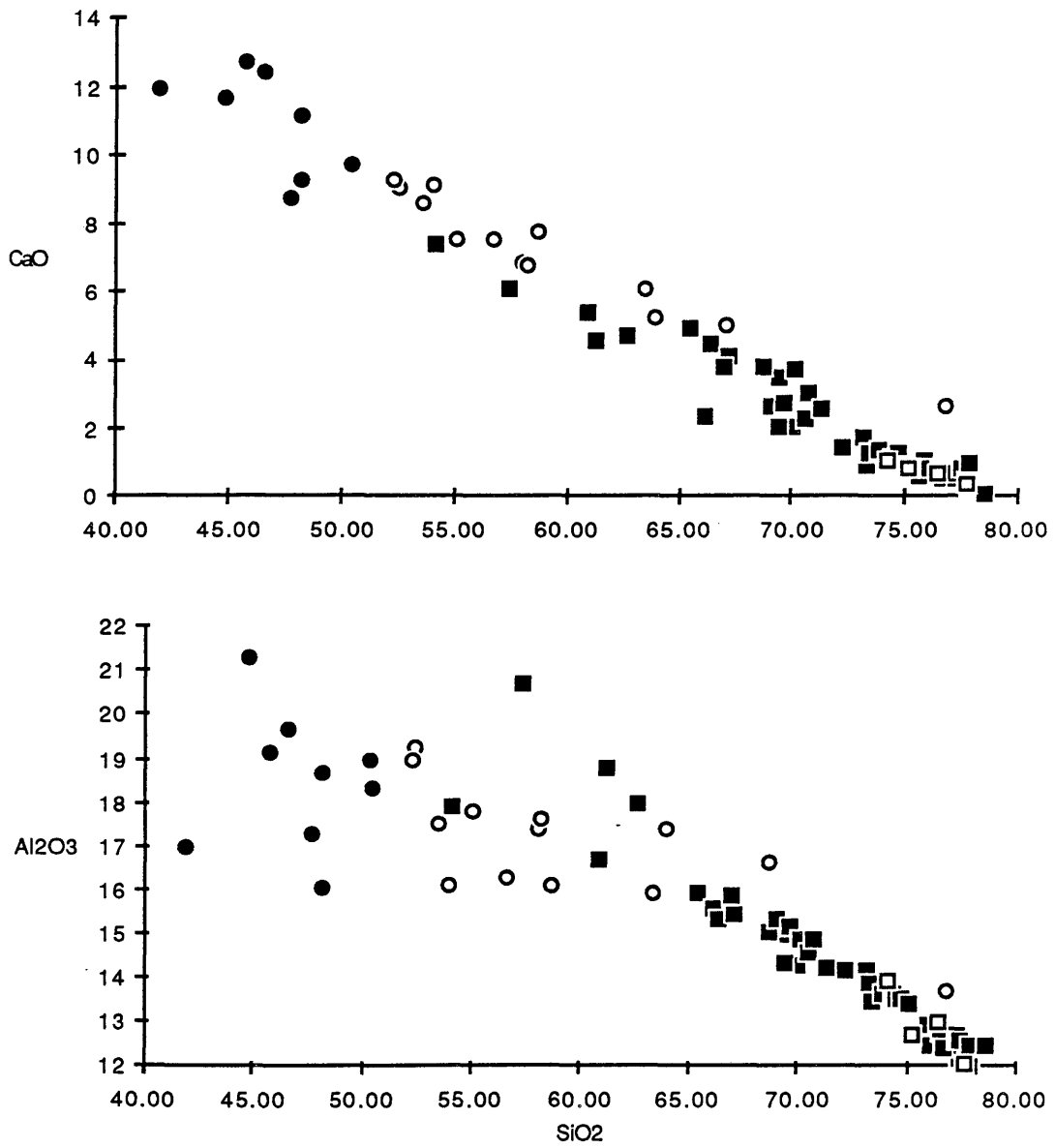


Fig. 1.10 Harker Diagrams (CaO, Al₂O₃)

Symbols as in Fig. 1.9.

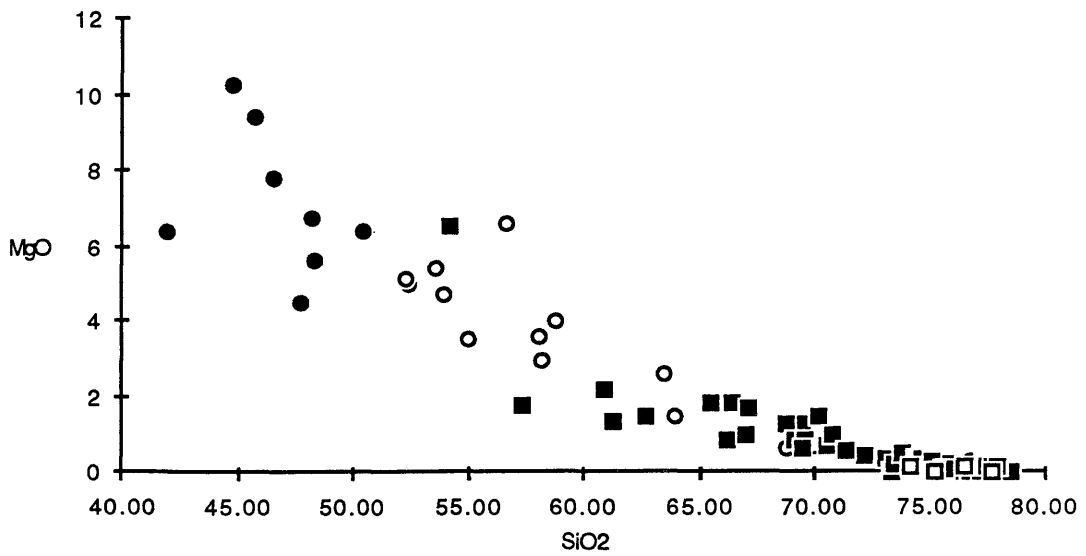
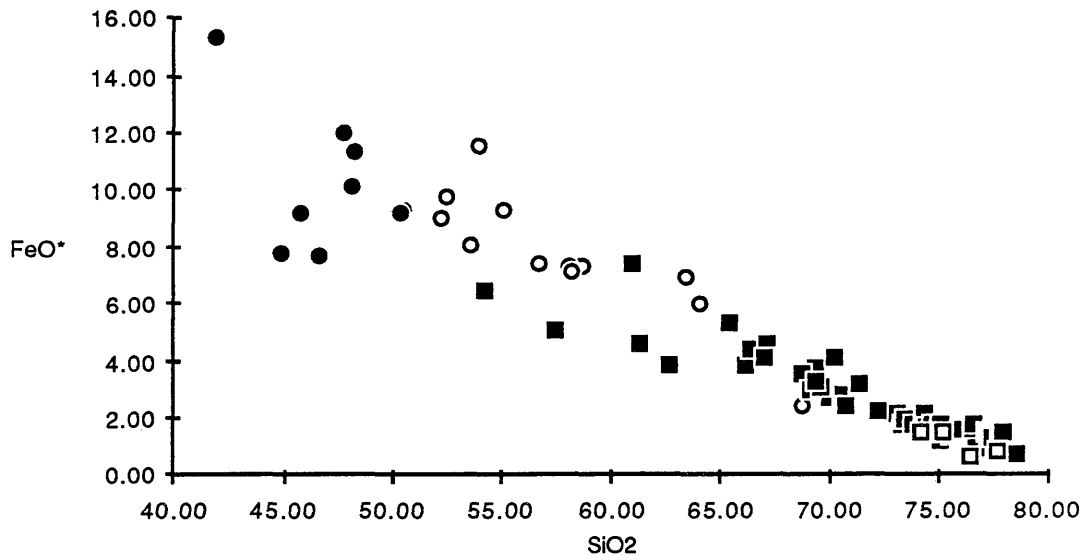


Fig. 1.11 Harker Diagrams (FeO*, MgO)

Symbols as in Fig. 1.9.

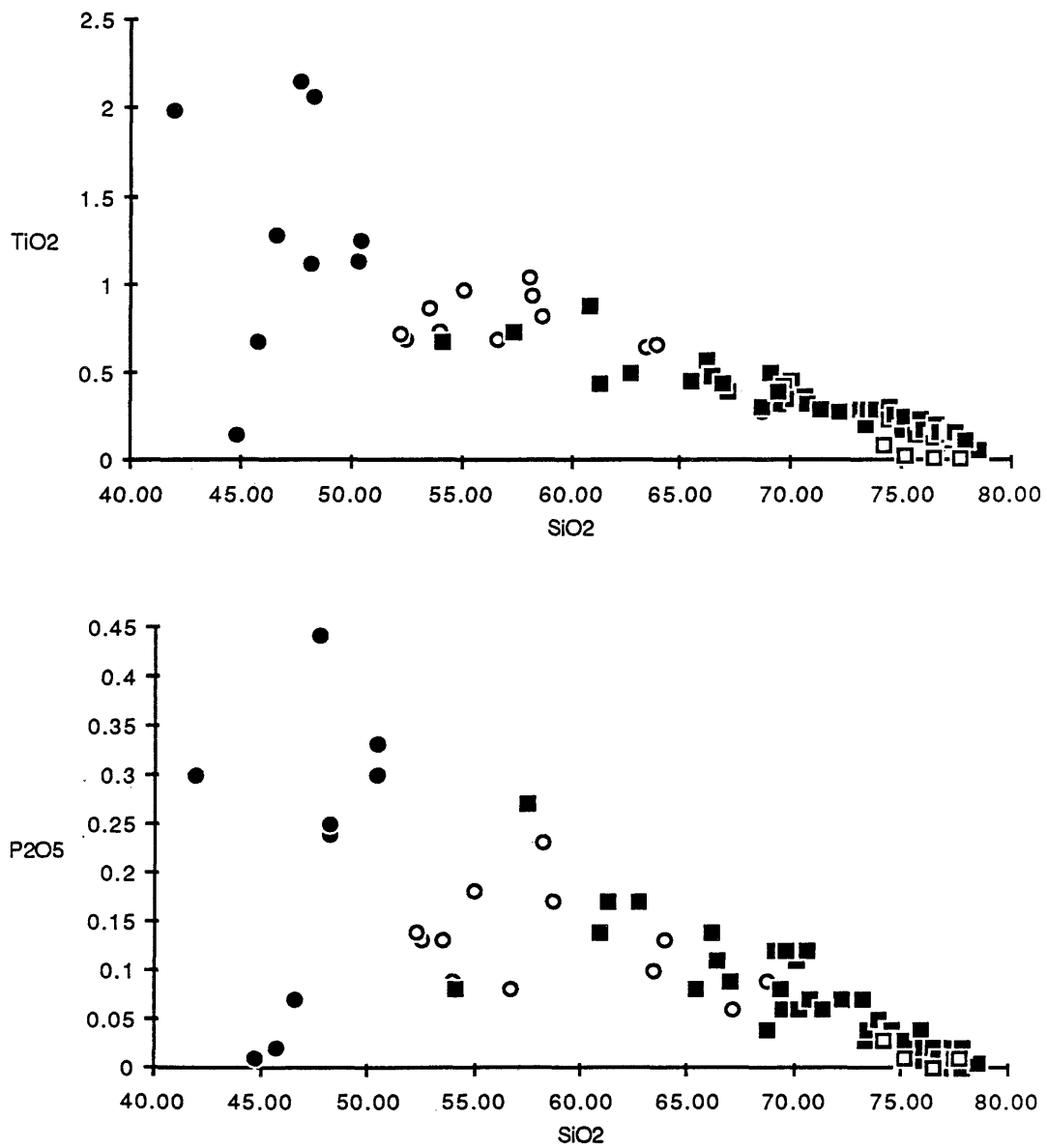


Fig. 1.12 Harker diagrams (TiO_2 , P_2O_5)

Symbols as in Fig. 1.9.

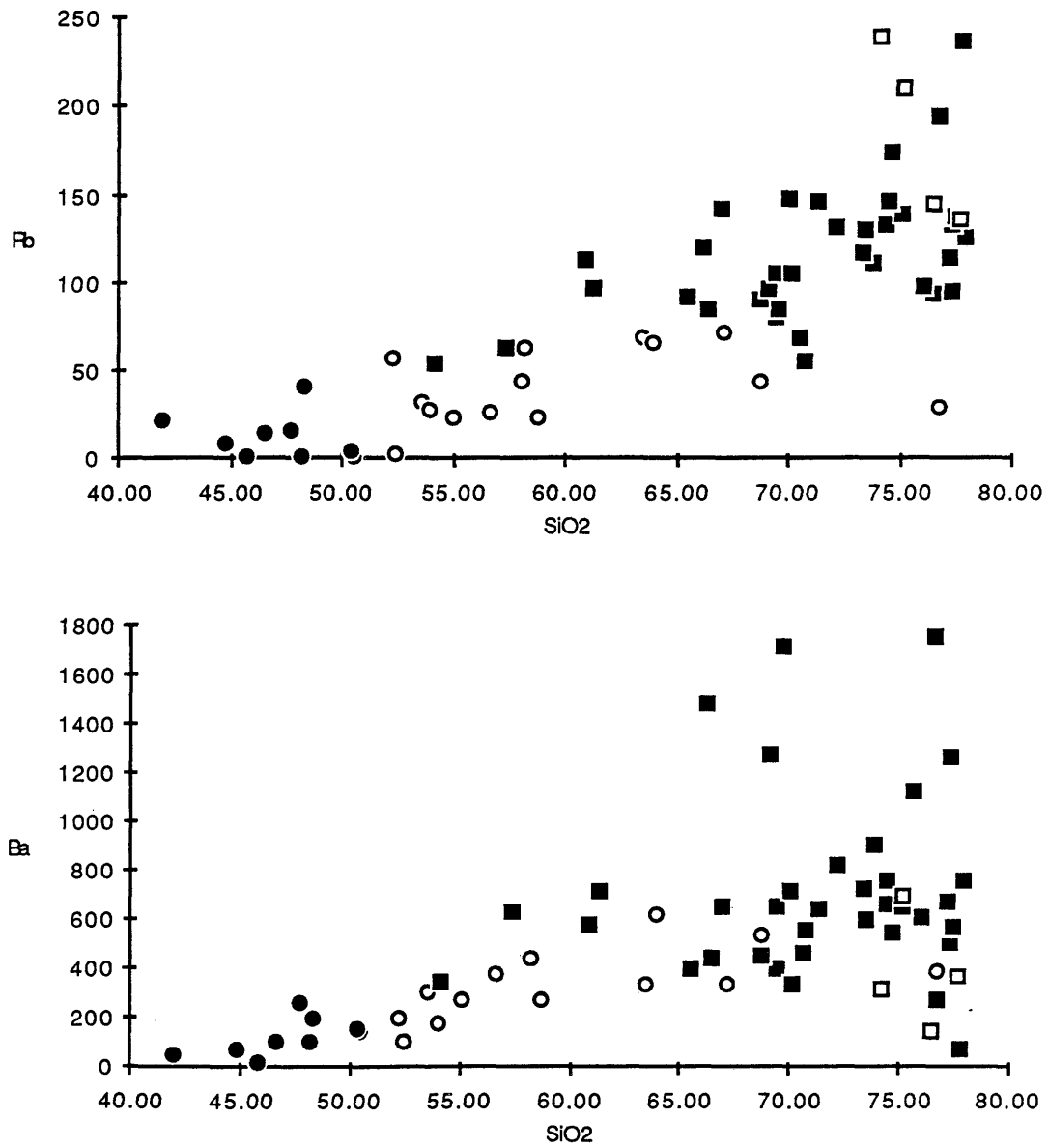


Fig. 1.13 Trace Element Harker Diagrams (Rb, Ba)

Symbols as in Fig. 1.9. Trace elements in ppm.

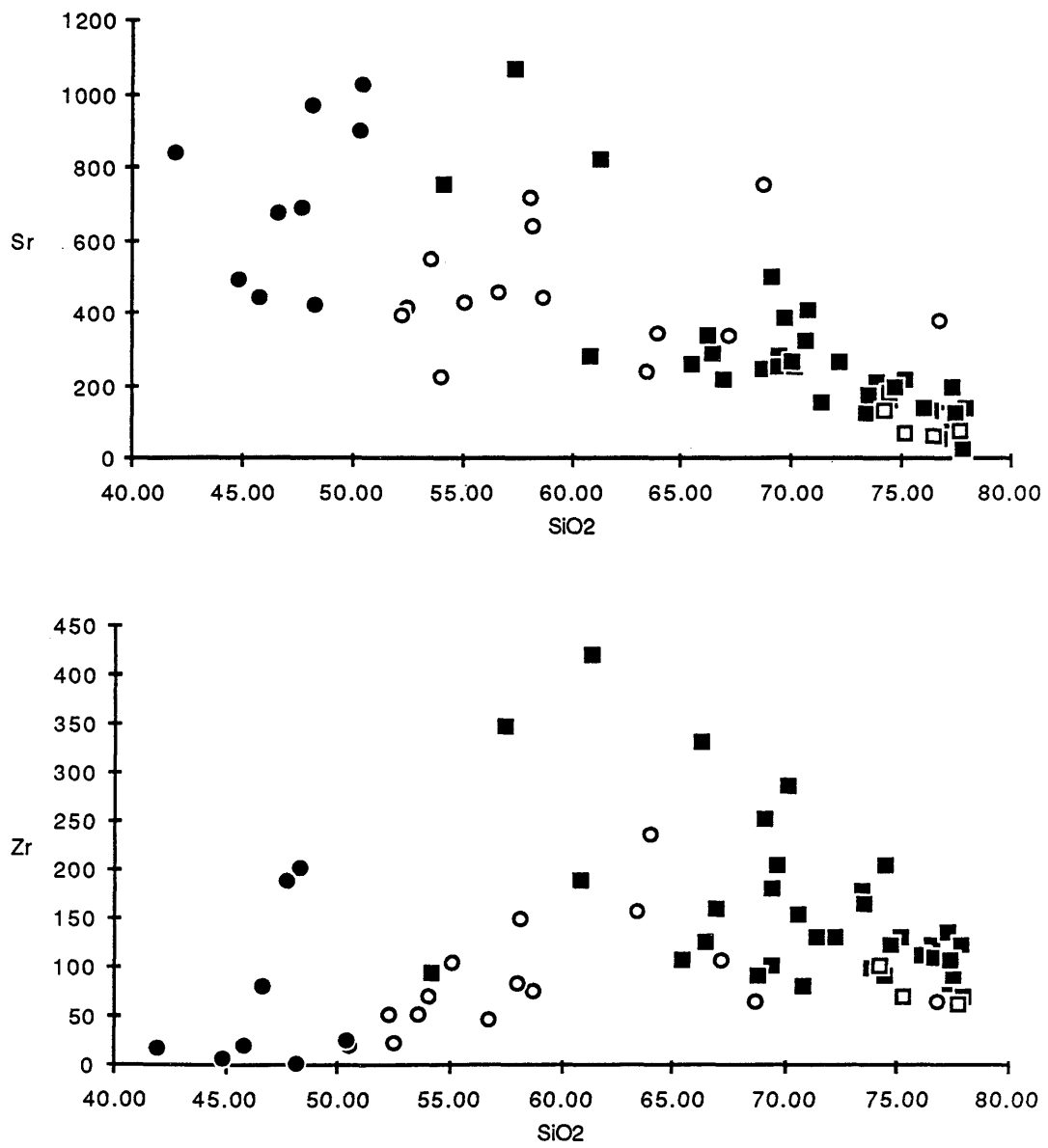


Fig. 1.14 Trace Element Harker Diagrams (Sr, Zr)

Symbols as in Fig. 1.9.

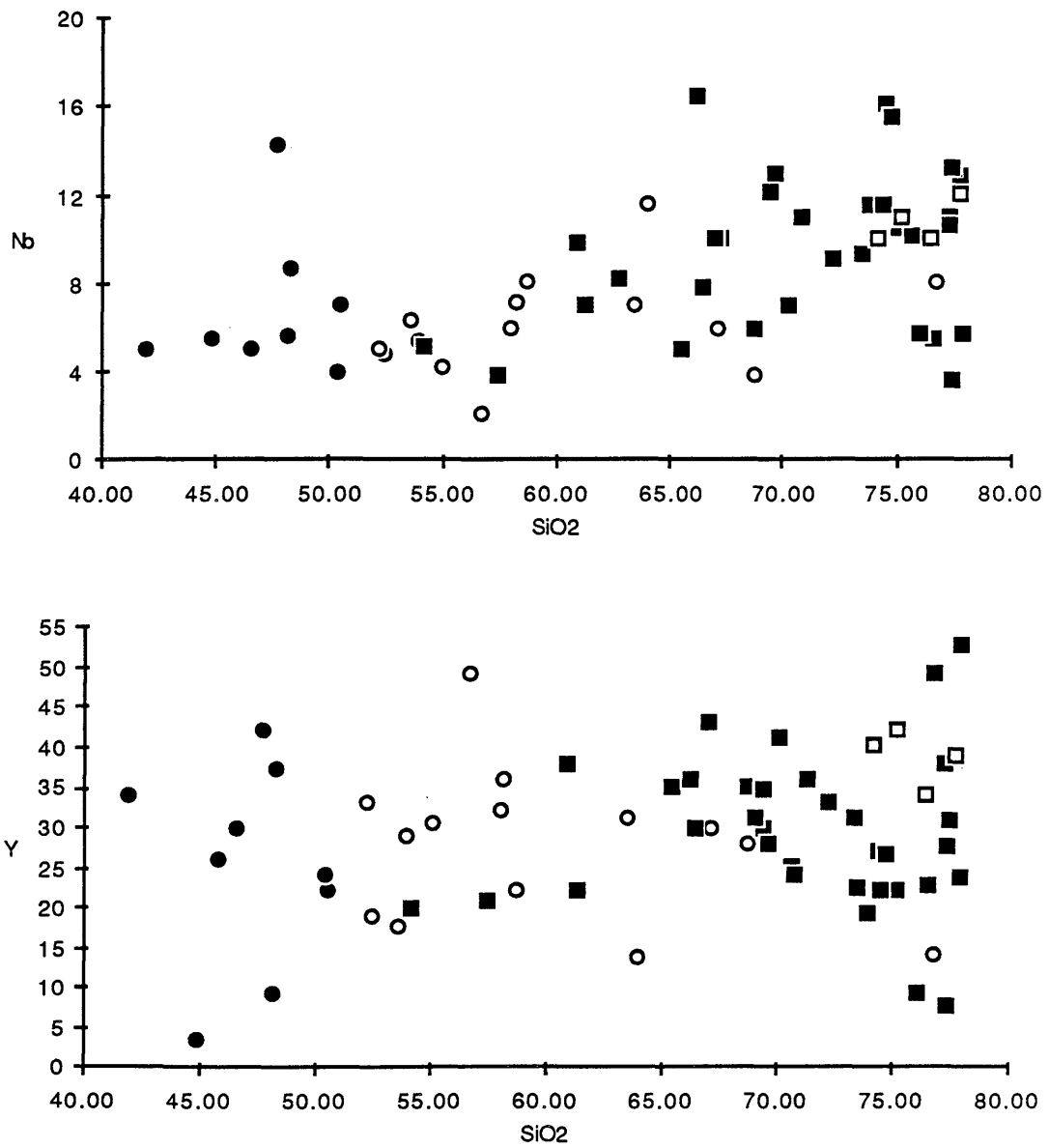


Fig. 1.15 Trace Element Harker Diagrams (Nb, Y)

Symbols as in Fig. 1.9.

Chemical Differences between Low K Calc-alkaline (CAT) and Normal K (CAG)

Rocks. Major element Harker diagrams (Fig. 1.9 - 1.12) generally exhibit linear trends for the CAT and CAG series rocks. These trends suggest a chemical coherency and probable genetic relationship within the two series. However, these linear trends cannot be viewed as specific fractionation or mixing trends relating the most mafic sample to the most silicic sample. The widely scattered locations, lack of detailed field relationships, and lack of extensive geochronology prevent a realistic evaluation of such petrologic evolution within each series. However, the coherent behavior of the two groups on the Harker diagrams does substantiate the presence of two distinct magmas series with distinct chemical characteristics.

The most notable differences in the two series are present in the concentrations of the large ion lithophile (LIL) elements, K, Rb, Ba. For lithologies with similar SiO₂ content (Table 1.2, and Figs. 1.9 and 1.13). The CAT series rocks always contain lower concentrations of LIL elements than the CAG series. CaO, FeO*, MgO and TiO₂ tend to be higher in the CAT series rocks. Na₂O, Al₂O₃, and P₂O₅ tend to be scattered and do not discriminate well between the two series. Na₂O, in particular, exhibits a wide range of values for samples of similar SiO₂ content in both the CAT and CAG series.

Trace elements (Figs. 1.13 - 1.15) tend to exhibit more scatter within the series than major elements. As previously mentioned, Rb and Ba concentrations readily discriminate between the CAT and CAG series, however both elements show a substantial variation within the evolved granites of the CAG series. Zr concentrations also tend to be higher in the CAG series, but also show a wide variation in the granites. Sr, Nb, and Y exhibit a wide degree of scatter among and between series and generally tend to be poor discriminators for the two series. This scatter among trace elements may be due to the

Table 1.2

Comparison of CAT and CAG Series Rocks

sample # lithology *	CAT series			CAG series		
	OE-11 Qd	OE-10 Ton	OE-4 Ton	BK-15 Qd	RB-98 Ton	RB-96 Gd
<u>mode ~</u>						
Quartz	6.7	30.6	29.4	6.9	21.0	33.1
K-feldspar	-	-	2.0	-	5.0	14.3
Plagioclase	44.57	50.0	40.8	51.4	61.0	41.1
Biotite	5.98	10.95	8.6	18.5	10.0	5.3
Hornblende	42.7	7.46	6.0	22.1	2.0	6.1
Pyroxene	-	1.0	-	-	-	-
<u>Chemistry ^</u>						
SiO ₂	54.01	63.39	67.12	54.16	61.27	66.98
K ₂ O	0.72	1.37	1.65	1.92	1.80	3.10
Rb	27	69	72	55	96	142
Ba	174	340	337	351	710	648
Sr	227	240	337	747	818	219
Zr	72	158	107	93	420	160

* Qd = quartz diorite, Ton = tonalite, Gd = granodiorite

~ mode in volume %

^ SiO₂ and K₂O in wt %, trace elements in ppm

probability that the analyses of these plutonic rocks do not represent liquid compositions, but rather are mixtures of crystals and liquids. For example, the presence or absence of certain trace minerals such as zircon, allanite, and apatite will clearly effect the concentrations of Zr, Y, and Nb (Pearce and Norry, 1979).

Chemical Characteristics of the 2-Mica Granites. Major element chemistry of the 2-mica granites is similar to the evolved granites of the CAG series rocks. On Harker diagrams (Figs.1.9 -1.12) the 2-mica granites tend to cluster within the field of the CAG granites. The best major element discriminant is TiO_2 , which is consistently lower in the 2-mica granites. Na_2O also tends to be lower than most of the CAG granites. The 2-mica granites are also more peraluminous than most of the CAG granites, with an $\text{AI} > 1.1$ (Fig.1.8). Trace elements also are scattered somewhat, but Sr, Ba, and Zr tend to be lower and Rb and Y tend to be higher in the 2-mica granites than the CAG granites.

Chemical Characteristics of the Gabbros. The gabbros when examined as a collective group, exhibit wide scatter on major and trace element Harker diagrams (Figs. 1.9 - 1.15). This may be due to their probable cumulate nature. It is also evident that they include the mafic members of both the CAT and CAG rock series. This is clearly evident in the K_2O , Rb and Ba diagrams, where several gabbro samples clearly have higher LIL concentrations than other gabbros with similar SiO_2 values, suggesting that the series classification extends to mafic rocks with no modal K- feldspar.

Geochemical Variations in Space and Time

Transverse Geochemical Variations Across the Batholith

Regular variations in LIL element concentrations across calc-alkaline batholiths have been well established in several magmatic arc complexes. The trends seen in the Sierra Nevada batholith (Bateman, 1983) and in the plutons of the Antarctic Peninsula (Saunders et al., 1980), clearly exhibit an increase in K_2O with increasing distance away from the subduction zone. The Patagonian batholith at $48^\circ S$ also exhibits such a trend, as is evident in Fig. 1.16, a plot of total alkalis vs. SiO_2 . The majority of plutons present in the western zone of the batholith (Fig.1.4) clearly have lower total alkalis for a particular SiO_2 value than those in the eastern zone. K_2O , Rb, and Zr exhibit the same areal variations, with the highest concentrations being in the eastern plutons. Similar trends in the Patagonian batholith at $52^\circ S$ have been noted by Stern and Stroup (1982).

Temporal Geochemical Variations Within the Batholith

The areal geochemical variations described in the previous section do not appear to have any systematic relationship to the time of intrusion. Samples in the eastern zone range in age from 149 Ma to 83 Ma and all tend to have higher LIL than those in the west that range in age from 130 Ma to 93 Ma. This suggests that the observed compositional variations are spatially dependent rather than time dependent.

Geochemical variations in the Patagonian batholith that are time dependent can be seen in Fig. 1.17, a plot of initial $^{87}Sr/^{86}Sr$ ratio (Sr_i) vs. time. A clear continuous trend of decreasing Sr_i with decreasing age can be seen for three regions of the Patagonian batholith. This relationship holds true irrespective of lithology. Weaver et al. (in press) have interpreted this relationship as a decrease in crustal contamination with time produced

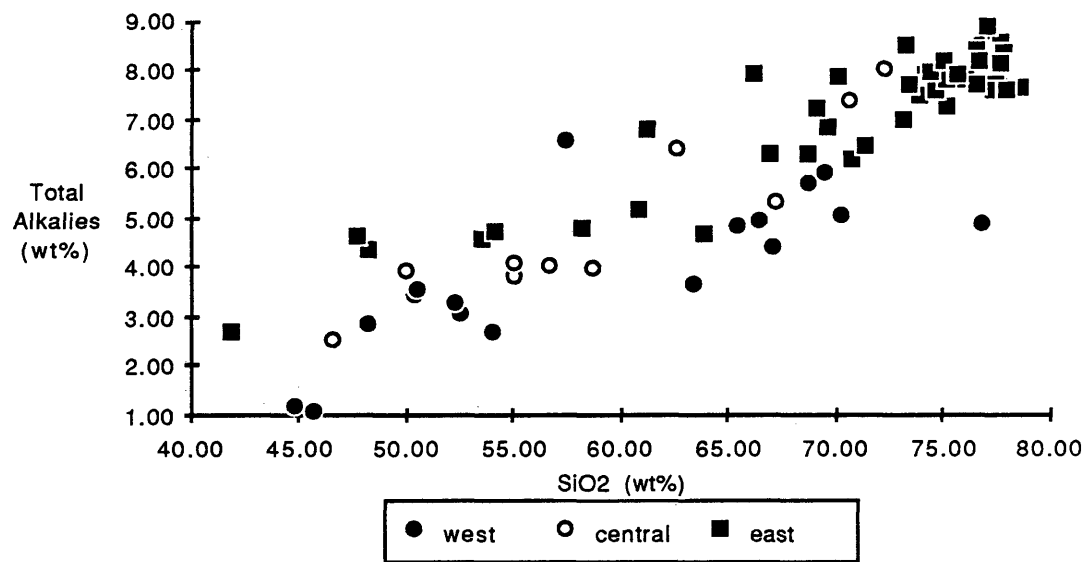


Fig. 1.16 Total Alkalies vs. SiO₂ Diagram

Note that the western area samples consistently have lower alkalies than the eastern area samples.

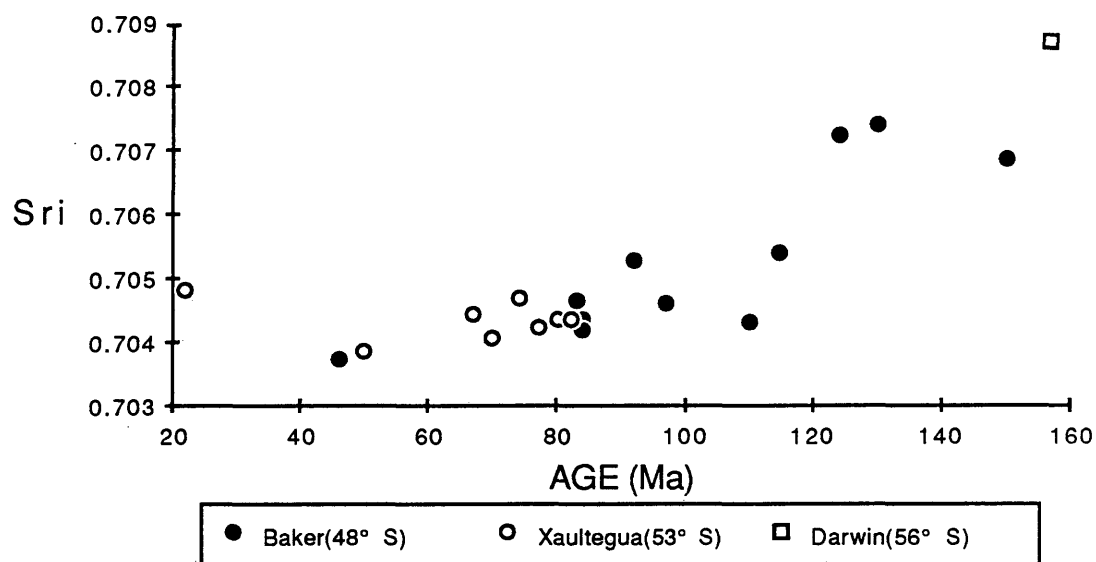


Fig. 1.17 $^{87}\text{Sr}/^{86}\text{Sr}$ Initial Ratio (Sri) vs. Age Diagram

Data from three areas in the batholith are plotted. Note the trend of decreasing Sri with age.

by the evolution of the accretionary fore-arc prism complex which hosts the batholith. Mixing models (Weaver et al., in press; Nelson et al., 1987), using Sr and Nd isotope data, support the suggestion that the early plutons of the Patagonian batholith were produced from mixtures of mantle-derived-magmas and partial melts of the continental crust. Hot mafic magmas, encountering water-bearing sediments of an accretionary forearc prism complex, could partially melt the complex and become contaminated by these melts. It is suggested that the complex dried out and became more refractory with time, resulting in decreased ability for chemical interaction between magmas and basement material, and thus less contaminated plutons were produced. Physical isolation of younger plutons from basement by older plutons occupying space previously filled by basement could also have contributed to the decrease in crustal component present in the younger plutons.

Discussion

The origin and evolution of calc-alkaline magmas in subduction related granite batholiths is a major question which still does not have a precise and unquestionable answer. The dynamic environment of the active continental margin provides a complex set of sources and mechanisms which interact to produce a wide variety of magmatic products. Wyllie (1983, 1984) in a review of the petrogenesis of granitoid magmas at convergent plate boundaries suggested that they represent the end product of a complex multi-stage process initiated by the the dehydration of oceanic crust in a subduction zone. The fluids released from the slab contain concentrations of alkalis and other LIL elements and ultimately enrich the overlying mantle wedge by metasomatism. These fluids also will induce partial melting in the mantle wedge to produce mafic magmas which underplate, or intrude into, the lower crust. Thus the mantle material enriched in LIL elements ultimately provides the

source of LIL enriched magmas typical of calc-alkaline magmatic arcs. Tonalites that make up most calc-alkaline batholiths are probably the result of fractionation of this mafic mantle magma along with varying degrees of interaction (contamination) with crustal material (Barker et al., 1981). Subsequent partial melting of these tonalites in the lower crust (initiated by prolonged intrusion of hot mafic magmas, or by crustal thickening) may ultimately produce more evolved magmas. Wyllie (1984) suggested that a wide range of granitoid rock types can be produced by mixing granitic liquid and restite material. If subduction is continued over a long period of time, a complex pattern of magma production, differentiation, and contamination could be recorded within a magmatic arc system.

An application of the above model to the Patagonian batholith must explain the lithologic and chemical variations which have been noted in the Baker area. Geochemical and petrographic data suggest the presence of two distinct rock series with different LIL element contents, and isotopic data suggest that crustal components also have contributed to the genesis of many of the plutons in the area. Since rocks of the continental crust in general tend to have high LIL element contents, a logical assumption would suggest that the plutons in the CAG series would be the most contaminated with crustal components. However, this is not the case. The oldest dated CAG series pluton, a granodiorite with $Sr = 0.7068$ and $\epsilon Nd = -3.2$, has a significant component from the continental crust. However, the evolved 84 Ma biotite granite and granodiorite of the CAG series have Sr ratios of 0.7042-0.7047 and ϵNd of 1.3 - 1.7, values suggesting little crustal contamination. In contrast the oldest dated CAT tonalite has Sr of 0.7074 and $\epsilon Nd = -6.0$, values suggesting major amounts of an older crustal component. Clearly the early CAT rocks cannot represent uncontaminated mantle-derived magmas. The question of

whether the difference in K_2O and other LIL elements is a function of original concentrations in mantle-derived magmas or is a function of contamination cannot be answered from evidence in the Baker area alone. However, our isotopic studies of other areas of the southern Patagonian batholith have suggested that the Xualtegua area at $53^\circ S$ has younger plutons which are uncontaminated (Fig. 1.17). Geochemical studies of plutons from the Xualtegua area (Bruce et al., in press) have identified both a low K_2O rock series and a higher K_2O rock series, like the CAT and CAG series in the Baker area, and their similarity invites a comparison. The lack of an older crustal component in the Xualtegua area suggests that the K_2O and LIL element difference is inherited from their primary mantle magma compositions. A chemical comparison of representative rocks of the two series from the Baker and Xualtegua areas is presented in Fig. 1.18. The two spider diagrams of mafic and intermediate rocks from the two areas illustrate the differences between the two rock series. In both areas, the LIL elements are higher in the CAG series than the CAT series. However, the concentrations in both series from the Xualtegua area are consistently lower than their counterparts in the Baker area. This confirms the isotopic data which suggest that the Baker plutons on the whole contain a greater component of continental crust. It also suggests that the differences in LIL content of the two rock series can be originally attributed to differences in primary mantle-derived magmas.

The genesis of two mantle magmas series with distinct differences in LIL content can be attributed to differences in the source material. Classically, the production of magmas with different K_2O values in magmatic arcs has been attributed to different depths of melting (Nielson and Stoiber, 1975; Dickinson, 1975). We propose an alternative model to account for variably enriched parental magmas produced by partial melting in the mantle wedge above the subducting oceanic slab. Partial melting of metasomatized mantle

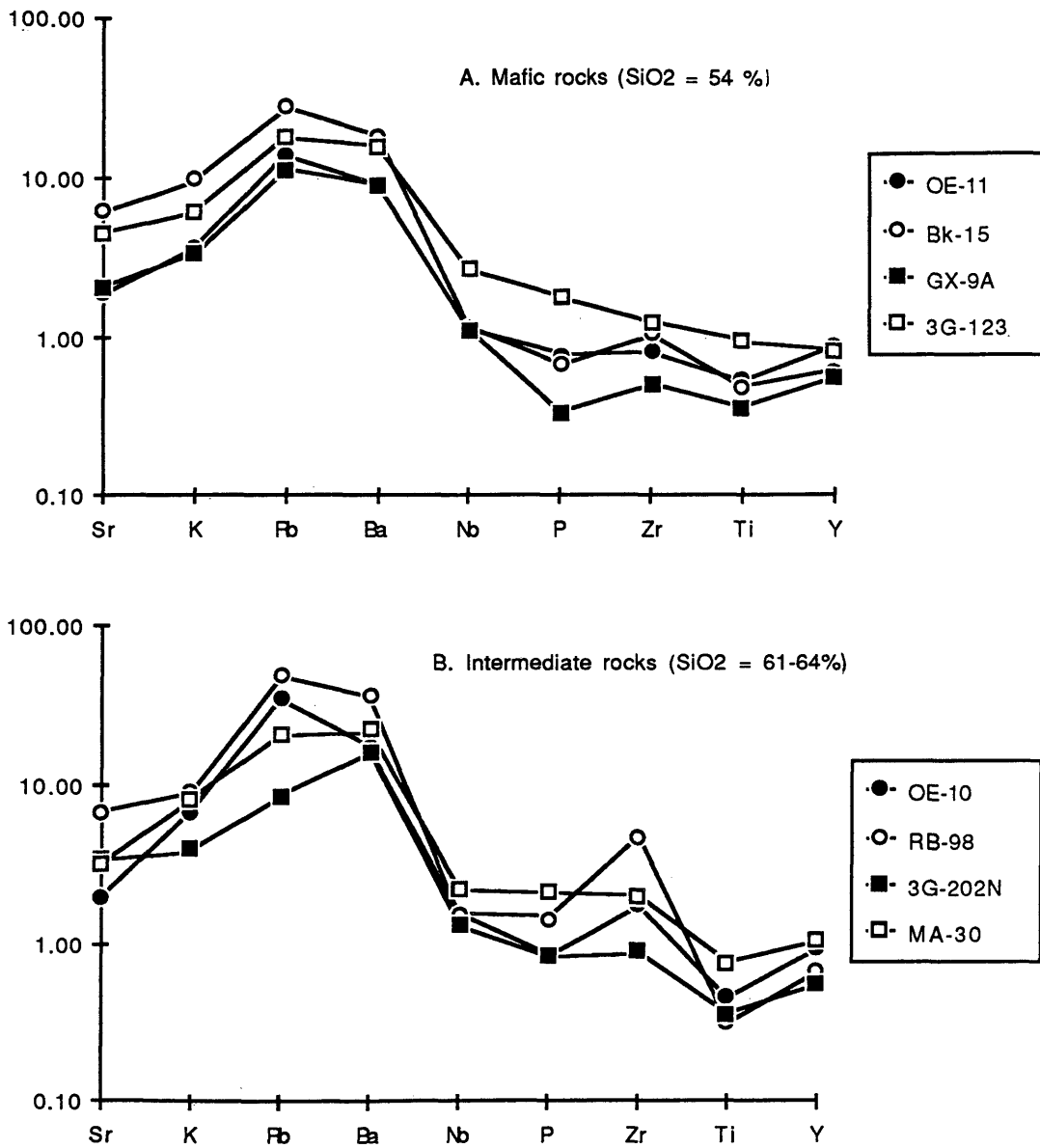


Fig. 1.18 Spider Diagrams Comparing CAT and CAG Series Rocks

Filled symbols = CAT series rocks. Open symbols = CAG series rocks. Circles from Baker area (48° S) and squares from Xualtegua area (53° S). Samples normalized to MORB (Pearce, 1983).

peridotite rich in LIL elements will produce a melt rich in the incompatible LIL elements. This melt rises and becomes the parental magma to the normal calc-alkaline CAG series rocks. The residue of this initial melting event will be depleted in LIL elements, and if it should undergo partial melting, it would produce a magma with lower LIL concentrations than the initial melt. We speculate that the density of the residue may be less than the surrounding mantle peridotite, which would allow the residue to rise and encounter higher temperatures ($>1400^{\circ}\text{C}$) in the center the mantle wedge beneath the magmatic arc (Tatsumi, 1983). Partial melting of the residue in this thermal high will then produce the parental magmas of the CAT series.

The variable petrologic and geochemical characteristics of the plutons of the Patagonian batholith probably reflect a complex scenario of partial melting, fractionation and contamination events during the evolution of the magmatic arc. Partial melting of early mafic and intermediate lithologies was most likely responsible for the genesis of the more silicic and evolved plutons of both the CAG and CAT rock series. For example, the large quantities of CAG biotite granite present in the eastern zone of the Baker area make an origin by fractional crystallization of mafic magma unlikely. Generation of an intermediate to silicic magma by partial melting of previously emplaced CAG series mafic or intermediate rocks, followed by crystal fractionation could produce the CAG biotite granites. The presence of micro-diorite inclusions as possible restite material in these granites supports this hypothesis. Plagioclase fractionation is suggested by the regular decrease in Sr with CaO (Fig. 19). The peraluminous nature of the CAG granites suggests that hornblende was present in the source as restite phase (Helz, 1976). Hornblende fractionation of metaluminous magmas can also produce weakly peraluminous lithologies (Zen, 1986; Cawthorn et al., 1976; Cawthorn and Brown, 1976), however, the lack of

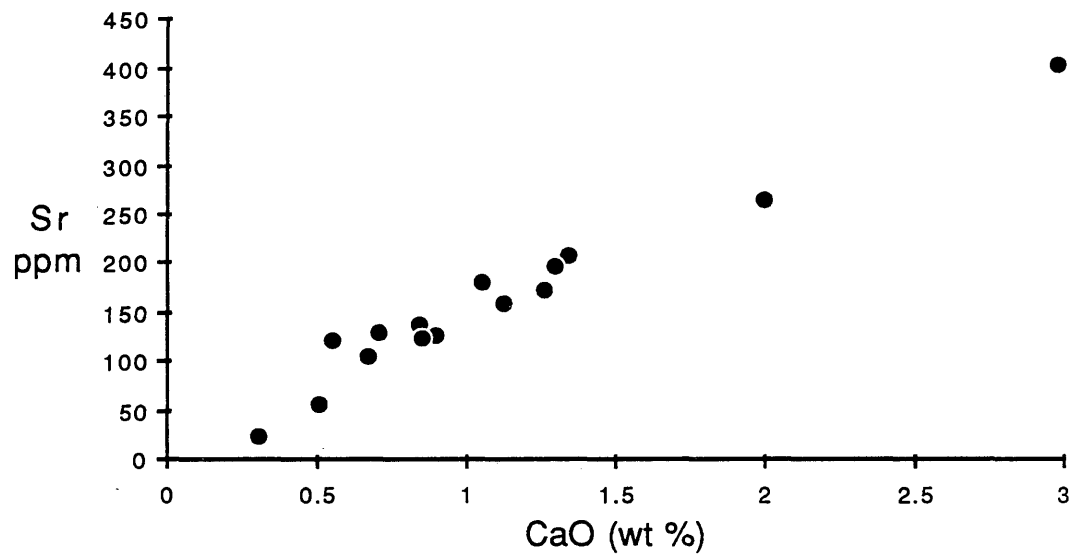


Fig. 1.19 CaO vs. Sr diagram for the 84 Ma CAG Biotite Granites.

Note the near linear decrease suggesting plagioclase fractionation.

hornblende in these granites makes this unlikely. The low Sr ratios preclude mixing of large amounts of a much older crustal component, although assimilation - fractional crystallization models (AFC) suggest that some contamination is feasible (see Chapter 2)

The age of the CAG biotite granites (84 Ma) lies within the apparent maximum magmatic activity (100-70 Ma) of the Patagonian batholith which also corresponds with a worldwide maximum in seafloor spreading rates (Larson and Pitman, 1972). Increase in spreading could result in an increased production of mafic mantle magmas that could intrude into the lower crust and promote partial melting of previously emplaced plutons. The heat required for such melting cannot be generated from a normal continental geothermal gradient, and thus, heat input from mantle sources is required (Clemens and Vielzeuf, 1987). This suggests that the evolution of a calc-alkaline batholithic complex is dependent on a complex multi-step process in which mantle derived material may evolve through several cycles of magma generation, fractional crystallization, and contamination within the crust to produce the plutons of the batholith.

The small population of strongly peraluminous ($AI > 1.1$) 2-mica granites present in the Baker area probably represent melts of continental crust, although Sr and Nd isotope data suggest a mantle-derived component is also present. The low Ti contents of these rocks are typical of crustal melts (Leeman and Hawkesworth, 1986). Mixing models suggest that 40-80 % crustal component is needed to explain the isotopic signature of these rocks (Weaver et al., in press). Miller (1985) has suggested that strongly peraluminous 2-mica granites are not necessarily solely the product of melting of a chemically mature sedimentary source, but rather, are dominantly derived from intermediate to felsic crustal sources which can include immature sedimentary rocks and metaluminous mafic and intermediate igneous rocks. Thus the magmas of the 2-mica granites in the Baker area may

be partial melts of the early contaminated plutons, and not necessarily partial melts of the accretionary prism basement complex. The ages (124 and 110 Ma) of these 2-mica granites, supports this theory, as the oldest contaminated plutons in the area has been dated at 150 Ma.

Summary and Conclusion

The Patagonian batholith of southern Chile is a typical example of a subduction related calc-alkaline batholith. The batholith at 48° S is composed of numerous plutons of varying lithologies, ranging from gabbro to granite. The ages of the plutons in this area range from 150 to 46 Ma. Two major rock series have been identified by lithologic and chemical characteristics. The first series is classified as calc-alkaline tonalitic (CAT) and is characterized by low K₂O and other LIL element concentrations and dominantly consists of tonalite and leucotonalite with little or no K-feldspar. The second series is classified as calc-alkaline granodioritic (CAG) and is characterized by higher K₂O and LIL element concentrations and consists of granite, granodiorite, and quartz monzodiorite with significant K-feldspar. We suggest that both rock series evolved from mafic parental magmas. The fundamental chemical differences of these two rock series suggest that two distinct parental magmas types were involved in the formation of the Patagonian batholith. Geochemical studies from other regions in the batholith confirm the existence of these two primary magma groups, and suggest that they were derived from different mantle sources or different depths in the mantle wedge beneath the magmatic arc. The more evolved granites and leucotonalites found in the batholith are likely partial melts of mafic and intermediate rocks of both magma series induced by a continuing magma flux from the mantle.

Sr and Nd isotope data suggest that mixing of mantle-derived material with an older crustal component derived from the basement accretionary prism complex, has played an important role in the petrologic and chemical evolution of the batholith at 48° S. The earliest plutons tend to be the most highly contaminated with a crustal component, and increasingly younger plutons show less contamination. This can be explained by an evolution of the basement material which resulted in it becoming less reactive due to dehydration and an increase in refractory material produced by partial melting. Mixing models (Weaver et al., in press; Nelson et al., 1987) support the suggestion that the early plutons of the Patagonian batholith were produced from mixtures of mantle-derived magmas and partial melts of the basement accretionary prism material.

In conclusion, the Patagonian batholith at 48° S is a product of a complex and variable set of magma sources and petrogenetic processes. As has been suggested for most calc-alkaline batholiths formed at convergent continental margins, the dominant components of the Patagonian batholith are of mantle origin. However, the processes which most affect the overall evolution of the batholith clearly have taken place in the crustal envelope in which it is hosted.

Chapter 2

**SR, ND, AND PB ISOTOPE VARIATIONS IN THE PATAGONIAN
BATHOLITH, 48° S LATITUDE, CHILE: IMPLICATIONS
FOR THE EVOLUTION OF CRUSTAL
CONTRIBUTIONS.**

Introduction

The study of major batholithic complexes formed by subduction-related magmatism at continental margins is important for understanding granitoid petrogenesis and the development of new continental crust. Previous isotopic studies (DePaolo, 1981a; McCulloch & Chappell, 1982) have suggested that such batholiths are mixtures of mantle-derived magmas with components derived from the continental crust. This paper presents Sr, Nd, and Pb isotope data from a suite of samples from the Patagonian batholith that suggests several types of mixing processes were involved in the petrogenesis of the plutons and that there was a progressive decrease in crustal involvement during evolution of the batholith.

The Patagonian batholith is one of the largest, yet least studied of the Mesozoic-Cenozoic circum-Pacific batholiths. Located in the Andes of southern Chile, the batholith forms a 1500 km long and 50-100 km wide curvilinear outcrop belt extending from approximately 41° S to 56° S. Much of the batholith is exposed in the rugged unpopulated fjord and canal region of southern Chile. A suite of samples was collected from sea level exposures along an east-west transect across the batholith at 48° S in a region we shall call the Baker area after the prominent west trending Canal Baker (Fig. 2.1).

Regional Geologic and Tectonic setting

The Patagonian batholith is situated along the active continental margin of southern South America where the Nazca and Antarctic plates are being subducted beneath the South America plate. Subduction in this region has probably been active semi-continuously since the Late Paleozoic (Dalziel, 1981; Forsythe, 1982). Paleozoic subduction produced a magmatic arc east of the Patagonian batholith. By mid-Jurassic

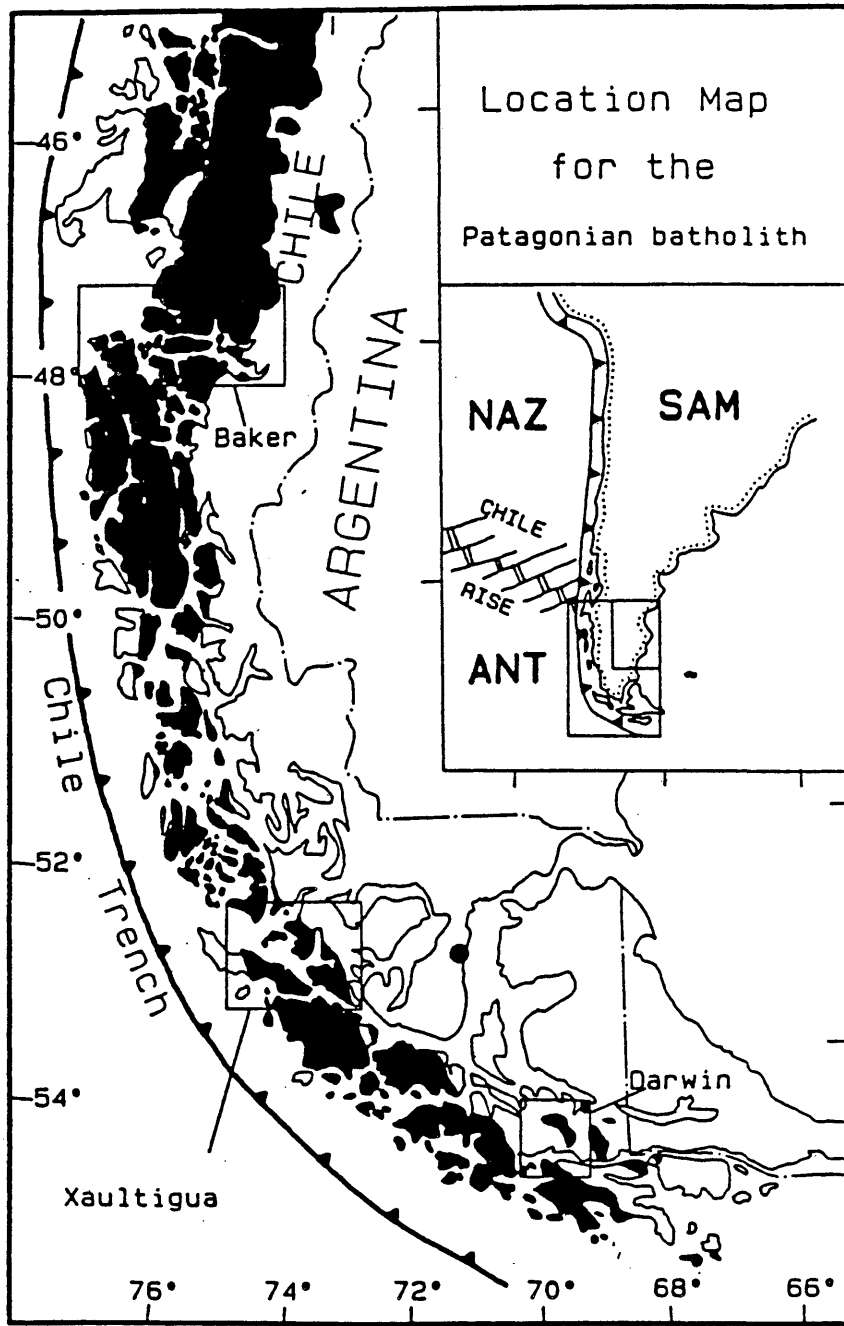


Fig. 2.1 Patagonian Batholith Location Map

time the locus of magmatism had moved west with intrusion of plutons into the Paleozoic fore-arc sequence and eruption of extension related bi-modal volcanics (Bruhn et al., 1978). The Early Cretaceous marked the formation the Rocas Verdes marginal basin and associated ophiolitic magmatism in the area presently south of 50° (Dalziel, 1981). Subsequent arc-continent collision during the Andean orogeny closed this marginal basin by mid-Cretaceous time with compressional tectonics continuing into the Tertiary (Nelson et al., 1980).

Patagonian batholith magmatism commenced in the Late Jurassic and continued until the Late Tertiary. Geochronological determinations (Halpern, 1973; Herve` et al., 1981; Bruce et al., 1986; Weaver et al., 1986) suggest that intrusive magmatism occurred semi-continually from about 166 Ma to 10 Ma.

Plutons in the batholith range in composition from noritic and hornblende gabbro to granodiorite and granite with biotite-hornblende tonalite making up the greatest percentage of the batholith. (Nelson et al., in press). Peraluminous garnet-bearing 2-mica granite and trondjhemites also are present in several areas.

The basement sequence into which much of the Patagonian batholith was intruded is an accretionary forearc complex of a Late Paleozoic magmatic arc to the east. Basement lithologies include: 1) a volcanoclastic flysch sequence of graywacke and shale, 2) radiolarian ribbon chert, 3) limestone, 4) mafic-ultramafic rocks containing high pressure mineral parageneses, 5) pillow basalt, and 6) quartz-veined phyllite (Mpodozis and Forsythe, 1983; Nelson et al., in press). These lithologic elements suggest that a volcanoclastic flysch sequence and a mixture of oceanic crustal material and allochthonous terranes were accreted to the margin prior to the Late Jurassic (Forsythe, 1982). Studies of this basement sequence at 46° S (Bartholomew and Tarney, 1984) suggest that it has been tectonically

mixed and represents a relatively homogeneous sequence in terms of its chemical and isotopic characteristics.

Patagonian Batholith at 48° S

Lithologies present in the Baker area include the typical range of rock types found throughout the batholith. Mafic lithologies include hornblende gabbros, noritic gabbro, and hornblende quartz diorite. Biotite-hornblende tonalite is common although the dominant lithologies in this area tend to be more siliceous and include biotite granite and granodiorite. The dominant lithology in the eastern section of the transect is biotite granite. Small stocks of garnet-bearing two-mica granite are present at the southeast margin of the area. With the exception of exposures along the major north-trending canal (Canal Meiser, 75° 45' Long.), none of the plutons are foliated. Plutons west of this disrupted zone locally contain euhedral magmatic epidote in association with hornblende and biotite suggesting crystallization at pressures of at least 6 kb (Zen and Hammarstrom, 1984).

Dating of biotite and hornblende separates using the $^{40}\text{Ar}/^{39}\text{Ar}$ method along with U-Pb zircon determinations and Rb-Sr mineral-WR isochrons suggest that magmatism occurred in the area from about 150 Ma to about 48 Ma (Weaver et al., 1986). The unidirectional migration of plutonism noted farther north in the Andes (Farrar et al., 1970) does not appear to have occurred in the Canal Baker area. The oldest dated sample (149 Ma-U/Pb, 146 Ma-Ar/Ar) is a granodiorite from the eastern margin of the batholith (Fig. 2.2). The next oldest dated sample (130 Ma-Ar/Ar) is a tonalite from the far western margin of the batholith. Younger dated samples (125 - 48Ma) are randomly scattered in between (Fig. 2.2). The biotite granite, which makes up much of the eastern area of the batholith, has been dated at 83 - 84 Ma ($^{40}\text{Ar}/^{39}\text{Ar}$ on biotite). Although the youngest

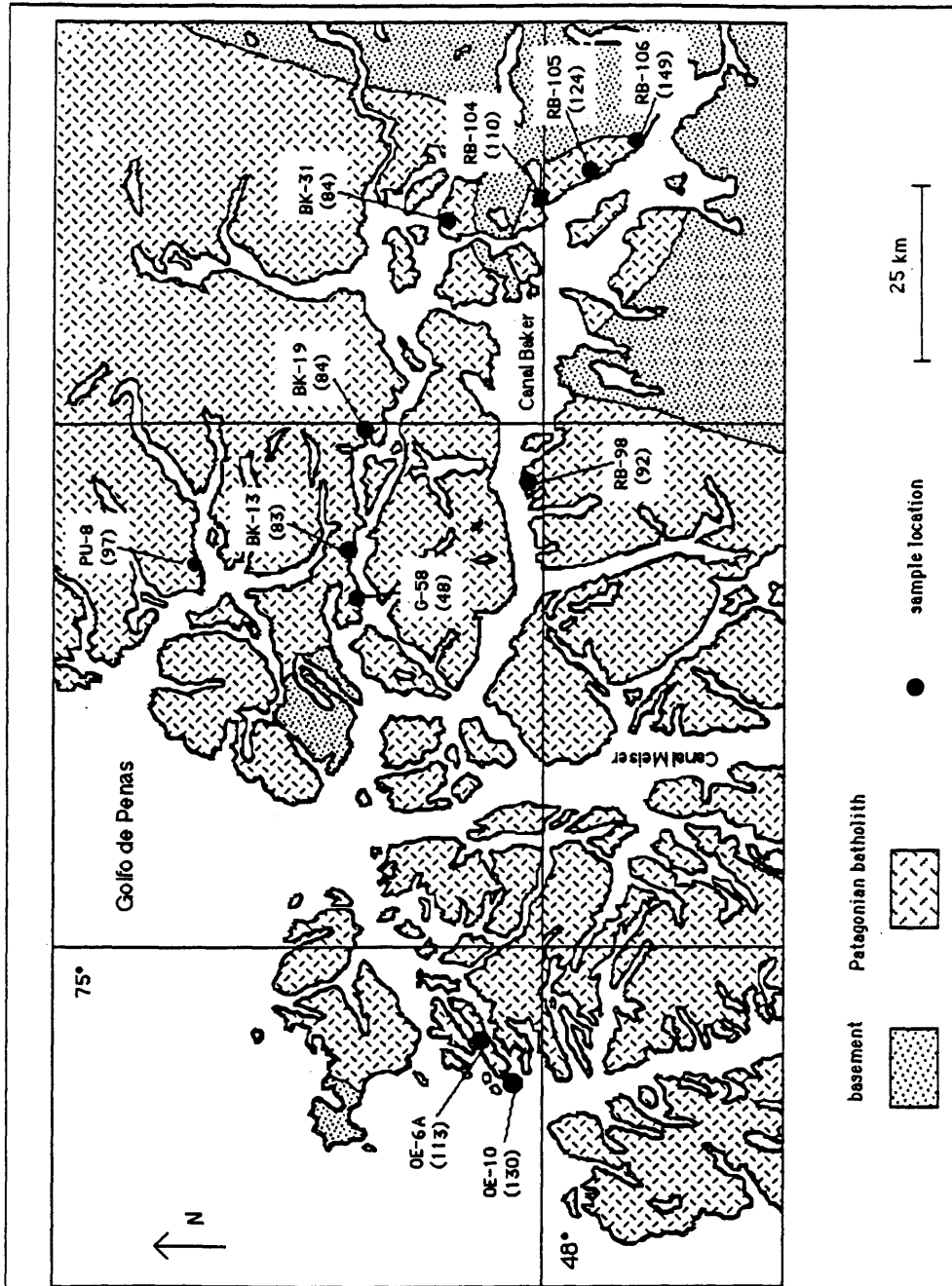


Fig. 2.2 Map of Baker Area Isotope Sample Locations

The ages of the samples in millions of years are shown in parentheses.

dated sample (48 Ma- $^{40}\text{Ar}/^{39}\text{Ar}$) is a hornblende gabbro, field relations suggest that most mafic rocks intruded during early phases of batholith development.

Most of the plutons have compositions that plot in the calc-alkaline field on an AFM diagram, although they are calcic according to Peacock's (1931) classification with an alkali-lime index of 64 (Weaver, unpublished data). The calc-alkaline rocks may be subdivided into a low K and normal K series based on the classification of Lameyre and Bowden (1982). The majority of analyzed samples with SiO_2 contents $> 60\%$ are peraluminous with molecular $\text{Al}_2\text{O}_3/\text{CaO}+\text{Na}_2\text{O}+\text{K}_2\text{O} > 1$, and have corundum in their norm.

Isotope Data

Analytical Methods

Sr, Nd and Pb isotope analyses were carried out in the isotope geochemistry lab at Lamont-Doherty Geological Observatory. Mass spectrometry procedures and Sr and Nd separation techniques utilized at Lamont are described by Zindler et al. (1984). Samples (1-2 Kg) were crushed and ground and ~ 50 g splits were tumbled and mixed for 48 hours to ensure homogeneity. Splits (100 mg) were spiked and dissolved in teflon bombs to ensure the dissolution of all refractory accessory minerals that might concentrate the REE. Blank levels were insignificant for all samples. All $^{87}\text{Sr}/^{86}\text{Sr}$ measurements were normalized to $^{86}\text{Sr}/^{88}\text{Sr} = 0.11940$ and are relative to $^{87}\text{Sr}/^{86}\text{Sr} = .70800$ for the Eimer and Amend SrCO_3 standard. Nd was analyzed as Nd^+ with measurements normalized to $^{146}\text{Nd}/^{144}\text{Nd} = 0.72190$.

Preliminary Pb isotope analyses were carried out on carefully separated and leached K-feldspar separates from several samples analyzed for Sr and Nd isotopes. The separates (1-1.5 g) were leached according to the method of Ludwig and Silver (1977), decomposed,

and Pb separated in ion exchange columns using HBr elution. The samples were electroplated to remove impurities and loaded on zone-refined Rh filaments with H₃PO₄ and silica gel. Measured ratios were standardized to NBS 981. The reported ratios are an average of two runs and have precisions of 0.1%.

Sr and Nd Isotope Variations

All isotopic and trace element data are presented in Tables 2.1- 2.2. The initial ⁸⁷Sr/⁸⁶Sr and ¹⁴³Nd/¹⁴⁴Nd ratios are also presented in ε notation (DePaolo and Wasserburgh, 1976). Reference values are the same as used by Carlson et al., 1981.

Initial Sr and Nd isotope data for rocks from the Patagonian batholith and basement are plotted on an ε Sr - ε Nd diagram in Fig. 2.3. The data for the batholith define a curvilinear array ranging from ε Nd = 6.7 to -6.0 and ε Sr = -14.0 to 39.8. Data for gabbros and diorites plot within, or to the right of, the mantle array, suggesting that an isotopically-depleted primary mantle-derived component was involved in development of the more mafic rocks. Three of these mafic units plot to the right of the mantle array (Zindler et al., 1979), suggesting the presence of an oceanic crust component that had been altered by reaction with seawater (Hawkesworth , 1982). Most of the data for intermediate to silicic granitoids plot in the negative ε Nd and positive ε Sr field suggesting a component of continental crustal in their isotopic composition. Such a component could be represented by the field of three basement samples plotted in Fig. 2 3. The two basement symbols plotted represent the spread of isotopic values calculated at 150 Ma and 80 Ma.

The 2-mica granites have quite different ε Sr values, one positive and the other negative. This disparity most likely reflects large uncertainties in their calculated ⁸⁷Sr/⁸⁶Sr initial ratios caused by their high Rb/Sr ratios coupled with age uncertainties.

Table 2.1

Sr and Nd Isotope Data

Sample #	lithology	Rb (ppm)	Sr (ppm)	Sm (ppm)	Nd (ppm)	$^{87}\text{Rb}/^{86}\text{Sr}$	$^{147}\text{Sm}/^{144}\text{Nd}$	$^{87}\text{Sr}/^{86}\text{Sr}$ ^	$^{143}\text{Nd}/^{144}\text{Nd}$ ^
BK-46	noritic gabbro	4*	894	3.3	14.22	0.0032	0.1404	0.70465 ± 4	0.51273 ± 1
G-58	gabbro	14*	675	4.02	14.3	0.06	0.1694	0.70374 ± 3	0.51296 ± 3
RB-115B	gabbro	1*	438	1.2	3.9	0.0066	0.1904	0.70509 ± 2	0.51277 ± 5
PU-8	diorite	24*	441	0.85	24.18	0.1573	0.1210	0.70483 ± 3	0.51282 ± 3
OE-10	tonalite	68*	217	2.41	11.53	0.9072	0.1258	0.70910 ± 3	0.51227 ± 2
RB-98	tonalite	96	818	4.3	25.88	0.3381	0.1001	0.70570 ± 4	0.51255 ± 2
BK-13	granodiorite	56	404	2.46	15.4	0.3996	0.0962	0.70512 ± 3	0.51256 ± 2
OE-6A	granodiorite	91	248	2.89	10.24	1.0668	0.1702	0.70712 ± 3	0.51253 ± 2
OE-7	granodiorite	92	262	nd	nd	1.01885	nd	0.70692 ± 4	nd
RB-106	granodiorite	113*	259	7.1	37.78	1.174	0.1132	0.70935 ± 3	0.51240 ± 2
BK-19	granite	130	155	4.67	29.65	2.4404	0.0949	0.70728 ± 4	0.51265 ± 2
BK-21	granite	127	128	nd	nd	2.8825	nd	0.70767 ± 4	nd
BK-22	granite	116	127	nd	nd	2.6431	nd	0.70730 ± 4	nd
BK-31	granite	80	112	7.31	46.52	2.0591	0.0947	0.70662 ± 3	0.51267 ± 5
OE-5	granite	115	255	nd	nd	1.193	nd	0.70729 ± 2	nd
RB-104	2 mica granite	240*	131	6.55	33.07	5.2963	0.1194	0.71259 ± 3	0.51251 ± 2
RB-105	2 mica granite	210	68	12.58	55.48	8.9824	0.1367	0.72305 ± 3	0.51241 ± 1
BK-39	meta-pellite	36	77	12.51	50.58	1.3569	0.1491	0.71690 ± 10	0.51237 ± 6
GP-5**	meta-arenite	116	169	5.47	26.99	2.0509	0.1233	0.71547 ± 3	0.51225 ± 2
4G-185**	meta-arenite	100	157	3.57	22.15	1.9342	0.0981	0.71649 ± 7	0.51222 ± 2

* - denotes analysis by XRF, all other concentrations by isotope dilution

** - data from Kaeding, 1986

^ - error is two standard deviations on the mean and refers to the last significant figures

nd - not determined

Table 2.2

Sr and Nd Initial Ratios

Sample #	Age ^a (Ma)	⁸⁷ Sr/ ⁸⁶ Sr (T)	¹⁴³ Nd/ ¹⁴⁴ Nd (T)	ϵ Sr* (T)	ϵ Nd* (T)
G-58	48.2 ± 2.2	0.7036	0.51279	-14.0	6.7
BK-13	82.2 ± 2.2	0.7047	0.51250	-0.4	-0.6
BK-19	83.0 ± 0.6	0.7044	0.51260	-4.4	1.3
BK-31	84.0 ± 1	0.7042	0.51262	-7.3	1.7
RB-98	92 ± 6 ^b	0.7053	0.51248	8.4	-0.7
PU-8	95.8 ± 2.4	0.7046	0.51274	-0.6	4.4
RB-104	110 ± 3 ^b	0.7043	0.51242	-4.8	-1.6
OE-6A	113.1 ± 0.7 ^c	0.7053	0.51240	10.5	-1.7
RB-105	124 ± 27 ^b	0.7072	0.51230	36.8	-3.6
OE-10	128.5 ± 1.2	0.7074	0.51217	39.8	-6.0
RB-106	149.3 ± 0.8 ^c	0.7068	0.51229	32.0	-3.2
BK-46	(150) ^d	0.7046	0.51259	0.6	2.8
RB-115B	(150) ^d	0.7051	0.51259	6.9	2.7
BK-39	(150) ^e	0.7140	0.51223	133	-4.3
GP-5	(150) ^e	0.7111	0.51213	92.4	-6.3
4G-185	(150) ^e	0.7124	0.51212	110.2	-6.4

a) age determination by ⁴⁰Ar/³⁹Ar (biotite, hornblende)

b) age determination by Rb-Sr whole rock-mineral isochrons

c) age determination by U/Pb zircons (concordant)

d) age estimated from field relations

e) initial ratios of basement calculated at 150 Ma

*) typical uncertainties ~ ± 1 ϵ unit for Nd and ± 5 ϵ units for Sr

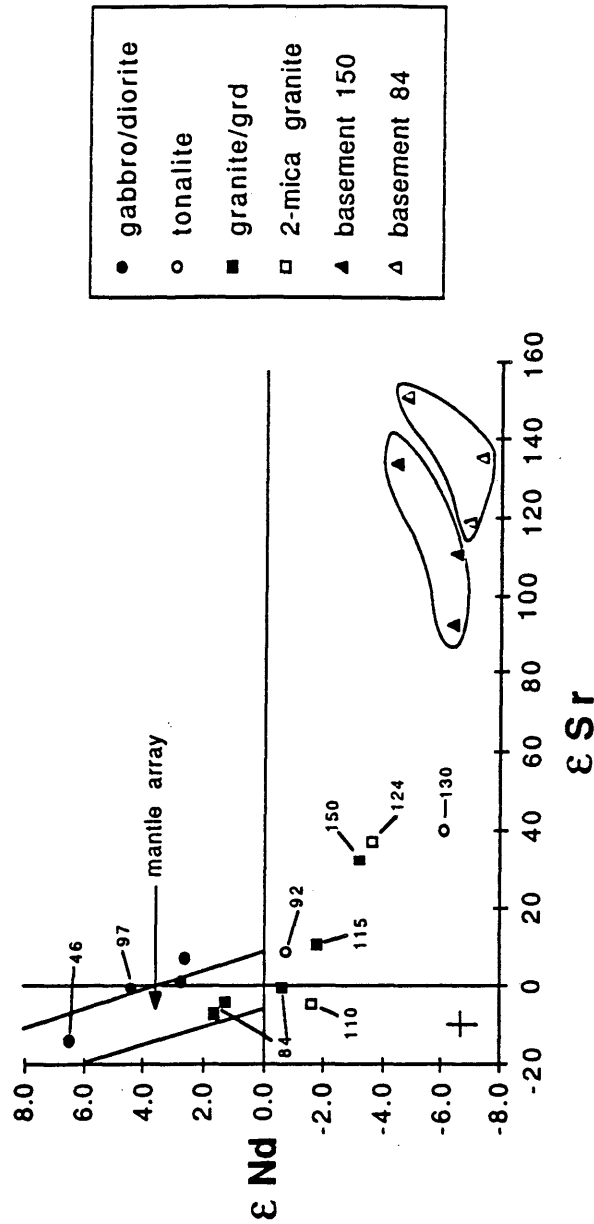


Fig. 2.3 ϵ_{Sr} vs. ϵ_{Nd} diagram

Samples are plotted by lithology and the age in millions of years is indicated. Grd = granodiorite. Values for three basement samples have been plotted for 150 Ma and 84 Ma. The mantle array (Zindler et al., 1979) is also plotted. Typical uncertainties are shown in the lower left.

Isotopic Variations in Time

A distinct correlation exists between the age and the isotopic composition of the Patagonian batholith plutons analyzed from the Baker area. This correlation is best illustrated in a plot of $^{87}\text{Sr}/^{86}\text{Sr}$ initial ratio against age (Fig. 2.4). A trend of decreasing $^{87}\text{Sr}/^{86}\text{Sr}$ initial ratio with decreasing age is clearly evident. The age-isotope composition trends are also evident in Fig. 2.3. Note that the intermediate and silicic samples which plot with the highest ϵ Sr (32-39.8) and lowest ϵ Nd (-3.2 to -6.0) are also the oldest dated units (125-150 Ma). The next youngest group of samples (90-115 Ma) have more depleted compositions and the youngest intermediate and silicic samples (84-85 Ma) plot on the mantle array. A similar relationship is also present in the mafic units that have been dated. The most depleted sample (ϵ Sr = -14, ϵ Nd = 6.7) is a hornblende gabbro (G-58) which has been dated at 46 Ma. The oldest dated mafic unit (97 Ma) is a hornblende quartz diorite and its isotopic composition is more enriched (ϵ Sr = -0.6, ϵ Nd = 4.4) than the young hornblende gabbro. Two additional mafic samples, which have not been isotopically dated but show field relations that suggest intrusion during the early phases of batholith development, are the most enriched with ϵ Sr = 0.6-6.9 and ϵ Nd = 2.7-2.8 (calculated at 150 Ma). One of these samples (BK-46) is a noritic gabbro, a lithology that can be formed by assimilation of aluminous sediments by a mafic magma (Bowen, 1928). The decrease in enriched component in progressively younger plutons suggests that the amount of continental crustal component, or the degree of crustal contamination of magmas, has decreased through time during evolution of the Patagonian batholith in the Baker area.

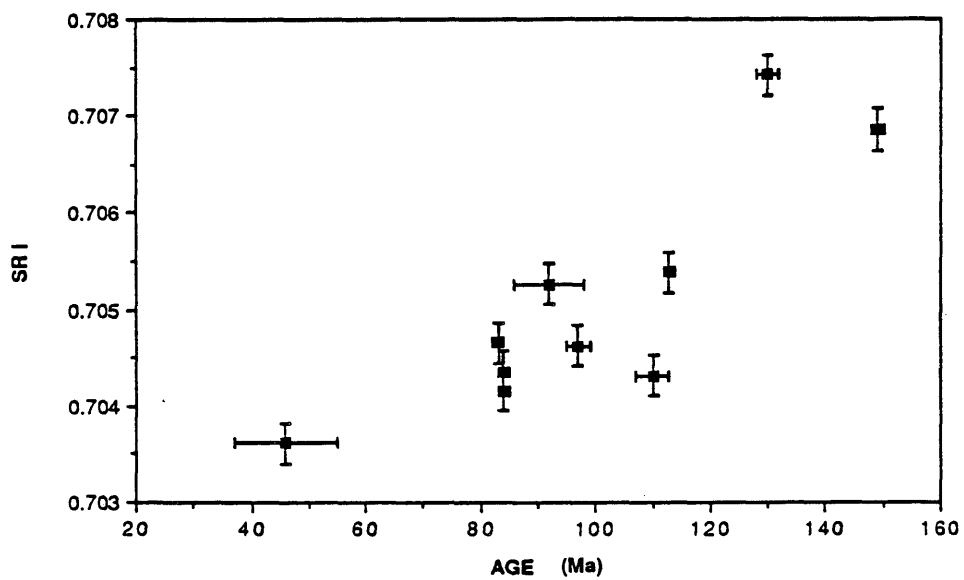


Fig. 2.4 Sri vs. Age Diagram

Sample RB-105, a 2-mica granite, is not plotted because of its large age uncertainty. Uncertainties on the Sri are $\pm 0.05\%$

Mixing Between Mantle and Crustal Components

The suggestion that the plutons of Patagonian batholith in the Baker area formed by interaction between mantle-derived magmas and some crust-derived component can be evaluated by calculating mixing curves between potential end-member compositions. For such calculations to be meaningful, accurate determination of the isotopic and elemental composition of each end-member composition is necessary. An initial choice for the crustal component would logically be the basement material into which the plutons were intruded. The assumption that the lithologies exposed today correspond directly with the basement materials that interacted with the intrusions may or may not be valid, but it at least provides a starting point for a mixing analysis. The isotopic and elemental compositions of the basement component used in the mixing models were calculated as the average of three basement samples. The two primary mantle components used in the mixing calculations were chosen from mafic samples with the highest positive ϵ Nd values which represent the most LREE depleted source material. In the following discussion, various mixing scenarios between a depleted mantle component represented by two mafic samples (G-58 and PU-8) and the assumed basement component will illustrate the difficulty in quantitatively evaluating specific mixing or contamination events.

Fig. 2.5 illustrates bulk mixing curves calculated between the average basement composition calculated at 150 Ma and 84 Ma, and the two most isotopically-depleted mafic samples. The two basement ages were used because they span the major period of plutonism in the Baker area. The position of the curves does not change appreciably with the change in basement age. The only differences are small changes in mixing ratio along the curves. The majority of data plot in reasonable agreement with the two bulk mixing

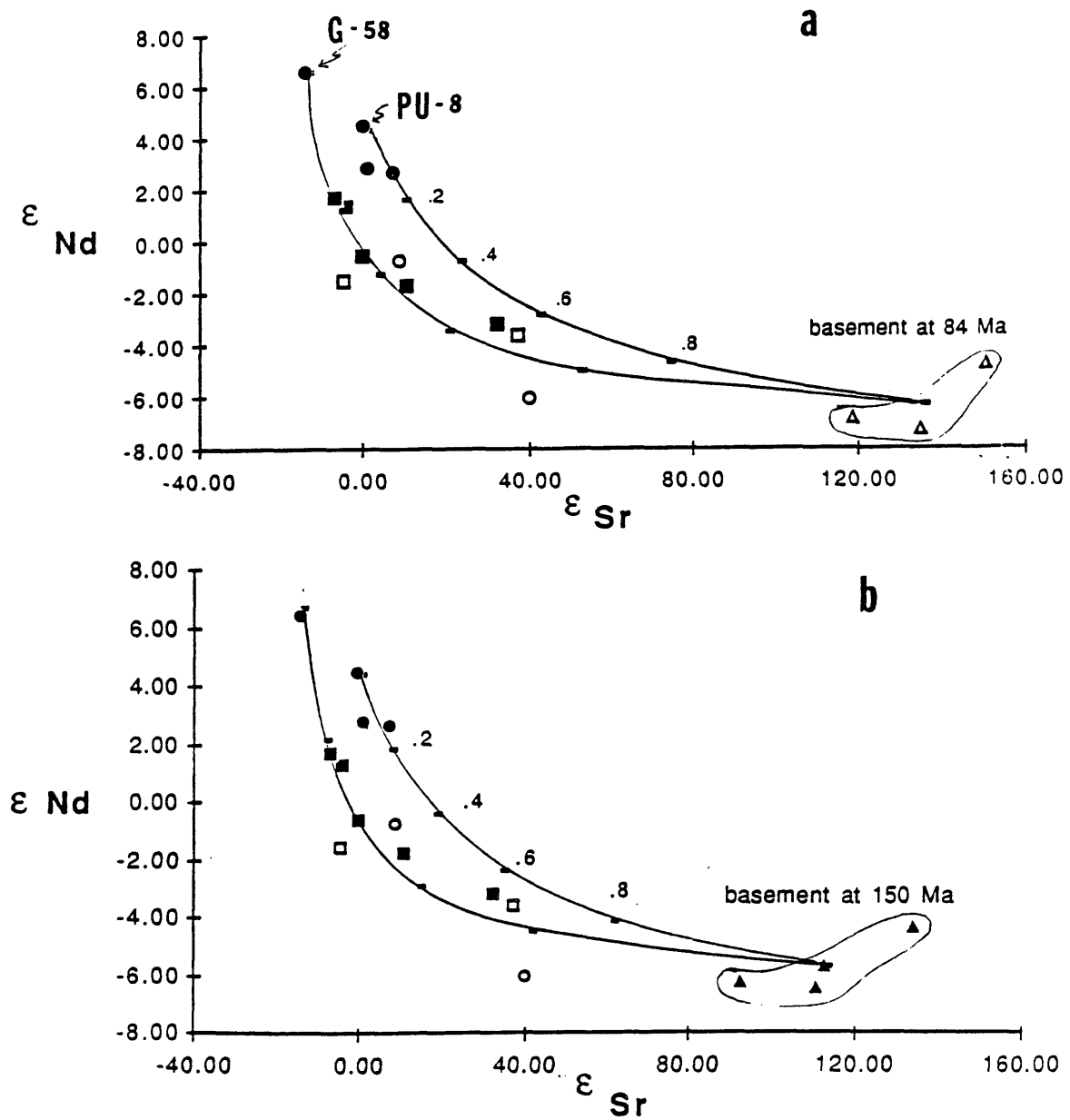


Fig. 2.5 Bulk Mixing Models

Simple bulk mixing curves plotted between the two most primitive mafic samples (G-58 and PU-8) and the average basement. Horizontal ticks on the curves indicate the mass fraction of basement needed for that particular isotope signature. The mass fraction values are labelled on the upper curve. Sample symbols as in Fig.2.3. a) mixing with 84Ma basement, b) mixing with 150 Ma basement

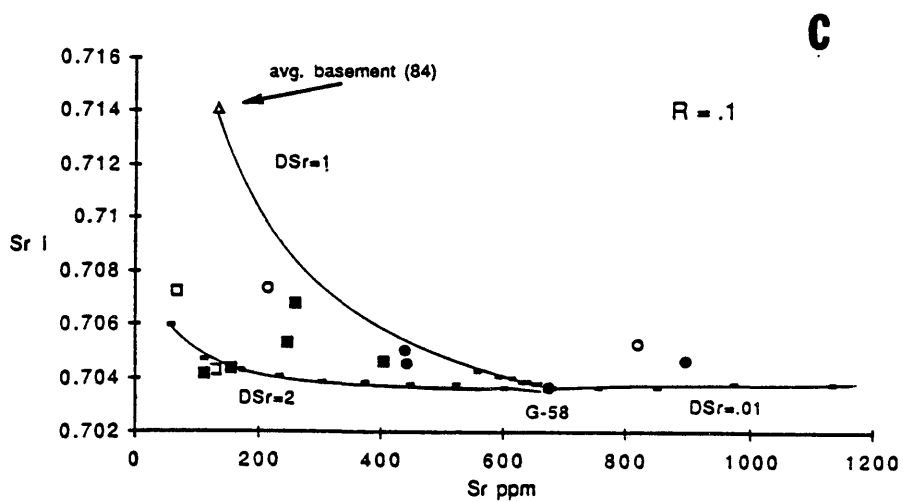
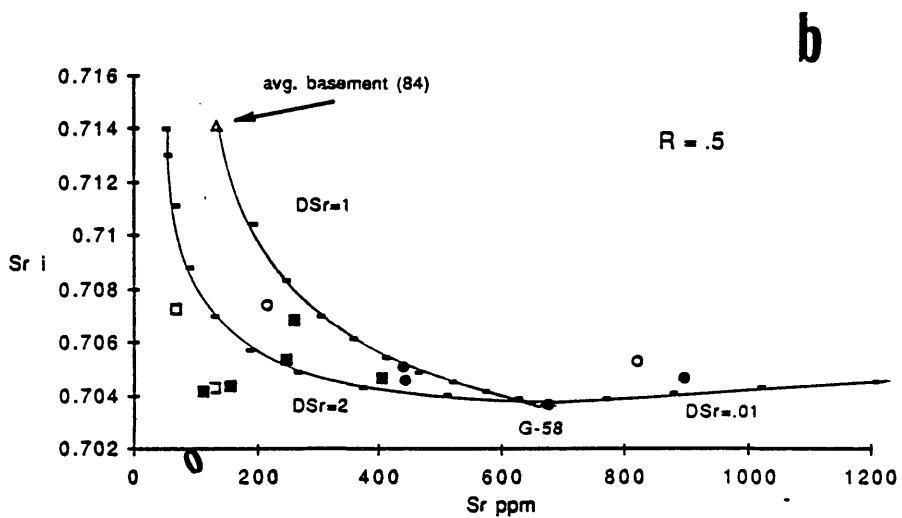
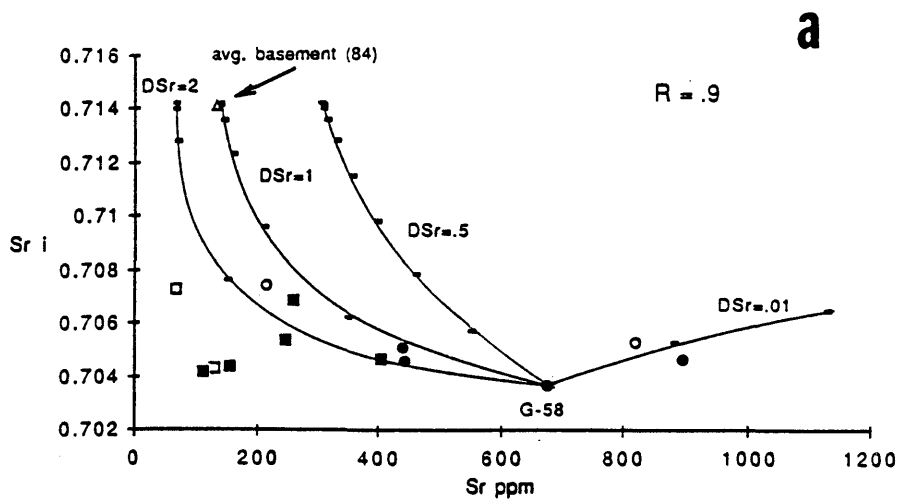
and an isotopically depleted component. Some scatter is expected given the analytical uncertainties of the data points and probable variation in the actual end-member compositions. However, care must be taken in analyzing such graphical representations of mixing models, particularly when realistic geological constraints are taken into consideration. In its most simple concept, bulk mixing is defined as a complete physical and chemical blending of two components. In order for this to realistically occur in the geologic environment both components must be magmas. Assimilation of a solid by a magma does not usually occur without the concomitant crystallization of mineral phases. This combined process of assimilation with fractional crystallization (AFC) results in mixtures which do not lie on simple bulk mixing curves. This suggests that if the simple bulk mixing curves illustrated in Fig. 2.5 are relevant, the Sr and Nd concentrations and isotopic ratios of the basement component must represent a total melt of the basement material. Clearly this is difficult to justify given unrealistic thermal requirements and the relatively cool nature of the young accretionary prism complex. With this discussion in mind, the more geologically feasible processes of AFC and mixing with a partial melt of the basement material are modeled in the following two sections.

Assimilation with Fractional Crystallization (AFC). A proper evaluation of contamination of a magma by assimilation of a solid must acknowledge that fractional crystallization is coupled with assimilation (AFC), because the heat required for assimilation is provided by the latent heat of crystallization of the magma. The amount of assimilation will depend on the temperature contrast between the magma and the wall rock, the fusion temperature of the wallrock and magma, and the rate of magma ascent. Under ideal conditions, where the wallrocks have been heated to high temperatures prior to assimilation the maximum amount

of assimilation possible would correspond to a magma to contaminant ratio of 1:1 (Taylor, 1980). Fig. 2.6 illustrates Patagonian batholith Sr isotope and concentration data plotted with a series of Sr AFC curves calculated using the methods of DePaolo (1981b). The curves were calculated for a range of D^{Sr} (bulk distribution coefficient) values using hornblende gabbro G-58 as the initial magma composition and the average basement at 84 Ma as the contaminant. Three values of r (0.9, 0.5, & 0.1), which is the ratio of the mass rate of assimilation to the mass rate of crystal fractionation in the magma, were used for the calculations (Fig. 2.6). A value of $r = 1$ would be approximately equal to a 1:1 mix of magma to contaminant (DePaolo 1981b). The curves plotted for $D^{Sr} = 1$ are also equivalent to simple two component mixing. Note that the most radiogenic samples show the best agreement with curves calculated with r values of 0.9 or 0.5, which is consistent with the suggestion of substantial basement assimilation. The majority of the Patagonian batholith samples plot in proximity to the AFC curves for $D^{Sr} = 1$ or greater suggesting that plagioclase fractionation occurred if AFC processes produced the isotopic and elemental compositions of the samples. Two samples that plot near the $D^{Sr} = .01$ curve suggest plagioclase was not fractionating during assimilation, or perhaps the parental magmas had very high Sr contents. The 84 Ma granites show excellent agreement with the AFC curve calculated for $r = .1$ and $D^{Sr} = 2$ (Fig 2.6c). A granodiorite (BK-13) of the same suite plots on the $r = .9$ and $D^{Sr} = 2$ curve (Fig. 2.6a), which may suggest that the rate of assimilation decreased with the thermal and chemical evolution of that magma series.

Fig. 2.6 Sr Isotope Assimilation-Fractional Crystallization (AFC) Models

Calculated AFC curves (Depaolo, 1981b) using G-58 as the parental magma assimilating an average 84 Ma basement. Three curves are plotted for different bulk distribution coefficients of Sr ($DSr = 2$, $DSr = 1$, and $DSr = 0.01$). The horizontal ticks on the curves represent the fraction of liquid (f) remaining in 0.1 intervals, starting with 0.9 closest to the parental magma. The three different plots represent AFC calculations using different r values (a: $r = 0.9$, b: $r = 0.5$, c: $r = 0.1$). The r value is the ratio of the mass rate of assimilation to the mass rate of crystal fractionation in the magma. Sample symbols as in Fig. 2.3



Mixing Between a Mantle Magma and a Partial Melt of Basement. Another way of explaining the isotopic patterns of the most contaminated plutons could be by mixing between a mantle-derived magma and a partial melt of the basement material. Influx of hot mafic mantle magmas with liquidus temperatures at $\sim 1100^\circ\text{C}$ into a sequence of accretionary wedge sediments that were potentially water saturated could have produced substantial crustal melting. Accurate quantitative trace element modeling of such partial melting is difficult primarily because of uncertainties in the modal mineralogy of the material being melted and the lack of well constrained distribution coefficients for minerals such as muscovite and other aluminosilicates which may be important modal constituents. Nevertheless, available K_d values (Philpotts & Schnetzler, 1970; Nagasawa & Schnetzler, 1971) were used to calculate the Sr and Nd contents of a likely crustal melt. The average basement material was assumed to be a 1:3 composite of shale to graywacke, with the average modal mineralogy of shale consisting of 20% quartz, 10% plagioclase, 5% K-feldspar, and 65% mica (clay minerals) and the average modal mineralogy of graywacke consisting of 37% quartz, 15% plagioclase, 15% K-feldspar, and 33% mica (Wedepohl, 1967; Pettijohn et al., 1973). These mineralogies are consistent with petrographic data for the Patagonian batholith basement material. The bulk partition coefficients calculated for these compositions are $D^{\text{Sr}} = \sim 1$ and $D^{\text{Nd}} = \sim 0.1$. A 30% melt of the basement, using the equilibrium melting equation of Shaw (1970), leads to a Sr concentration of 140 ppm and a Nd concentration of 89 ppm in the melt. Fig. 2.7 illustrates the resulting mixing curves for mixing this 30% partial melt with melts represented by the two depleted mafic samples. Note again the proximity of most of the data to the two curves. Changes in the degree of partial melting of the basement will change the Sr/Nd ratio of the melt which will change, in turn, the degree of curvature of the mixing curves (DePaolo & Wasserburg,

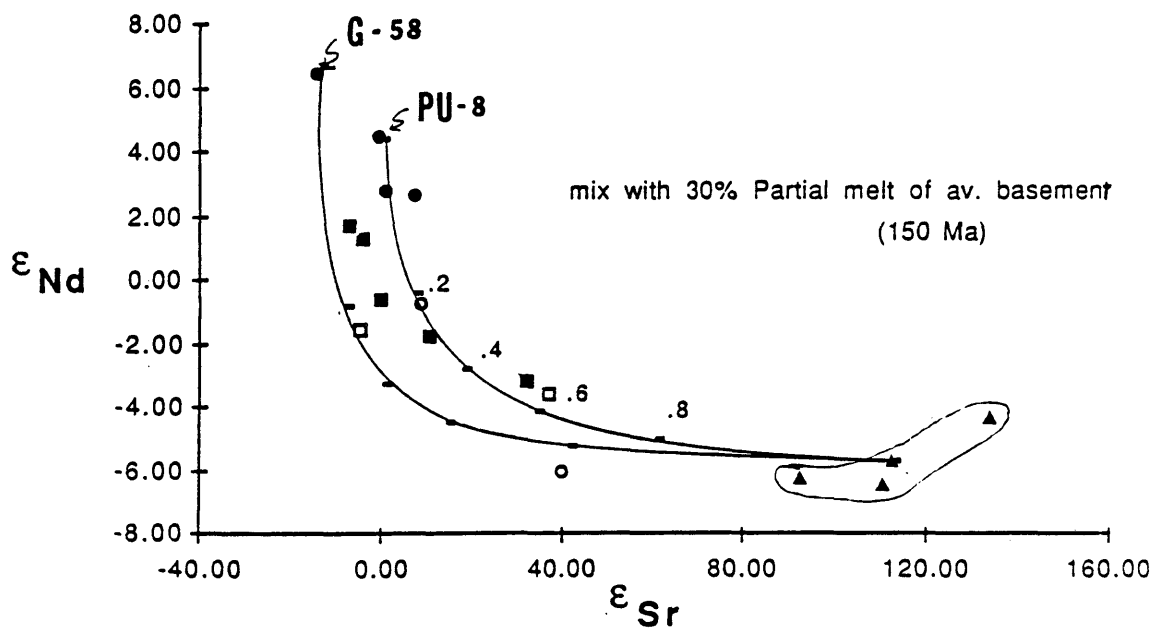


Fig. 2.7 Partial Melt Mixing Model

Mixing model with curves calculated for the two most primitive samples (G-58 and PU-8) mixed with a 30% partial melt of the average basement at 150 Ma (see text). Sample symbols as in Fig. 2.3

1976). Higher percents of melts will have higher Sr/Nd ratios resulting in a decrease in the curvature of the mixing line.

The mass balance constraints of this mixing model suggest that the oldest most contaminated plutons require magmas that are 20-40% mantle melt and 60-80% crustal melt. The presence of a large crustal component in these rocks is supported by their lithology and bulk chemistry. These early plutons tend to be peraluminous and RB-105 and RB-104 are garnet bearing 2-mica granites, a lithology consistent with crustal melting.

Pb Isotope Data

Pb isotope data for five K-feldspar separates from plutons in the study area are tabulated in Table 2.3:

Pb isotope data

sample #	$^{206}\text{Pb}/^{204}\text{Pb}$	$^{207}\text{Pb}/^{204}\text{Pb}$	$^{208}\text{Pb}/^{204}\text{Pb}$
BK-22	18.54	15.58	38.41
BK-13	18.51	15.56	38.33
RB-98	18.49	15.57	38.39
RB-104	18.51	15.59	38.45
RB-105	18.56	15.63	38.55

The variation in the isotopic ratios is small. With the exception of RB-105, a peraluminous 2-mica granite with a high $^{207}\text{Pb}/^{204}\text{Pb}$ ratio, the remaining Pb isotope values are all within the analytical error of 0.1% of each other in $^{206}\text{Pb}/^{204}\text{Pb}$, $^{207}\text{Pb}/^{204}\text{Pb}$, and

$^{208}\text{Pb}/^{204}\text{Pb}$. All samples except, again, RB-105, give Stacey & Kramer (1975) (S&K) model ages that are much younger than the age of the plutons, indicating that a simple single stage model relative to the S & K growth curve does not apply to these samples. Fig. 2.8 is a $^{207}\text{Pb}/^{204}\text{Pb}$ vs. $^{206}\text{Pb}/^{204}\text{Pb}$ plot of the data with Doe & Zartman's (1979) growth curve for the orogene superimposed on the plot. The Patagonian batholith data form a steeply inclined array that defines a regression line with a slope of 0.83. This corresponds to a $^{207}\text{Pb}^*/^{206}\text{Pb}^*$ age of approximately 3.9 Ga, an age which has no geologic meaning in the context of the geologic setting of the Patagonian batholith. The apparent linear array of data may therefore be explained in terms of a mixing model instead of an isochronous relationship. The Patagonian batholith data plot within the field for arc magmas and lie close to the growth curve defined by the orogene in the plumbotectonics model of Doe & Zartman (1979). Data in this field can be explained qualitatively as mixtures produced during orogenic (subduction related) magmatism between radiogenic upper crustal material with high $^{207}\text{Pb}/^{204}\text{Pb}$ and $^{206}\text{Pb}/^{204}\text{Pb}$ ratios and mantle material with low $^{207}\text{Pb}/^{204}\text{Pb}$ and $^{206}\text{Pb}/^{204}\text{Pb}$ ratios. The sample with the highest $^{207}\text{Pb}/^{204}\text{Pb}$ ratio is RB-105, a peraluminous 2-mica granite that required a large component of older continental crustal material during its genesis. The other Patagonian batholith Pb data points have lower $^{207}\text{Pb}/^{204}\text{Pb}$ suggesting a greater amount of mantle-derived component with less radiogenic Pb. The other 2-mica granite RB-104 has a lower $^{207}\text{Pb}/^{204}\text{Pb}$ value, plotting with the less radiogenic samples. Either less crustal component is present in this sample or possibly a less radiogenic lower crustal material was involved in its genesis. The Sr and Nd data for RB-104 plot in the lower left quadrant of the $\epsilon\text{Sr}-\epsilon\text{Nd}$ diagram (Fig. 2.3) with $\epsilon\text{Sr}_i = -4.8$ and $\epsilon\text{Nd}_i = -1.6$, supporting the suggestion of lower crustal involvement. However the high RB/Sr ratio of this sample

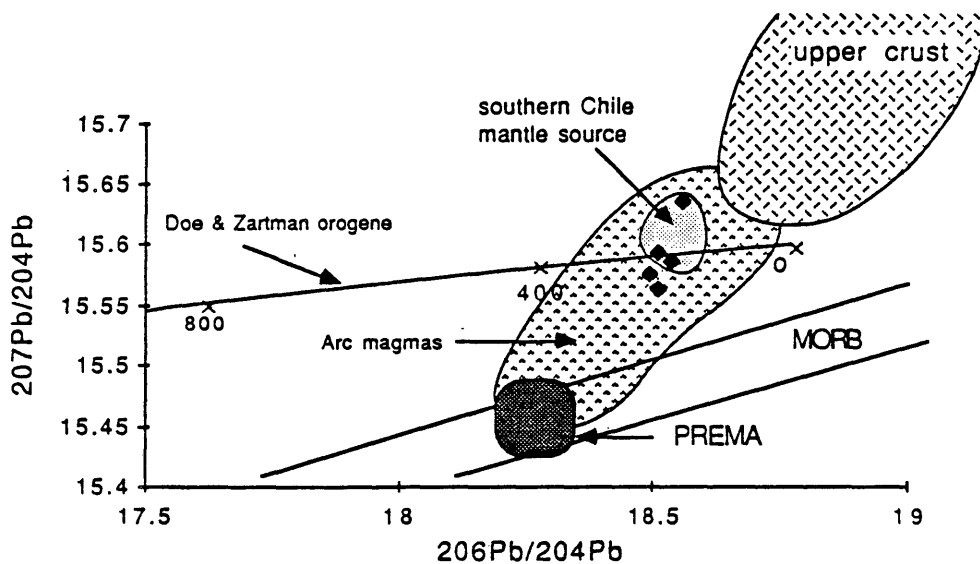


Fig. 2.8 $^{207}\text{Pb}/^{204}\text{Pb}$ vs. $^{206}\text{Pb}/^{204}\text{Pb}$ Diagram

Plotted are the Patagonian batholith data and the fields of components which could have mixed to produce the Pb isotope signatures of the batholith. Batholith data are plotted as diamonds and the orogene evolution curve of Doe and Zartman (1979) is plotted as x's at 400 my intervals. Field of PREMA from Zindler and Hart (1986). Fields of upper crust, arc magmas, and MORB from Doe and Zartman (1979). Field of southern Chile mantle source from Tilton (1979).

prevents a precise calculation of its initial $^{87}\text{Sr}/^{86}\text{Sr}$ ratio, thus its location in negative ϵ Sr space is not conclusive of the presence of a lower crustal component.

Fig. 2.8 also illustrates fields for potential components that may have mixed to produce the Patagonian batholith Pb isotope compositions. Mixing on this diagram is indicated by linear relationships. The field labeled Southern Chile mantle source was defined by Tilton (1979) to represent the "enriched" Pb isotope composition of the mantle beneath southern South America. The data that define this field are from several northern Chilean porphyry copper deposits that have Sr i ratios of .7040, also consistent with derivation from an enriched mantle. However, Sr and Nd isotope data from ultramafic xenoliths from Patagonian alkali basalts suggest that the southern South America subcontinental mantle lithosphere has a depleted nature in the Patagonian region (Stern et al., 1985). Tilton's field of Pb isotope values can also be explained as mixes between a mantle component shown as PREMA (Prevalent mantle component) and a component represented by the upper crust. PREMA has been defined by Zindler and Hart (1986) as a hypothetical overall average mantle component found dominantly beneath continental crust. It is defined by Sr and Nd isotope values of the least radiogenic continental basalts which typically are not as depleted as MORB basalts. Mixtures of PREMA derived melts with continental crust could generate the Pb isotope values of the Patagonian batholith.

Discussion

The decrease in the radiogenic character of the isotopic signatures of the Patagonian batholith plutons through time is interpreted to reflect an overall decrease in the amount of contamination by basement components. A similar trend of decreasing Sr initial ratio with decreasing age was noted in the Mesozoic and Tertiary plutonism of Graham Land in the

Antarctic Peninsula (Pankhurst, 1982). This trend has been ascribed to early magma generation in the lower crust or enriched sub-crustal lithosphere evolving to deeper sub-crustal mantle magma generation as a result of steepening of the subduction angle or an increase in magma production (Pankhurst, 1982). The Antarctic Peninsula is geologically analogous to southern South America and a continuous subduction-related magmatic arc may have existed from the Andes to the Antarctic Peninsula during the Mesozoic and early Tertiary (Dalziel & Elliot, 1973). Thus it is not surprising that similar trends exist in the two regions, and a similar explanation may apply to both regions.

We present two additional models that focus on the changing contribution of crustal components to mantle derived magmas emplaced into thin immature continental crust typical of accretionary prism complexes. The first model requires that early mantle-derived magmas intruded the base of the accretionary wedge complex and encountered sedimentary rocks or low grade meta-sedimentary rocks that contained substantial amounts of pore fluid. The influx of hot mafic magmas initiated partial melting of these water rich sedimentary sequences and the resultant anatectic melts mixed with the mafic magmas to produce contaminated hybrid magmas. As time progressed, the basement material lost its fluid phase through upward migration brought on by progressive metamorphism (Walther & Orville, 1982). This "drying out" raised the temperature required for partial melting of the basement material. Also, the basement became more refractory as early formed melts were extracted from it. Partial melting of the remaining basement became less likely and contamination by magma mixing decreased. Further crustal contamination could only occur by minor assimilation concurrent with fractional crystallization of the intruding magma (AFC).

A second explanation for decreasing contamination with time in the Patagonian batholith is purely physical. Younger intrusions may have been isolated from contact with the basement by the older intrusions that occupied space once filled by basement. Reduced contact with basement material lowered the potential for crustal contamination. In reality, processes from both models may have contributed to the progressive decrease in crustal contamination seen in the Patagonian batholith.

Summary

Sr, Nd, and Pb isotope data for the Patagonian batholith complex suggest that it is composed of mantle-derived magmas mixed that with components derived from the intruded crust. This conclusion is in agreement with isotopic studies of other major subduction-related batholiths (DePaolo, 1981a; McCulloch & Chappell, 1982). Mass balance constraints limit the amount of realistically possible assimilated solid crust and thus suggest that the early highly contaminated plutons were produced by mixtures of mantle magmas and crustal melts. Calculated mixing models support this hypothesis. Younger less contaminated plutons show characteristics consistent with AFC processes. In reality, some combination of AFC, and magma mixing most likely contributed to the genesis and evolution of the batholith. Although such mixing scenarios may not meet rigorous mass balance chemical constraints, the pattern of the Patagonian batholith isotope data does suggest that mixing between material from isotopically distinct sources did occur, and their contribution to arc magmatism changed progressively through time.

The apparent decrease in contamination through time as suggested by the isotope data can be explained by an evolution of the basement accretionary wedge complex that dried out and became more refractory with time. This evolution resulted in decreased potential

for chemical interaction between magmas and basement material, and thus less contaminated plutons are produced. Physical isolation of younger plutons from basement by older plutons occupying space previously filled by basement could also have contributed to the decrease in crustal component present in the younger plutons of the Patagonian batholith.

REFERENCES CITED

- Alexander, E. C. ; Mickelson, C. M.; and Lanphere, M. A. 1978. MMhb-1, a new ^{40}Ar - ^{39}Ar dating standard. in Short papers of the fourth international conference, geochronology, cosmochronology, isotope geology, R. Zartman, ed., U. S. Geol. Survey Open File Report # 78-701, p. 6-8
- Barker, F.; Arth, J. G.; and Hudson, T. 1981. Tonalites in crustal evolution. Phil. Trans. R. Soc. Lond., A301, p. 293-303
- Bartholomew, D. S. ; and Tarney, J. 1984. Geochemical characteristics of magmatism in the southern Andes(45-46°). in Andean Magmatism - Chemical and Isotopic Constraints, R.S. Harmon and B.A. Barrieco, eds., Shiva, London , p.220-230
- Bateman, P. C.; and Nockelberg, W. J. 1978. Solidification of the Mount Givens Granodiorite, Sierra Nevada, California. J. Geology, 86, p. 563-579
- Bateman, P. C. 1983. A summary of critical relations in the central part of the Sierra Nevada batholith, California. in Circum-Pacific plutonic terranes, J. A. Roddick, ed, Geological Society of America Memoir 159, p. 241- 254
- Bowden, P.; Batchelor, R. A.; Chappell, B. W.; Didier, J.; and Lameyre, J. 1984. Petrological, geochemical and source criteria for the classification of granitic rocks: a discussion. Phys. Earth Planet. Int., 35, p. 1-11
- Bowen, N.L. 1928. The Evolution of the Igneous Rocks. (Dover, New York, 1956) reprint of 1928 ed. 332 pp.
- Brown, G. C. 1982. Calc-alkaline intrusive rocks: their diversity, evolution, and relation to volcanic arcs. in Andesites, R. S. Thorpe, ed., Wiley, London, p. 437-461
- Bruce, R.; Nelson, E.; Weaver, S.; and Lux, D. 1986. Geochronology and petrology of the Patagonian batholith: implications for magma genesis and arc evolution. EOS, 67 #16, p.413
- Bruce, R.; Nelson, E.P.; and Weaver, S.G. in press. Effects of Synchronous uplift and intrusion during magmatic arc construction. Tectonophysics
- Bruhn, R. L.; Stern; C. R.; and De Witt, M. J. 1978. Field and geochemical data bearing on the development of a Mesozoic volcano-tectonic rift zone and back-arc basin in southernmost South America. Earth Planet. Sci. Lett., 41, p. 32-46
- Carlson, R. W.; Lugmair, G. W.; and MacDougall, J. D. 1981. Columbia river volcanism: The question of mantle heterogeneity or crustal contamination. Geochimica Cosmochim Acta, 45, p. 2483-2499

- Cawthorn, R. G.; and Brown, P. A. 1976. A model for the formation and crystallization of corundum- normative calc-alkaline magmas through amphibole fractionation. J. Geology, 141, p. 467-476
- Dalrymple, G. B.; and Lanphere, M. A. 1971. $^{40}\text{Ar}/^{39}\text{Ar}$ technique of K-Ar of dating, a comparison with conventional isotope dilution technique. EOS, 52 #4, p.367
- Dalrymple, G. B.; Alexander, E. C.; Lanphere, M. A.; and Kraker, G. P. 1981. Irradiation of samples for $^{40}\text{Ar}/^{39}\text{Ar}$ dating using the Geological Survey TRIGA reactor. U. S. Geol. Survey, Prof. Paper # 1176, 55pp.
- Darwin, C. 1846. Geological Notes on South America, London
- DePaolo, D. J ;and Wasserburg, G. J. 1976. Nd isotopic variations and petrogenetic models. Geophys. Res. Lett., 3, p. 249-252
- DePaolo, D. J. 1981a. A neodymium and strontium isotopic study of Mesozoic calc-alkaline granitic batholiths of the Sierra Nevada and Peninsular Ranges, California. J.Geophys. Res., 86, p. 10470-10488
- DePaolo, D. J. 1981b. Trace element and isotopic effects of combined wall rock assimilation and fractional crystallization. Earth Plant. Sci. Lett., 53, p. 189-202
- Dalziel, I. W. D. 1981. Back-arc extension in the southern Andes: a review and critical reappraisal. Phil. Trans. R. Soc. London , A300, p. 319-35
- Dalziel, I. W. D ; and Elliot, D. H. 1973. The Scotia Arc and Antarctic margin, in The Ocean Basins and Margins, A. E. M. Nairn and F. G. Stehli, eds., Plenum Pub. Corp., New York, p. 171-246
- Dickenson, W. R. 1975. Potash-depth (K-h) relations in continental margin and intra-oceanic magmatic arcs. Geology, 3, p. 53-56
- Doe, B. ; and Zartman, R. 1979. Plumbotectonics I, the Phanerozoic, in Geochemistry of Hydrothermal Ore Deposits, 2nd Ed., H.L. Barnes, ed., Wiley Interscience, p. 22-70
- Farrar, E.; Clark, A. H.; Haynes, S. J.; Quirt, G. S.; Conn, H. ;and Zentilli, M. 1970. K-Ar evidence for post-Paleozoic migration of granitic foci in the Andes of northern Chile. Earth Plant. Sci. Lett., 10, p. 60-66
- Forsythe, R. 1982. The late Paleozoic to early Mesozoic evolution of southern South America: a plate tectonic interpretation. Jour. Geol. Soc. London, 139, p. 671-82
- Goldich, S. S. 1984. Determination of ferrous iron in silicate rocks. Chemical Geology, 42, p 343-347

- Gromet, L. P.; and Silver, L. T. 1987. REE variations across the Peninsular range batholith : implications for batholithic petrogenesis and crustal growth in magmatic arcs. J. Petrology, 28, p. 122-136
- Halpern, M. 1973. Regional geochronology of Chile south of 50° latitude, Geol. Soc. Am. Bull., 84, p 2407-22
- Halpern, M.; and Fuenzalida, R. 1978. Rubidium-strontium geochronology of a transect of the Chilean Andes between latitudes 45° and 46°. Earth Planet. Sci. Lett., 41, p.60-66.
- Hart, S. R.; and Brooks, C. 1977. The geochemistry and evolution of the Early Precambrian mantle. Contrib. Mineral. Petrol., 61, p. 109
- Hawkesworth, C. J. 1982. Isotope characteristics of magmas erupted along destructive plate margins, in Andesites, R. S. Thorpe , ed, Wiley, London p. 549-571
- Helz, R. T. 1976. Phase relations of basalts in their melting ranges at PH₂₀= 5 kb Part II melt compositions. J. Petrology, 17, p. 139-193
- Herve, F. 1976. Estudio geologica del la falla Linguine-Reloncavi en el area de Liguine: antecedentes de un movimiento 1976 transcurrente: Santiago, Chile. Acta I Congresso Geologico Chileno, 1, p. B39-B56
- Herve, F.; Nelson, E.; Kawashita, K.; and Suarez, M. 1981. New isotopic ages and the timing of orogenic events in the Cordillera Darwin, southernmost Chilean Andes. Earth Planetary Sci. Lett., 55, p. 257-65
- Hower, J. 1959. Matrix corrections in the x-ray spectrographic trace element analysis of rocks and minerals. American Mineralogist, 44, p. 19-32
- Irvine, T. N.; and Baragar, W. R. B. 1971. A guide to the chemical classification of the common igneous rocks. Can. Jour. Earth Sci., 8, p. 523-548
- Kaeding, M. E. 1986. Geochemistry of near-trench magmatic rocks from the Taitao Peninsula, southern Chile: implications for ridge subduction, unpublished M.S. thesis, Rutgers University, 80 pp
- Krank, E. H. 1932. Geological investigation in the Cordillera of Tierra del Fuego. Acta Geog. Helsingfors, 4, 231p
- Lameyre, J.; and Bowden, P. 1982. Plutonic rock type series: discrimination of various granitoid series and related rocks. Jour. of Volcanology and Geothermal Res., 14, p. 169-186
- Larson, R. L.; and Pitman, W. C. 1972. World-wide correlation of Mesozoic magnetic anomalies, and its implications. Geol Soc. Am. Bull., 83, p. 3645-3662

- Ludwig, K.; and Silver, L.T. 1977. Lead isotope inhomogeneity in Precambrian igneous feldspars. Geochim Cosmochim. Acta, 41, p. 1457-1472
- McCulloch, M. T.; and Chappel, B. W. 1982. Nd isotopic characteristics of S- and I- type granites. Earth Planetary Sci. Lett., 58, p. 51-64
- Miller, C. F. 1985. Are strongly peraluminous magmas derived from pelitic sedimentary sources. J. Geology, 93, p. 673-689
- Mpodozis, C.; and Forsythe, R. 1983. Stratigraphy and geochemistry of accreted fragments of the ancestral Pacific floor in southern South America. Paleogeography, Paleoclimatology, Paleoecology, 41, p. 103-24
- Nagasawa, H.; and Schnetzler, C. C. 1971. Partitioning of rare earth, alkalic, and alkaline earth elements between phenocrysts and acidic igneous magma. Geochim. Cosmochim. Acta, 35, p. 953
- Nelson, E. P.; Dalziel, I.; and Milnes, A. G. 1980. Structural geology of the Cordillera Darwin-collisional style orogenesis in the southernmost Chilean Andes. Ecologae Geol. Helv., 73, p. 27-51
- Nelson, E. P.; Bruce, R.; Elthon, D.; Kammer, D.; and Weaver, S. in press. Regional lithological variations in the Patagonian batholith, J. of South American Geology
- Nielson, D. R.; and Stoiber, R. E. 1975. Relationship of potassium content in andesitic lavas and depth to the seismic zone. J. Geophys. Res., 78, p. 6887-6892
- Pankhurst, R. J. 1982. Rb-Sr geochronology of Graham Land, Antarctica. Jour. Geol. Soc. London, 139, p. 701-711
- Peacock, M. A. 1931. Classification of igneous rock series. J. Geol., 39, 65-67
- Pettijohn, F. J.; Potter, P. E.; and Siever, R. 1973. Sand and Sandstone, Springer Verlag, New York, 618 pp
- Pitcher, W. S. 1978. The anatomy of a batholith. Jour. Geol. Soc. London, 135, p. 157-182
- Pitcher, W. S.; Atherton M. P.; Cobbing, E. J.; and Beckinsdale, R. D. 1986. Magmatism at a Plate Edge: The Peruvian Andes, Blackie, Wiley, London, 328 pp.
- Philpotts, J. A.; and Schnetzler, C. C. 1970. Phenocryst-matrix partition coefficients for K, Rb, Sr and Ba, with applications to anorthosite and basalt genesis. Geochim. Cosmochim. Acta, 34, p. 307
- Quensel, P. 1910. Beitrag zur Geologie der patagonischen Cordillera. Geologische Rundschau, I, p. 297-302

- Richard P.; Shimuzu, N.; and Allegre, C. J. 1976. $^{143}\text{Nd}/^{144}\text{Nd}$, a natural tracer: an application to oceanic basalts. Earth Planetary Sci. Lett., 31, p. 269
- Shand, S. J. 1927. The Eruptive Rocks, Wiley, New York
- Shaw, D. M. 1970. Trace element fractionation during anatexis. Geochim Cosmochim. Acta, 34, p. 237-243
- Stacey, J. S.; and Kramer, J. D. 1975. Approximation of terrestrial lead isotope evolution by a two stage model. Earth Planetary Sci. Lett., 26, p. 207-221
- Steiger, R. H.; and Jaeger, E. 1977. Subcommittee on geochronology, convention on the use of decay constants in geo-cosmochronology. Earth Planetary Sci. Lett., 36 #3, p.359-362
- Stern, C.; and Stroup, J. B. 1982. The petrochemistry of the Patagonian batholith, Ultima esperanza, Chile. in Antarctic Geoscience, C. Craddock, ed., Univerity of Wisconsin Press, Madison, p. 135-142
- Stern, C.; Futa, K.; Saul, S.; and Skewes, M. 1985. Evolution of the subcontinental mantle lithosphere below southernmost South America. Comunicaciones, # 35, p. 227-231
- Streckeisen, A. L. 1974. Classification and nomenclature of plutonic rocks. Geologische Rundschau, 63, p. 773-786
- Suarez, M. 1978. Notas geochimicas preliminares del batolito Patigonico al sur de Tierra del Fuego, Chile. Revista Geologica de Chile, 4, p. 15-33
- Tatsumi, Y. 1983. Generation of arc basalt magmas and thermal structure of the mantle wedge in subduction zones. J. Geophys. Res., 88, p. 5815-5825
- Taylor, H. P. 1980. The effects of assimilation of country rocks by magmas on $^{18}\text{O}/^{16}\text{O}$ and $^{87}\text{Sr}/^{86}\text{Sr}$ systematics in igneous rocks. Earth Planetary Sci. Lett., 47, p. 243-254
- Tilton, G. R. 1979. Isotopic studies of Cenozoic Andean calc-alkaline rocks. Carnegie Year Book, p. 298-304
- Walther, J. V.; and Orville, P. M. 1982. Volatile production and transport in regional metamorphism. Contrib. Mineral. Petrol., 79, p. 252-257
- Weaver, S. G.; Nelson, E. P.; Bruce, R.; Brueckner, H. K.; and Zindler, A. 1986. Sr and Nd isotope systematics of the Patagonian batholith, 48° S, Chile. EOS, 67 #16, p. 13

- Wedepohl, K. H. 1971. Environmental influences on the chemical deposition of clays. Phys. Chem. Earth, 8, p. 305
- White, A. J. R.; and Chappell, B. W. 1977. Ultrametamorphism and granitoid genesis. Tectonophysics, 43, p. 7-22
- Wyllie, P. J. 1983. Experimental and thermal constraints on the deep-seated parentage of some granitoid magmas in subduction zones. in Migmatites, Melting, and Metamorphism, M. P Atherton and C. D. Gribble, eds., Shiva, London, p. 37-51
- Wyllie, P. J. 1984. Sources of granitoid magmas at convergent plate boundaries. Phys. Earth Planet. Int., 35, p. 12-18
- Zen, E.; and Hammarstrom J. 1984. Magmatic epidote and its petrologic significance. Geology, 12, p. 515-518
- Zen, E. 1986. Aluminum enrichment in silicate melts by fractional crystallization: some mineralogic and petrographic constraints. J. Petrology, 27 # 5, p. 1095-1118
- Zindler, A.; and Hart, S. 1986. Chemical geodynamics. Ann Rev. Earth Planet. Sci., 14, p. 493-571
- Zindler, A.; Staudigel, H.; and Batiza, R. 1984. Isotopic and trace element variations in young pacific seamounts: implications for the scale of mantle heterogeneity. Earth Planetary Sci. Lett, 70, p. 175-195
- Zindler, A.; Hart, S.; Frey, F.; and Jakobsson, S. P. 1979. Nd and Sr isotope ratios and rare earth element abundances in Reykjanes Peninsula basalts: evidence for mantle heterogeneity beneath Iceland. Earth Planetary Sci. Lett., 45, p. 249-262

APPENDICES

Appendix A: SAMPLES AND LOCATIONS

Table A-1 Patagonian Batholith Sample Locations and Descriptions

map # ^a	sample #	lithology	rock series
1	OE-11	quartz diorite	CAT
2	OE-10	tonalite	CAT
3	OE-8	tonalite	CAT
4	OE-7	granodiorite	CAG
5	OE-6	2-mica granite	2-mica granite
	OE-6A	granodiorite	CAG
6	OE-5	granite	CAG
	OE-5A	granodiorite	CAG
7	OE-4	tonalite	CAT
8	OE-3	gabbro	CAT
9	OE-2	quartz diorite	CAT
10	RB-117	granodiorite	CAG
11	RB-116	leuco-tonalite	CAT
12	RB-115B	gabbro	CAT
13	BK-48	tonalite	CAT
	BK-48A	noritic gabbro	CAT
14	BK-47	noritic gabbro	CAT
15	BK-46	noritic gabbro	CAT
16	BK-45	quartz-monzodiorite	CAT
17	BK-42	granite	CAG
	BK-42A	granodiorite	CAG
18	BK-5A	diorite (dike)	CAT
	BK-5B	tonalite	CAT
19	BK-6B	tonalite	CAT
20	G-58	gabbro	CAT
21	G-59	tonalite	CAT
22	BK-7	granite	CAG
23	BK-8	granite	CAG
24	BK-10	granodiorite	CAG
25	BK-11	tonalite	CAT
26	BK-13	granodiorite	CAG
27	BK-14B	tonalite	CAT
28	BK-15	quartz diorite	CAG
29	BK-16	quartz diorite	CAT
30	BK-18	granite	CAG
31	BK-19	granite	CAG
32	BK-20	granite	CAG
33	BK-21	granite	CAG
34	BK-22	granite	CAG
35	G-69	granite	CAG

(continued)

Table A-1 (continued)

map # ^a	sample #	lithology	rock series
36	BK-23	granite	CAG
37	BK-25	granite	CAG
38	BK-26	granite	CAG
39	BK-27	granite	CAG
40	BK-29	granite	CAG
41	BK-31	granite	CAG
42	BK-33	granite	CAG
43	BK-34	granite	CAG
44	BK-35	granite	CAG
45	BK-26	granite	CAG
46	RB-80	granodiorite	CAG
47	RB-82	granodiorite	CAG
48	RB-83	granite	CAG
49	RB-84	granite	CAG
50	RB-85	granite	CAG
51	RB-86	granite	CAG
52	RB-106	granodiorite	CAG
53	RB-105	2-mica granite	2-mica granite
54	RB-104	2-mica granite	2-mica granite
55	RB-103	gabbro	CAG
56	RB-96	granodiorite	CAG
57	RB-101	granodiorite	CAG
58	RB-98	tonalite	CAG
59	RB-97	granodiorite	CAG
60	4G-111A	quartz diorite	CAG
61	4G-110	granodiorite	CAG
62	4G-106	granodiorite	CAG
63	4G-104	2-mica granite	2-mica granite
64	PU-6	quartz diorite	CAT
65	PU-8	quartz diorite	CAT
66	PU-9	gabbro	CAG
67	PU-10A	granite	CAG
	PU-10B	tonalite	CAT
68	PU-11	tonalite	CAT

^a see plate A-1

Appendix B: PETROGRAPHIC DESCRIPTIONS

This appendix will provide more detailed petrographic descriptions of the major lithologies found in the Patagonian batholith in the Baker area. The specific locations of the samples discussed may be found by referring to appendix A and plate A-1. In addition to the petrographic descriptions, table B-1 provides a complete list of modal data.

Lithologies of the Western Zone

Tonalite and Quartz Diorite of Cabo Bynoe & Is Jungfrauen

The western most plutons of the Patagonian batholith in the Baker area consist of mafic biotite hornblende quartz diorite and hornblende biotite tonalite. The quartz diorite (OE-11) has a medium grained hypidiomorphic granular texture with a color index (CI) of 49. Plagioclase is present as tabular phenocrysts which often show a zonation from two distinct generations. The cores of the plagioclase are usually highly corroded and resorbed and exhibit sericitic alteration. The rims are distinctly fresh and undisturbed. Green hornblende makes up 43% of the rock and occurs as tabular phenocrysts which occasionally exhibit resorption features. Minor biotite (6%) occurs as small tabular crystals often replacing hornblende. Apatite and Fe oxides are present as accessory minerals. Late crystalizing quartz occurs interstitially between the hornblende and plagioclase.

The tonalite (OE-10) is also medium grained with a hypidiomorphic granular texture. Its CI is 19 with biotite (11%) being slightly more abundant than hornblende (7%). Textures suggest that biotite followed the hornblende in the paragenetic sequence. Trace amounts of orthopyroxene are enclosed in some of the biotite. Plagioclase makes up 50% of the rock and occurs as euhedral to subhedral tabular crystals (An 48-55) with normal

zoning. Quartz occurs as anhedral to subhedral grains which occasionally show and undulatory extinction patterns typical of grains which have been strained. Accessory apatite is poikilitically enclosed with plagioclase, hornblende, and biotite. Ilmenite is the dominant Fe-Ti oxide. This sample (OE-10) has been dated at 135 Ma by $^{49}\text{Ar}/^{39}\text{Ar}$ analysis of biotite. Numerous mafic dikes cut outcrops of this tonalite.

Epidote Bearing Tonalite and Granodiorite of Isla Juan Stiven.

This suite of samples is characterized by the presence of phenocrysts of primary epidote which occur up to 2.6% in the mode. The epidote always occurs in close proximity to biotite or hornblende grains as subhedral grains up to 1-2 mm in size. Zen and Hammarstrom (1984) have suggested that the presence of magmatic epidote indicates crystallization at at least 6 kb. At least two distinct plutons in this region contain the magmatic epidote. One of these is a hornblende biotite tonalite (OE-4) which has been dated at 93 Ma by $^{49}\text{Ar}/^{39}\text{Ar}$ and the other is a hornblende biotite granodiorite (OE-5, OE-6A, & OE-7) which has been dated at 114 Ma by U-Pb.

The main distinguishing petrographic characteristic of the 114 Ma granodiorite is the presence of late crystallizing xenomorphic intergranular microcline which comprises from 8 to 29% of its modal composition. Plagioclase forms tabular phenocrysts which are normally zoned and often have rims of myrmekite when in contact with microcline. Some plagioclase also shows signs of resorption and oscillatory zoning is occasionally present. The overall texture is medium to coarse grained hypidiomorphic granular, with quartz being anhedral to subhedral. Green hornblende is always subordinate to biotite and some hornblende poikilitically encloses plagioclase and biotite. CI ranges from 12-14. Trace amounts of apatite, zircon, and magnetite are present, and trace amounts of blue green

tourmaline were noted in sample OE-6A. As this sample shows no indication of hydrothermal alteration, the tourmaline is believed to be primary. Fine grained granite aplite dikes (OE-6) with trace amounts of magmatic garnet cut this pluton.

The 93 Ma tonalite is medium grained hypidiomorphic granular with a CI of 18. Tabular phenocrysts of plagioclase up to 5mm comprise 41% of the rock. Normal zoning predominates although minor oscillatory zoning also present. Minor potassium feldspar (2%) occurs as intergranular xenomorphic grains. The K-spar is perthitic and does not exhibit well developed tartan twinning suggesting that it probably is orthoclase. Green hornblende (6%) is subordinate to biotite (9%). The hornblende and biotite often form glomeroporphyritic clots with epidote. Trace zircon, apatite and magnetite are also present. Numerous mafic dikes cut this pluton

Noritic Gabbro of Entrada Nassau

This mafic complex is located just west of Canal Meisier on Isla Millar and along Entrada Nassau. The fine to medium grained gabbro (BK-45A, BK-46, BK47, BK-48A) contains tabular plagioclase (56%) which often shows a distinct planar flow fabric. The plagioclase is normally zoned (An₈₄₋₇₂). Orthopyroxene (18%) predominates over clinopyroxene (11%), and the pyroxenes often occur together in glomeroporphyritic clumps. Up to 8% green hornblende occurs as rims on the pyroxenes. Magnetite is present up to 3% and often exhibits skeletal textures. Apatite occurs up to 1%.

A fine to medium grained biotite hornblende tonalite (BK-48) located at the west end of Entrada Nassau may be genetically related to the noritic gabbro. Green hornblende is the dominant mafic (19%) Much of the hornblende has remnant pyroxenes cores. Biotite (10%) follows hornblende in the paragenetic sequence. Tabular euhedral -subhedral

plagioclase which shows crude alignment makes up 51% of the rock. Anhedral quartz (16%) was the last mineral to crystallize. Zircon occurs up to 1.3%, and large (.5mm) stubby apatite crystals are also present.

Quartz Monzo-Diorite of Isla Millar

Sample BK-45 from the north end of Isla Millar is a medium grained quartz monzo-diorite with a CI of 18. Euhedral-subhedral tabular grains of plagioclase make up 60% of the rock and quartz occurs at 12% as anhedral grains. Microcline crystallized last and occurs as intergranular material making up 9% of the rock. The initial ferro-magnesian minerals were pyroxene and biotite which now are almost completely replaced by chlorite and minor epidote. Some fresh biotite remains (4.6%). Fe oxides are present at 1.4%. This unit has been intruded by the noritic gabbro described above.

Lithologies of Isla Wager

Samples collected from the south side of Isla Wager include hornblende gabbro (RB-115) and a 2-mica leucotonalite (RB-116). The hornblende gabbro is fine to medium grained and is composed of up to 61% tabular actinolitic hornblende and 35% plagioclase. Trace amounts of biotite are also present, as is minor (~2%) chlorite after the amphibole. Ilmenite (1%) is the oxide phase. The leucotonalite is medium grained hypidiomorphic granular containing 53% tabular plagioclase grains up to 2 mm. (An 35-30). Quartz (43%) occurs as polycrystalline grains which occasionally exhibit undulatory extinction. Trace amounts of K-feldspar occur as late intergranular material. Biotite (2.9%) and muscovite (1.3%) define a crude foliation in the unit.

Lithologies of the Central Zone

Hornblende Gabbro and Tonalites of Peninsula Luz

The south shore of Peninsula Luz contains outcrops of hornblende gabbro and tonalites with varying percentages of hornblende and biotite. The hornblende gabbro (G-58) is medium grained and contains 52% long tabular hornblende grains up to 5 mm. These hornblendes often poikilitically enclose small plagioclase and biotite grains. Plagioclase (43%) occurs as tabular euhedral to subhedral crystals and exhibits normal zoning (\sim An₉₀₋₇₅). Biotite is minor at 2.7%. This sample has an age of 46 ± 9 Ma as determined by $^{40}\text{Ar}/^{39}\text{Ar}$ analysis of hornblende.

Sample G-59 is a biotite tonalite with trace amounts of hornblende. The sample is medium grained hypidiomorphic granular and contains 68% tabular euhedral to subhedral plagioclase which occasionally exhibits oscillatory zoning. The plagioclase composition ranges from \sim An₄₅-An₂₅ and some grains show evidence of resorption. Quartz (18%) is intergranular, as is trace amounts (.5%) of K-spar. Biotite is present at 13% with some replaced by chlorite.

Sample BK-6B is a medium grained biotite hornblende tonalite with a CI of 39. Green hornblende is the dominant mafic mineral making up 30% of the rock, followed by biotite at 8%. Euhedral to subhedral tabular plagioclase crystals make up 47% of the sample. These plagioclase grains are normally zoned and often exhibit resorbed and corroded cores with clean rims suggestive of two generations. A composition of An₃₈ was determined on an uncorroded rim of one grain. Quartz (14%) occurs as anhedral intergranular material. This lithology was cut by a garnet bearing 2- mica aplite dike with a granophyric texture (Bk-6A).

Sample BK-5B is a hornblende biotite tonalite which is likely a more felsic phase of BK-6B, as evidenced by similar textures and mineralogy. Plagioclase exhibits the corroded cores with fresh rims as in BK-6B. Biotite predominates (10%) over green hornblende (6%) and quartz makes up 35% of the rock. This outcrop was cut by a dike of fine grained hornblende diorite (BK-5A).

Hornblende quartz diorite of Fiordo Pulpo

Outcrops along northern shore of the central stretch of Fiordo Pulpo are dominated by fine to medium grained hypidiomorphic granular hornblende quartz diorites (stations PU-6 to 8). PU-8 is typical example, consisting of 34% tabular hornblende grains up to 5mm and 49% euhedral plagioclase grains up to 2 mm. The plagioclase is ~ An 50 and exhibits normal zoning. The sample is moderately altered with minor chlorite replacing hornblende and sericitized cores of plagioclase. Small clots (5%) of chlorite, epidote, and sphene have probably replaced primary biotite.

Lithologies of the Eastern Zone

Biotite Granite

A large complex of biotite granite (~ 1250 km²) is found exposed from central Isla Merino Jarpa east into Fiordo Mitchell and north into Fiordo Steffen. The large area that this granite is exposed over suggests that several plutons of this lithology may be present within the region. Minor variations in modal abundance and textures do exist among the analyzed samples, however there is no apparent mineralogic or textural zonation within the complex. Mafic dikes are rare and micro-diorite inclusions are occasionally present in these granites. Samples (BK18 to BK-31) are typically medium grained, hypidiomorphic

granular biotite granite with CI ranging from 2 to 8. Plagioclase (25-30%) is present as normally zoned (~An₂₀₋₁₀) euhedral to subhedral grains, which often show resorption features, and minor sericite alteration in the cores. Myrmekite overgrowths are common at contact boundaries between plagioclase and K-feldspar. Quartz (25-35%) is usually anhedral, although occasional subhedral grains exhibiting β -quartz morphology are present. K-feldspar (25-30%) occurs as late anhedral intergranular material, commonly exhibiting patchy perthitic structure. Tartan twinning is rare. Biotite (2-6%) is the sole ferro-magnesium mineral present in these rocks, occurring as subhedral grains up to 4 mm. Trace constituents consist of apatite, zircon, and occasionally allanite. Sample BK-22 has been dated at 84 Ma by $^{49}\text{Ar}/^{39}\text{Ar}$ on biotite.

Hornblende Biotite Tonalite-Granodiorite

Hornblende and biotite bearing tonalite and granodiorite typical of much the Patagonian batholith makes up most of the remainder of the batholith in the eastern zone. RB-98 is typical medium grained hypidiomorphic tonalite with a CI of 13. Euhedral to subhedral plagioclase (~An₃₀) up to 3 mm makes up 60% of the unit. Anhedral intergranular quartz is present at 21% along with minor (5%) intergranular microcline. Biotite (10%) is the dominant ferromagnesium mineral, occurring as euhedral to subhedral grains up to 2 mm. Green hornblende is minor (2%) and often exhibits resorption features. Magnetite is present at 3%. Trace constituents consist of zircon and apatite which is poikilitic in all phases. This sample has been dated at 92 Ma by a Rb/Sr mineral-WR isochron and 90 Ma by $^{49}\text{Ar}/^{39}\text{Ar}$ on biotite.

The oldest intrusive rock so far dated from the Patagonian batholith at 48° S is a biotite hornblende granodiorite which occurs on Peninsula Vedidu at the eastern edge of the

batholith in the study area. Sample RB-106, dated at 149 Ma by U-Pb, is a mildly altered medium grained hypidiomorphic granular unit with a CI of 22 containing 50% plagioclase, 19% quartz and 8% K-feldspar. The plagioclase exhibits normal and oscillatory zoning and typically has sericite alteration in its cores and corroded edges. Minor myrmekite is also present as reaction rims on plagioclase. The K-feldspar occurs as late intergranular material. Hornblende is the dominant ferromagnesium mineral (12%). It often exhibits faint remnant cores of pyroxene and in some cases appears to be replaced by biotite. Some of the hornblende also appears to have been altered to actinolite. Biotite (8%) occurs as rims on hornblende and as discrete grains and is often altered to chlorite. Opaques, apatite and zircon occur as trace constituents.

Garnet Bearing 2-Mica Granite

Garnet bearing 2-Mica Granite occurs at two stations (RB-104, RB-105) on Peninsula Vedidu. These medium to coarse grained leucocratic rocks contain 2-3% biotite, 1-1.3% muscovite and less than 1% garnet. Quartz predominates (39-43%), and perthitic K-feldspar and plagioclase are present in roughly equal quantities (27-29%). Plagioclase is present as euhedral to subhedral grains which are often poikilitically enclosed in K-feldspar. The cores of most plagioclase grains are often resorbed and altered by sericite. Fresh rims (~ An₃₀) show no sign of resorption or alteration. This may be suggesting that the cores are relict restite material. Trace ilmenite is present in both samples and trace dumortierite is present in RB-104. RB-104 has been dated at 110 Ma by a RB/Sr mineral-WR isochron.

Mafic Rocks

Mafic rocks in the eastern zone occur in several scattered locations but volumetrically are minor. A Fine grained gabbro (RB-103) is present at Pta. Blanca on Peninsula Veditu. This gabbro has a porphyritic texture with scattered plagioclase phenocrysts up to 7 mm. Groundmass plagioclase (~An 60) averages 1 mm. Augite (20%) occurs up to 2 mm. Probable original olivine has been replaced by chlorite and Fe-oxides. The chlorite (17%) is present throughout the groundmass.

A medium grained hornblende gabbro (PU-9) is present along the eastern extension of Fiordo Pulpo in the northern part of the study area. CI is 54 with minor augite (6%) always rimmed by brown hornblende. Discrete hornblende grains up to 2 mm make up 39% of the unit and plagioclase laths up to 2 mm make up 45%. Fe-Ti oxides are prevalent (8%) with magnetite often rimming ilmenite.

Table B-1 Patagonian Batholith Modal Data

Sample #	quartz	k-feldspar	plagioclase	hornblende	biotite	cpx	opx	muscovite	chlorite	epidote	garnet	opaques	accessories
4G-104	43.5	31.8	22.8		0.4			1.5				0.3	0.6
4G-106	27.8	20.7	44.2	3.4	3							5.09	2
4G-110	28.4	9.4	39.2	11.4	11.6							0.5	1r
4G-111A	4.59		53.15	32.27	2.9				0.6			0.6	0.09
BK-10	30.4	9.1	52.2		7.3							0.5	0.7
BK-11	22.5		57.1	9.2	8.1							1	1
BK-13	32.67	9	51.52		5.11	0.2			1.04			0.6	0.09
BK-14B	15.4		54.5	13.1	13.9							2.3	0.7
BK-15	6.9		51.4	22.1	18.5							0.6	1
BK-16	7.4		48.2	33.6	10							0.6	0.2
BK-18	30.5	29.1	37.4		1.9							1	
BK-19	44.4	23.4	25.9		5.2							1.1	
BK-20	28.5	20.5	43.9		6.7							0.4	
BK-21	40.7	22.8	35.9		0.5							1	
BK-31	39.9	28.9	25.1		5.1							0.1	
BK-33	37.6	28.9	31.2		2.2							0.1	
BK-34	36.9	31.6	29.3		2.1							0.1	
BK-36	29.3	28.7	37.7		3.3							1	
BK-42	33.8	33.7	28.1						3.5				1.3
BK-42A	35.2	15	43.5		5.9							0.3	
BK-45	12	9.3	60		4.6				10.7			1.4	1.5
BK-47			56.08	8.14		11.4	18.4		2.06			3.14	0.78
BK-48	16.5		50.6	18.6	10.1				0.9			1.5	1.8
BK-5A			26.3	56.3	10.4							5.4	1.7
BK-5B	35		47.4	6.2	10.1							0.4	0.4
BK-6B	13.6		47.5	30.4	7.9							0.7	0.3
BK-7	37		12.9		1.1							0.4	
BK-8A	27.8	48.5	34.2		2.2							0.4	
G-58			43	52.3	2.7							1.9	0.1
G-59	17.6	0.5	67.8	0.5	12.8				0.2			0.2	0.4
G-69	41.3	39.8	17.8						0.8			0.4	
OE-10	30.62		50	7.46	10.95		0.77						0.2
OE-11	6.78		44.57	42.7	5.98							0.2	0.2
OE-2	6.4		65.5	18.3		6.3						2.4	1.1
OE-4	39.4	2	40.8	6	8.6					2.7		0.2	0.3
OE-5	30.9	29.7	26.3	0.1	11.6					0.4			
OE-6	36.6	28.7	33.3		0.2			0.4					0.2
OE-6A	30.7	15.5	41.2	2.3	8.5				0.5				0.2
OE-7	34.4	8.8	41.7	3.5	9.4					1.6			0.5
OE-8	12.7		47.3	31.2	4.9				1.5				0.7
PU-10A	43.8	34.9	18		3.2							0.1	
PU-10B	22.7		54.5	2	16.7							0.6	2.8

(continued)

Table B-1 (continued)

Sample #	quartz	k-feldspar	plagioclase	hornblende	biotite	cpx	opx	muscovite	chlorite	epidote	garnet	opaques	accessories
PU-11	32	10	48		8							1	
PU-6	11.1		58.3	22.5					6			2.2	
PU-8	10.78		48.63	34.02					4.02			1.67	0.9
PU-9			45.5	39.3		5.9						8.5	0.8
RB-101	35.1	15.7	43.8	0.8	4.6								
RB-103			58			20			17.2			4.8	
RB-104	39	29	27		3			1.3	0.9		0.6		
RB-105	43.9	22.1	29.7		2.5			1.2	0.6				
RB-106	19.33	7.65	50.64	12.07	7.75				2.35			0.3	
RB-115b			35.5	60.8	0.4			1.3	2			1	0.3
RB-116	42.7	0.3	52.8		2.9								
RB-117	24.6	13.9	45.3	7.4	7.6							1	0.1
RB-80	33.2	14.3	40.6		11.9								
RB-82	26.8	18.4	42.5	5.3	7								
RB-83	39.7	32.8	25.9		1.3							0.3	
RB-85	34.5	32.3	30.5		2.1							0.5	0.1
RB-86	39.4	33.9	24.6		1.6							0.6	
RB-90	36.4	29.6	30.3		3.4							0.1	0.2
RB-96	33.1	14.3	41.1	6.1	5.3								
RB-97	39.3	15	37.2		7							0.9	0.6
RB-98	21	5	61	2	10							0.6	0.5

cpx = clinopyroxene
 opx = orthopyroxene

Appendix C: ANALYTICAL METHODS

Sample Disaggregation

Powders for chemical analysis were obtained from fresh rock samples starting from an interior slab created during the preparation of thin section chips and mode counting slabs. Slab edges were removed and the interior portion broken so as to fit in the jaw crusher. Samples (1-2 kg) were crushed and split into ~50 gram portions, one of which was pulverized in a tungsten carbide puck mill to finer than 200 mesh. These stock powders were used for all subsequent whole rock analyses. Before use, the stock powders were mixed for 24 hours in a rotary mixing mill to ensure homogeneity.

Major Element Analysis by X-ray Fluorescence Spectrometry

Oven dried (100 ° C) whole rock powder (0.5000 grams) is mixed with 4.5000 grams of dry $\text{Li}_2\text{B}_4\text{O}_7$ for several hours in an inclined rotary ball mill. The mixture is placed in a Pt crucible (95% Pt, 5% Au) with three drops of 0.5 N LiI solution. The crucible is then covered with Pt mold/cover and the sample is fused over a bunsen burner. After all refractory phases melt, the mold is placed on a heat resistant surface and the sample is pored into it. When cool, the resultant glass disk is labeled and stored in a desiccator.

The major element glasses were analyzed by Stan Mertzman at Franklin and Marshall College on a computer automated Diano x-ray fluorescence spectrometer. Analytical precision is as follows: $\text{SiO}_2 \pm 0.4\%$, $\text{Al}_2\text{O}_3 \pm 0.12\%$, $\text{Fe}_2\text{O}_3 \pm 0.10\%$, $\text{TiO}_2 \pm 0.02\%$, $\text{MnO} \pm 0.01\%$, $\text{MgO} \pm 0.07\%$, $\text{CaO} \pm 0.03\%$, $\text{Na}_2\text{O} \pm 0.09\%$, $\text{K}_2\text{O} \pm 0.02\%$, and $\text{P}_2\text{O}_5 \pm 0.02\%$. The precision and accuracy of these analyses was confirmed by running blind standards and duplicate analyses.

Trace Element Analysis by X-ray Fluorescence

Oven dried whole rock powder and microcrystalline cellulose are mixed in a 2:1 ratio (2 parts sample, 1 part cellulose) for several hours. Sample size is dependent on the size of the pellet desired. The sample mixture is pressed into a pellet with a backing of additional microcrystalline cellulose at a pressure of 30,000 psi in a standard laboratory press, and stored in a desiccator.

Trace elements were analyzed on the XRF at Franklin nd Marshall or at CSM on a Rigaku XRF using procedures established by Carl Erickson. Blind standards were included in each run to test the accuracy and precision of the method. Data covering a six month period demonstrates the high precision of the technique. Accuracy varies from element to element and from standard to standard. Percent deviance vs. ppm diagrams were analyzed by visual inspection to determine realistic lower detection limits and the percent error at that concentration:

<u>Element</u>	<u>Detection limit ppm</u>	<u>Percent error</u>
Ba	300	10
Nb	10	10
Ni	30	10
Rb	10	5
Sr	50	5
V	15	10
Y	10	10
Zr	50	10

Trace element concentrations were corrected for mass absorption and matrix effects by the method of Hower (1959).

Iron Oxidation State and LOI

Ferrous iron was determined by the method of Goldich (1984). These data were used to refine loss on ignition (LOI) determinations. LOI was determined by measuring the weight loss of an oven dried sample during a 45 minute run at 900° C in a muffle furnace. A correction for the mass gained by oxidation of FeO is made by multiplying the wt% FeO by 0.111348 and adding this to the LOI value.

Mineral Proportions

Mineral modes were determined from 1000 point counts. Coarse grained rocks were analyzed by counting stained slabs using grid counting templates provided by Dr. Bruce Johnson of the USGS. Medium- and fine-grained rocks were counted using standard mechanical stage techniques.

Isotope Geochemistry

Sr and Nd isotope analyses were carried out at Lamont-Doherty Geological Observatory. All sample preparation was carried out in a clean lab to prevent sample contamination. Samples were spiked with enriched isotopes of ^{87}Rb , ^{84}Sr , ^{149}Sm , and ^{150}Nd . For Sr and Nd, concentrations and isotope ratios were measured on the same sample aliquot.

Sample Dissolution. Fifty to 100 mg of sample powder was dissolved in ~ 3-8 ml of ~1:4 HClO_4 : HF in a 10 ml TFE beaker. This solution was evaporated at ~150 °C until the majority of HF was gone; temperature then increased incrementally to 280° to drive off HClO_4 . Samples were dried down three times in 6.2 N HCl. Samples were then

dissolved in 0.2 ml of 2.5 N HCl, centrifuged, and loaded into the first ion exchange column.

First Column Step (Cation Columns). The first column (described by Hart and Brooks, 1977) consists of a 0.5 cm (diameter) x 19 cm (height) column filled with 37 ml of cleaned Dowex AG50-8 cation exchange resin. The sample was loaded in 0.2 ml of 2.5 N HCl and washed with three aliquots of 2.5 N HCl totaling 1 ml. Elution with 19-20 ml of 2.5 N HCl follows and during this stage of elution, alkalies and Sr were passed off the column and collected. The elutant was then changed to 6.2 N HCl and approximately 6-8 ml were required to remove the REE. The column was then cleaned with 30 ml of 6.2 N HCl and backwashed with 2.5 N HCl.

Second Column (REE). The procedure for Nd-Sm separation is modified after the method of Richard et al. (1976). The column consists of 50 cm of 0.5 cm I.D. supersil quartz tubing attached to a 100 ml round bottomed flask which serves as a reservoir for elutants, and provides a constant pressure head. The bottom end of the column is fitted with a polyethelene fiber "frit". A 2mm hole is blown into the column 12.5 cm from the bottom to allow sample loading. Teflon tape cleaned in 1:1 HNO₃ is wrapped around the hole to prevent leakage. Ten cm of column material is loaded into the column in H₂O and compressed uniformly to desired compaction (~ 10 ml/ hr flow rate) by a combination of aspiration from the bottom and tamping from the top with a glass rod. The column material is composed of a mixture of teflon powder and HDEP [Bis (2-ethylhexyl) hydrogen phosphate] in a weight ratio of 10:1 (teflon powder : HDEP). This column material is capped by 0.5 cm of Dowex AG1-X8 anion resin to prevent teflon flotation.

REE were loaded onto the column in 0.1 ml of 0.25 N HCl and washed onto the column with three 0.2ml aliquots of 0.25 N HCl. The reservoir was then loaded with 30 ml of 0.25 N HCl and Nd was collected at the proper time interval as determined by column calibration using the indicator erichrome black. The reservoir was then emptied and Sm was eluted with 0.6 N HCl.

Mass Spectrometry. Rb, Sr, Sm, and Nd concentrations and Sr and Nd isotope ratios were measured on a modified V.G. Micromass 30 mass spectrometer with computer controlled data collection functions and focusing and filament control. Sr was loaded on single W filament as a nitrate, Rb was loaded on a Ta single filament with H₂O, and Nd and Sm were loaded as chlorides on Ta side filaments of a triple filament assembly (Rh center). All $^{87}\text{Sr}/^{86}\text{Sr}$ measurements were normalized to $^{86}\text{Sr}/^{88}\text{Sr} = 0.11940$ and are relative to $^{87}\text{Sr}/^{86}\text{Sr} = .70800$ for the Eimer and Amend SrCO₃ standard. Nd was analyzed as Nd⁺ with measurements normalized to $^{146}\text{Nd}/^{144}\text{Nd} = 0.72910$.

Argon Isotopic Analysis

$^{40}\text{Ar}/^{39}\text{Ar}$ isotopic dating was accomplished by Robert Bruce using the facilities of the department of Geological Sciences at the University of Maine in Orono. Following standard mineral separation procedures, conducted at CSM, samples with an estimated purity of 99.9% were weighed, encapsulated in Al foil and sealed in silica glass vials. They were irradiated at Phoenix Memorial Laboratory in the Ford Nuclear Reactor at the University of Michigan. Included in each silica vial as flux monitors are samples of an international standard, MMhb-1, whose accepted age is 519.4 Ma (Alexander et al., 1978) and in-house (UMO) laboratory standards.

Argon was liberated from samples by radio frequency induction heating of a Mo crucible within a pyrex extraction furnace. Extraction temperatures were estimated by optical pyrometry. The inert gas extraction and purification system utilized standard purification methods including Cu-CuO getter and SAES cartridge getters (50 l/s and 10 l/s). Argon isotope compositions were determined using a Nuclide 6-60-SGS gas source, 15 cm radius, 60 degree sector Nier-type mass spectrometer with automated operations controlled by an IBM PC computer.

Ages were calculated using the equations and correction factors given by Dalrymple et al. (1981). Decay constants for ^{40}K and the isotopic composition of K used in the age calculation are the values recommended by Steiger and Jaeger (1977). Atmospheric argon was analyzed several times a week to make accurate mass discrimination corrections. The ^{37}Ar was corrected for decay during the time interval between irradiation and isotopic analysis using a half life of 35.1 days. Data was corrected for mass fractionation during analysis. The reported analytical uncertainty for individual analyses is a one sigma estimate determined by the equation of Dalrymple et al. (1981) using uncertainties in time zero extrapolations and an uncertainty in J of 0.25%. Plateau ages represent an average for consecutive increments which constitute a significant proportion (> 50%) of the total ^{39}Ar in the sample and whose apparent ages cannot be considered different on the basis of the critical value test of Dalrymple and Lanphere (1971). The uncertainty estimates used in the critical value test for plateaus in individual samples exclude uncertainties in J-value and are considered at the 2-sigma level. Uncertainties reported for plateau ages are one standard deviation with n-1 weighting.

Appendix D : GEOCHEMICAL DATA

Table D-1 Major Element Data

Sample #	Patagonian batholith series	SiO ₂	TiO ₂	Al ₂ O ₃	Fe ₂ O ₃	FeO	MnO	MgO	CaO	Na ₂ O	K ₂ O	P ₂ O ₅	LOI	FeO*	Total
BK-14B	CAT	58.18	0.94	17.58	4.63	2.89	0.12	2.86	6.75	3.44	1.35	0.23	1.17	7.06	100.24
BK-16	CAT	53.54	0.86	17.49	2.93	5.4	0.15	5.39	8.5	3.45	1.1	0.13	1	8.04	99.94
BK-46	CAT	50.37	1.12	18.93	3.56	5.92	0.15	6.37	9.64	3.18	0.25	0.3	1.01	9.12	100.80
BK-47	CAT	48.16	1.11	18.64	4.36	6.16	0.15	6.73	11.14	2.77	0.09	0.24	1.01	10.08	100.56
BK-48	CAT	58.04	1.03	17.36	2.84	4.72	0.12	3.58	6.78	3.53	1.29	0.23	1.26	7.28	100.78
BK-48A	CAT	50.48	1.24	18.33	3.43	6.19	0.15	6.35	9.68	3.28	0.26	0.33	1.08	9.28	100.60
BK-6B	CAT	56.69	0.89	16.24	2.79	4.9	0.18	6.6	7.46	2.93	1.09	0.08	1.15	7.41	100.80
G-58	CAT	46.57	1.27	19.65	2.77	5.19	0.1	7.76	12.41	2.07	0.48	0.07	1.73	7.68	100.07
OE-10	CAT	63.44	0.64	15.88	1.14	5.84	0.11	2.57	6.08	2.32	1.35	0.10	1.93	6.87	101.38
OE-11	CAT	53.99	0.73	16.07	2.68	9.03	0.21	4.72	9.07	1.99	0.71	0.09	1.72	11.44	101.01
OE-2	CAT	52.47	0.89	19.23	3.91	6.24	0.18	4.98	8.99	2.95	0.14	0.13	1.05	9.76	100.96
OE-3	CAT	44.82	0.14	21.28	2.38	5.63	0.15	10.23	11.62	0.90	0.26	0.01	2.78	7.77	100.20
OE-4	CAT	67.12	0.39	15.56	1.73	3.15	0.10	1.75	4.95	2.74	1.65	0.06	1.22	4.71	100.42
OE-8	CAT	52.26	0.71	18.92	3.67	5.64	0.18	5.10	9.22	2.06	1.24	0.14	1.74	8.94	100.88
PU-10B	CAT	63.97	0.66	17.35	2.27	3.89	0.08	1.48	5.24	3.23	1.43	0.13	0.90	5.93	100.63
PU-11	CAT	68.73	0.28	16.63	1.17	1.37	0.06	0.66	3.80	4.61	1.68	0.09	0.54	2.42	99.62
PU-6	CAT	55.03	0.96	17.78	3.50	6.12	0.19	3.52	7.50	3.33	0.75	0.18	1.63	9.27	100.49
PU-8	CAT	58.72	0.81	16.06	2.99	4.62	0.14	4.02	7.68	3.15	0.82	0.17	1.52	7.31	100.70
RB-115b	CAT	45.74	0.67	19.14	2.53	6.86	0.14	9.36	12.71	0.92	0.12	0.02	1.97	9.14	100.18
RB-116	CAT	76.76	0.09	13.68	0.28	1.18	0.02	0.30	2.67	4.00	0.88	0.01	0.48	1.43	100.35
4G-106	CG	70.59	0.37	14.57	1.26	1.65	0.05	0.72	2.27	4.20	3.19	0.12	0.80	2.78	99.79
4G-110	CG	67.18	0.39	15.43	1.43	3.29	0.12	1.70	4.04	2.60	2.71	0.09	1.35	4.58	100.33
4G-111A	CG	47.72	2.15	17.27	5.50	6.99	0.20	4.45	8.68	3.84	0.70	0.44	1.05	11.94	99.09
BK-13	CG	70.77	0.32	14.84	1.18	1.38	0.07	0.96	2.98	3.88	2.34	0.07	1.3	2.44	100.09
BK-15	CG	54.16	0.87	17.91	2.07	4.58	0.12	6.54	7.36	2.8	1.92	0.08	1.36	6.44	99.57
BK-18	CG	75.91	0.23	12.92	0.73	0.8	0.06	0.2	1.07	3.82	3.99	0.04	0.6	1.46	100.37
BK-19	CG	74.49	0.24	13.53	1.09	0.67	0.06	0.34	1.05	3.74	4.25	0.04	0.24	1.65	99.74
BK-20	CG	73.88	0.29	13.61	0.86	0.95	0.06	0.49	1.34	3.91	3.58	0.05	0.37	1.72	98.39
BK-21	CG	77.45	0.16	12.58	0.87	0.52	0.04	0.11	0.85	3.8	3.89	0.01	0.27	1.30	100.55
BK-22	CG	73.32	0.21	13.95	0.49	1.36	0.06	0	0.9	4.29	4.24	0.03	0.75	1.80	99.50
BK-23	CG	76.53	0.13	12.75	0.73	0.43	0.04	0	0.54	3.93	4.49	0.01	0.45	1.09	100.03
BK-25	CG	73.14	0.29	14.17	0.81	1.3	0.04	0.36	1.72	4.79	2.21	0.07	0.57	2.12	99.57
BK-26	CG	77.25	0.15	12.67	0.82	0.77	0.07	0	0.55	4.74	3.38	0	0.23	1.51	100.63
BK-27	CG	77.85	0.09	12.45	0	1.27	0.06	0	0.31	3.77	4.6	0	0.33	1.27	100.73
BK-28	CG	77.32	0.17	12.59	1.42	0.13	0.06	0.18	0.67	3.5	4.12	0.02	0.42	1.41	100.60
BK-29	CG	76.06	0.18	12.47	0.88	0.81	0.03	0.08	0.84	3.11	4.84	0.02	0.43	1.60	99.75
BK-31	CG	76.56	0.21	13.02	0.76	1.07	0.03	0.16	0.71	4.07	3.62	0.02	0.36	1.75	100.59
BK-33	CG	74.70	0.26	13.52	1	0.9	0.06	0.32	1.3	4.03	3.58	0.03	0.54	1.80	100.24
BK-34	CG	75.15	0.25	13.37	0.96	0.9	0.05	0.28	0.93	4.09	3.73	0.03	0.73	1.76	100.47
BK-35	CG	74.41	0.3	13.63	0.73	1.5	0.05	0.33	1.12	4.38	3.61	0.04	0.69	2.16	100.79
BK-36	CG	73.44	0.29	13.46	1	1.06	0.06	0.18	1.26	4.15	3.54	0.04	0.63	1.96	99.11
BK-42	CG	72.24	0.28	14.16	1.16	1.23	0.05	0.45	1.43	3.92	4.09	0.07	0.97	2.27	100.05
BK-42A	CG	69.42	0.4	14.35	1.28	2.11	0.07	0.65	2.06	4.41	2.49	0.08	1.05	3.26	98.37
BK-45	CG	57.41	0.73	20.7	2.52	2.75	0.02	1.72	6.03	4.26	5.04	0.27	1.29	5.02	100.06
BK-7	CG	77.38	0.12	12.16	0.85	0.84	0.02	0.04	0.83	2.26	2.45	0.01	0.21	1.61	100.17
G-59	CG	62.71	0.5	17.96	1.71	2.29	0.07	1.5	4.69	4.71	1.68	0.17	0.75	3.83	98.74

(continued)

Table D-1 (continued)

Sample #	series	SiO2	TiO2	Al2O3	Fe2O3	FeO	MnO	MgO	CaO	Na2O	K2O	P2O5	LOI	FeO*	Total
G-69	C&G	77.74	0.12	12.13	0.46	0.46	0.03	0.12	0.41	3.09	5.03	0	0.34	0.87	99.93
OE-5	C&G	69.43	0.32	14.97	0.84	2.97	0.08	1.26	3.48	2.52	3.38	0.06	0.74	3.73	100.05
OE-5A	C&G	70.19	0.35	14.88	1.02	3.16	0.09	1.44	3.72	2.86	2.22	0.06	0.76	4.08	100.75
OE-6A	C&G	68.75	0.31	15.02	1.22	2.45	0.08	1.26	3.75	2.88	2.93	0.04	1.12	3.55	99.71
OE-7	C&G	65.45	0.45	15.91	2.21	3.33	0.19	1.81	4.89	2.71	2.12	0.08	1.06	5.32	100.21
PU-10A	C&G	77.90	0.12	12.02	0.59	0.92	0.02	0.12	0.97	2.00	5.58	0.02	0.36	1.45	100.62
PU-9	C&G	41.94	1.98	16.94	8.43	7.69	0.22	6.38	11.95	2.41	0.27	0.30	1.61	15.28	100.12
RB-101	C&G	71.34	0.29	14.21	0.78	2.51	0.06	0.53	2.58	3.03	3.43	0.06	0.80	3.21	99.62
RB-103	C&G	48.24	2.05	16.03	3.78	7.94	0.20	5.58	9.18	3.31	1.06	0.25	2.54	11.34	100.16
RB-106	C&G	60.86	0.88	16.69	1.73	5.81	0.12	2.17	5.34	2.76	2.42	0.14	1.97	7.37	100.88
RB-117	C&G	66.42	0.48	15.34	1.93	2.67	0.09	1.82	4.48	2.72	2.25	0.11	0.82	4.41	99.13
RB-80	C&G	69.64	0.42	15.15	1.15	2.01	0.07	0.84	2.74	3.48	3.36	0.12	0.58	3.05	99.56
RB-82	C&G	66.16	0.57	15.57	1.75	2.23	0.09	0.84	2.35	4.21	3.70	0.14	1.25	3.81	98.86
RB-83	C&G	78.56	0.06	12.46	0.43	0.37	0.02	0.03	0.04	3.64	3.98	0.00	0.73	0.76	100.33
RB-84	C&G	70.06	0.45	14.25	1.30	1.58	0.06	0.67	2.00	3.98	3.98	0.11	0.78	2.75	99.12
RB-85	C&G	75.09	0.17	12.73	0.68	0.58	0.01	0.09	0.89	3.31	4.97	0.03	0.48	1.19	98.93
RB-86	C&G	76.72	0.16	12.39	0.56	0.46	0.05	0.00	0.51	3.95	4.23	0.01	0.49	0.96	98.53
RB-90	C&G	75.64	0.14	12.74	0.59	0.88	0.03	0.10	0.62	3.69	4.21	0.01	0.42	1.41	99.07
RB-96	C&G	66.98	0.44	15.87	1.14	3.04	0.07	1.00	3.78	3.19	3.10	0.09	1.16	4.07	99.86
RB-97	C&G	69.07	0.49	15.34	1.55	1.60	0.09	0.86	2.61	4.46	2.75	0.12	0.54	3.00	99.48
RB-98	C&G	61.27	0.44	18.77	1.86	2.76	0.19	1.34	4.56	4.97	1.90	0.17	1.19	4.52	99.42
4G-104	2-mica granite	77.71	0.02	12.08	0.52	0.36	0.05	0.00	0.39	3.53	4.15	0.01	0.48	0.83	99.30
OE-6	2-mica granite	76.48	0.02	13.00	0.24	0.40	0.01	0.12	0.70	2.76	5.82	0.00	0.30	0.82	99.65
RB-104	2-mica granite	74.20	0.08	13.91	0.37	1.20	0.11	0.14	1.06	3.71	4.19	0.03	0.80	1.53	99.80
RB-105	2-mica granite	75.20	0.03	12.72	0.34	1.17	0.04	0.00	0.79	3.19	4.10	0.01	2.25	1.48	99.84

Table D-2 Trace Element Data

Sample #	series	Ba	Nb	Ni	Sr	Rb	V	Y	Zr	Rb/Sr	K/Rb
BK-14B	CAT	443	7.1	bd	638	63	180	36	150	0.10	178
BK-16	CAT	307	6.2	35	549	32	193	18	53	0.06	289
BK-46	CAT	157	4.0	72	894	4	215	24	25	0.00	519
BK-47	CAT	105	5.6	60	970	2	254	9	1	0.00	387
BK-48	CAT	446	6.0	15	711	44	206	32	85	0.06	243
BK-48A	CAT	147	7.0	70	1025	2	205	22	21	0.00	1079
BK-6B	CAT	375	2.0	80	453	26	158	49	47	0.06	342
G-58	CAT	102	5.0	67	675	14	325	30	81	0.02	285
OE-10	CAT	340	7.0	9	240	69	156	31	158	0.29	162
OE-11	CAT	174	5.3	20	227	27	358	29	72	0.12	217
OE-2	CAT	106	4.8	31	410	2	258	19	23	0.01	534
OE-3	CAT	70	5.4	126	493	8	49	4	8	0.02	257
OE-4	CAT	337	6.0	8	337	72	107	30	107	0.21	190
OE-8	CAT	198	5.0	19	392	57	271	33	52	0.15	181
PU-10B	CAT	624	11.5	19	345	66	85	14	236	0.19	179
PU-11	CAT	533	3.8	6	752	43	29	28	65	0.06	324
PU-6	CAT	276	4.2	25	430	24	201	31	105	0.05	265
PU-8	CAT	276	8.0	21	441	24	206	22	76	0.05	284
RB-115b	CAT	21	nd	74	438	1	266	26	22	0.00	996
RB-116	CAT	388	8.1	bd	377	29	bd	14	65	0.08	252
4G-106	CAG	461	nd	bd	319	69	23	25	155	0.22	384
4G-111A	CAG	262	14.2	19	686	15	319	42	189	0.02	377
BK-13	CAG	554	11.0	13	404	56	39	24	80	0.14	347
BK-15	CAG	351	5.2	108	748	55	109	20	93	0.07	292
BK-19	CAG	760	16.1	19	182	145	25	22	92	0.80	243
BK-20	CAG	905	11.6	18	207	111	27	19	99	0.54	267
BK-21	CAG	565	13.2	21	123	137	14	31	91	1.11	235
BK-22	CAG	720	nd	bd	127	116	9	31	179	0.91	303
BK-26	CAG	673	10.9	17	122	113	7	38	136	0.92	248
BK-27	CAG	78	33.7	20	24	237	10	53	124	9.67	161
BK-28	CAG	503	10.6	18	106	132	20	27	83	1.25	258
BK-29	CAG	608	5.7	17	138	98	21	9	114	0.71	410
BK-31	CAG	1751	5.5	18	130	93	13	23	124	0.71	324
BK-33	CAG	546	15.5	17	198	174	22	27	123	0.88	171
BK-34	CAG	656	10.5	18	219	139	21	22	131	0.64	222
BK-35	CAG	661	11.5	19	160	132	20	27	205	0.83	226
BK-36	CAG	598	9.4	13	172	130	7	22	165	0.75	227
BK-42	CAG	814	9.1	3	264	131	26	33	132	0.50	259
BK-42A	CAG	398	12.2	17	282	81	33	35	182	0.29	256

(continued)

Table D-2 (continued)

Sample #	series	Ba	Nb	Ni	Sr	Rb	V	Y	Zr	Rb/Sr	K/Rb
BK-45	CAG	633	3.8	6	1066	62	82	21	348	0.06	273
BK-7	CAG	1266	3.6	18	199	94	22	8	106	0.47	481
OE-5	CAG	651	nd	6	255	105	83	30	103	0.41	267
OE-5A	CAG	333	7.0	20	255	105	nd	20	nd	0.41	176
OE-6A	CAG	452	6.0	7	248	91	80	35	91	0.37	258
OE-7	CAG	404	5.0	7	262	92	113	35	107	0.35	191
PU-10A	CAG	756	5.7	17	140	125	14	24	71	0.89	371
PU-9	CAG	48	5.0	10	840	22	496	34	18	0.03	102
RB-101	CAG	644	nd	bd	157	146	26	36	131	0.93	195
RB-103	CAG	202	8.6	46	420	40	244	37	201	0.10	219
RB-106	CAG	581	9.8	5	279	113	103	38	190	0.41	178
RB-117	CAG	440	7.8	bd	287	84	115	30	127	0.29	222
RB-80	CAG	1713	13.0	bd	383	85	36	28	204	0.22	328
RB-82	CAG	1486	16.4	bd	333	119	30	36	330	0.36	258
RB-84	CAG	718	nd	bd	266	148	27	41	286	0.56	218
RB-86	CAG	271	nd	bd	55	194	bd	49	110	3.53	181
RB-96	CAG	648	10.0	bd	219	142	41	43	160	0.65	181
RB-97	CAG	1273	nd	bd	498	96	34	31	251	0.19	238
RB-98	CAG	710	7.0	bd	818	96	40	22	420	0.12	156
4G-104	2-mica granite	366	12.0	bd	75	136	bd	39	63	1.81	253
OE-6	2-mica granite	143	10.0	17	62	144	bd	34	nd	2.32	324
RB-104	2-mica granite	319	10.0	bd	131	240	bd	40	103	1.83	145
RB-105	2-mica granite	689	11.0	bd	68	210	bd	42	72	3.09	162

nd = not determined

bd = not detected

Appendix E: $^{40}\text{Ar}/^{39}\text{Ar}$ AGE DATA

This appendix presents tables of isotopic data used to calculate the $^{40}\text{Ar}/^{39}\text{Ar}$ plateau ages for the Baker area samples. See Appendix C for analytical techniques. Each table gives the isotopic data for successive Ar extraction temperatures, and ends with a fuse temperature when all ^{40}Ar has been released from the sample. The first column of data lists the specific extraction temperature, the second column the $^{40}\text{Ar}/^{39}\text{Ar}$ ratio, the third column the $^{37}\text{Ar}/^{39}\text{Ar}$ ratio, the fourth column the $^{36}\text{Ar}/^{39}\text{Ar}$ ratio, and the fifth column the moles of ^{39}Ar . The sixth column lists the % of total ^{40}Ar released and the seventh column lists the % of radiogenic ^{40}Ar released. The eighth column lists the K/Ca ratio, and the last column give the age calculated for that particular temperature Ar release spectrum. The sample number is followed by an H if it is hornblende and a B if it is biotite. The J value, which is the neutron flux of the irradiated sample, is also listed. The calculated plateau age is listed at the bottom. The lower table lists the errors in % of the $^{40}\text{Ar}/^{39}\text{Ar}$, $^{37}\text{Ar}/^{39}\text{Ar}$, and $^{36}\text{Ar}/^{39}\text{Ar}$ ratios at each extraction temperature.

Temp x°C	40Ar 39Ar	37Ar 39Ar	36Ar 39Ar	Moles 39Ar	40Ar %Total	%Ar40 Rad	K/Ca	Age (Ma)
PU-8-H				J = .005822				
855	149.99	1.9873	0.2877	2.1	0.3	43.4	0.2462	580.5 +/- 22.3
925	50.57	1.5585	0.1175	2.8	0.4	31.5	0.3140	160.4 +/- 16.0
975	31.61	4.0026	0.0845	3.5	0.5	21.9	0.1221	71.5 +/- 8.9
1000	17.15	7.6754	0.0295	40.5	5.8	52.5	0.0635	92.7 +/- 1.6
1010	15.23	7.9775	0.0222	175.8	25.1	60.8	0.0611	95.4 +/- 1.3
1025	14.31	8.0533	0.0190	53.4	7.6	65.1	0.0605	95.8 +/- 1.3
1040	14.05	8.1035	0.0184	59.4	8.4	65.8	0.0601	95.1 +/- 1.5
1065	13.27	8.1376	0.0157	92.1	13.2	69.8	0.0598	95.3 +/- 1.1
1085	12.32	8.1619	0.0117	91.1	13.0	76.9	0.0597	97.4 +/- 1.5
1110	12.07	8.2256	0.0106	71.5	10.2	79.2	0.0592	98.2 +/- 1.3
FUSE	11.86	8.1584	0.0095	108.0	15.4	81.7	0.0597	99.6 +/- 1.1
TOTAL				699.3	100.0			98.1
PLATEAU AGE								95.8 +/- 2.4

E-40/39	E-37/39	E-36/39	TEMP
.543	1.544	1.382	855
.698	1.731	2.166	925
.523	.532	1.633	975
.113	.121	.739	1000
.062	.059	.73	1010
.087	.124	.789	1025
.074	.101	1.027	1040
.063	.063	.706	1065
.057	.05	1.734	1085
.08	.098	1.487	1110
.14	.107	.624	FUSE

Temp x°C	40Ar 39Ar	37Ar 39Ar	36Ar 39Ar	Moles 39Ar	40Ar %Total	%Ar40 Rad	K/Ca	Age (Ma)
-------------	--------------	--------------	--------------	---------------	----------------	--------------	------	----------

OE-4-2

J = .00584

825	10.66	0.0341	0.0146	191.5	7.4	59.1	14.3519	65.2 +/- 1.5
925	9.60	0.0062	0.0025	478.1	18.4	91.9	78.7322	90.6 +/- 1.0
985	9.78	0.0075	0.0024	488.0	18.8	92.3	65.1803	92.8 +/- 1.0
1025	9.52	0.0085	0.0017	682.1	26.3	94.4	57.5401	92.3 +/- 0.9
FUSE	9.48	0.0107	0.0017	756.0	29.1	94.3	45.7453	91.8 +/- 0.9

TOTAL				2595.7	100.0			89.9
-------	--	--	--	--------	-------	--	--	------

PLATEAU AGE								92.1 +/- 1.1
-------------	--	--	--	--	--	--	--	--------------

E-40/39	E-37/39	E-36/39	TEMP
---------	---------	---------	------

.086	2.326	1.548	825
.074	11.038	3.05	925
.076	5.907	2.06	985
.082	3.426	1.603	1025
.038	2.832	2.826	FUSE

Temp x°C	40Ar 39Ar	37Ar 39Ar	36Ar 39Ar	Moles 39Ar	40Ar %Total	%Ar40 Rad	K/Ca	Age (Ma)
		0E-6A-B				J = .005835		
855	13.24	0.0621	0.0135	136.7	5.6	69.6	7.8890	94.5 +/- 1.4
940	11.24	0.0063	0.0022	521.1	21.5	94.0	77.6591	107.9 +/- 1.2
1000	11.19	0.0066	0.0018	469.5	19.3	95.0	73.8171	108.6 +/- 1.1
1025	10.99	0.0065	0.0011	455.0	18.7	96.7	75.8757	108.5 +/- 1.1
FUSE	10.99	0.0109	0.0012	846.7	34.9	96.3	44.9620	108.1 +/- 1.1
TOTAL				2429.1	100.0			107.5
PLATEAU AGE								108.3 +/- 1.2

E-40/39	E-37/39	E-36/39	TEMP
.059	2.301	1.388	855
.082	3.828	3.679	940
.036	5.845	1.152	1000
.089	6.961	2.407	1025
.058	1.86	1.512	FUSE

Temp	40Ar	37Ar	36Ar	Moles	40Ar	%Ar40	K/Ca	Age (Ma)
xC	39Ar	39Ar	39Ar	39Ar	%Total	Rad		

0E-110-B

J = .005811

800	15.42	0.0078	0.0101	219.5	8.7	80.4	62.6348	125.5 +/- 1.6
905	13.54	0.0053	0.0026	403.0	15.9	94.1	92.7094	128.9 +/- 1.3
967	13.41	0.0044	0.0016	481.9	19.0	96.2	111.6154	130.5 +/- 1.4
1010	13.07	0.0046	0.0012	832.7	32.9	97.0	106.1907	128.3 +/- 1.3
1050	13.15	0.0079	0.0013	440.8	17.4	96.8	62.1673	128.8 +/- 1.3
FUSE	14.84	0.0183	0.0071	153.2	6.1	85.6	26.7461	128.5 +/- 1.6

TOTAL				2531.1	100.0			128.7
-------	--	--	--	--------	-------	--	--	-------

PLATEAU AGE								128.5 +/- 1.2
-------------	--	--	--	--	--	--	--	---------------

E-40/39	E-37/39	E-36/39	TEMP
.147	6.099	1.637	800
.05	7.025	2.062	905
.055	16.727	6.011	967
.107	4.567	2.702	1010
.042	6.632	5.98	1050
.111	4.003	2.237	FUSE

Temp	40Ar	37Ar	36Ar	Moles	40Ar	%Ar40	K/Ca	Age (Ma)
xC	39Ar	39Ar	39Ar	39Ar	%Total	Rad		

RB-96-B

J = .005757

855	15.44	0.0966	0.0229	77.3	3.9	56.0	5.0737	87.6 +/- 2.5
940	15.19	0.0132	0.0047	235.5	11.7	90.6	37.0202	137.5 +/- 1.5
1000	15.26	0.0141	0.0031	493.5	24.6	93.8	34.6968	142.8 +/- 1.4
1025	14.74	0.0197	0.0014	442.6	22.1	97.0	26.1793	142.7 +/- 1.4
FUSE	14.42	0.0188	0.0008	757.3	37.7	98.0	26.0043	141.2 +/- 1.4
TOTAL				2006.2	100.0			139.4
PLATEAU AGE								142.8 +/- 0.9

E-40/39

E-37/39

E-36/39

TEMP

.1	1.811	1.739	855
.064	6.609	2.626	940
.056	2.567	1.548	1000
.042	1.569	4.498	1025
.034	2.631	7.555	FUSE

Temp	40Ar	37Ar	36Ar	Moles	40Ar	%Ar40	K/Ca	Age (Ma)
x°C	39Ar	39Ar	39Ar	39Ar	%Total	Rad		

RB-98-B

J = .005857

855	10.31	0.0183	0.0063	174.6	7.5	81.5	26.8006	86.7 +/- 1.0
940	9.29	0.0071	0.0016	400.8	17.1	94.6	69.3974	90.6 +/- 1.2
1000	9.05	0.0079	0.0011	550.5	23.5	95.8	62.3006	89.4 +/- 0.9
1025	8.88	0.0084	0.0006	437.8	18.7	97.7	58.3552	89.4 +/- 0.9
1040	8.80	0.0059	0.0002	325.9	13.9	98.8	82.5273	89.6 +/- 0.9
FUSE	9.00	0.0324	0.0008	451.2	19.3	96.8	15.1012	89.8 +/- 0.9

TOTAL				2340.8	100.0			89.5
-------	--	--	--	--------	-------	--	--	------

PLATEAU AGE								89.8 +/- 1.4
-------------	--	--	--	--	--	--	--	--------------

E-40/39	E-37/39	E-36/39	TEMP
---------	---------	---------	------

.051	2.048	1.469	855
.056	11.761	8.902001	940
.026	3.462	1.941	1000
.058	5.632	4.501	1025
.062	15.575	11.192	1040
.064	1.38	2.38	FUSE

Temp x C	40Ar 39Ar	37Ar 39Ar	36Ar 39Ar	Moles 39Ar	40Ar %Total	%Ar40 Rad	K/Ca	Age (Ma)
RB-106-B								
J = .00584								
840	14.13	0.1584	0.0152	116.7	5.4	68.0	3.0927	98.5 +/- 1.9
905	15.09	0.0377	0.0043	303.0	14.0	91.2	12.9831	139.6 +/- 1.5
960	15.21	0.0318	0.0026	271.8	12.6	94.6	15.4212	145.6 +/- 1.5
1000	15.73	0.0528	0.0021	268.7	12.4	95.9	9.2864	152.2 +/- 1.5
1040	15.01	0.0471	0.0009	486.0	22.5	97.9	10.3986	148.6 +/- 1.5
FUSE	14.69	0.0523	0.0010	714.7	33.1	97.7	9.3620	145.3 +/- 1.4
TOTAL				2161.0	100.0			143.6
PLATEAU AGE								146.9 +/- 5.4

E-40/39	E-37/39	E-36/39	TEMP
.106	.504	1.9	840
7.900001E-02	.925	2.898	905
.076	.51	3.02	960
.078	.443	1.786	1000
.075	.287	3.945	1040
.064	.265	3.488	FUSE

Temp	40Ar	37Ar	36Ar	Moles	40Ar	%Ar40	K/Ca	Age (Ma)
xC	39Ar	39Ar	39Ar	39Ar	%Total	Rad		

BK-13-B

J = .005848

855	9.68	0.0545	0.0119	81.9	3.7	63.2	8.9970	63.4 +/- 1.4
940	8.58	0.0102	0.0025	292.1	13.2	91.0	48.1758	80.5 +/- 1.1
1000	8.50	0.0093	0.0018	349.5	15.8	93.4	52.6423	81.9 +/- 0.9
1025	8.32	0.0092	0.0009	350.6	15.9	96.3	53.2918	82.7 +/- 0.8
FUSE	8.21	0.0111	0.0010	1136.9	51.4	96.1	43.9975	81.4 +/- 0.8

TOTAL				2211.0	100.0			80.9
-------	--	--	--	--------	-------	--	--	------

PLATEAU AGE								82.0 +/- 2.2
-------------	--	--	--	--	--	--	--	--------------

E-40/39

E-37/39

E-36/39

TEMP

.064	2.11	1.783	855
.053	4.285	4.709	940
.051	3.836	2.903	1000
.033	4.321	4.395	1025
.045	3.01	1.555	FUSE

Temp	40Ar	37Ar	36Ar	Moles	40Ar	%Ar40	K/Ca	Age (Ma)
xC	39Ar	39Ar	39Ar	39Ar	%Total	Rad		

BK-22-B

J = .005765

855	10.17	0.0046	0.0093	312.1	12.9	72.5	106.2934	75.1 +/- 1.0
940	8.65	0.0030	0.0015	403.4	16.7	94.4	163.1589	82.9 +/- 0.9
1010	8.61	0.0032	0.0013	717.0	29.6	94.9	155.1542	83.1 +/- 0.8
1040	8.44	0.0040	0.0008	602.1	24.9	96.9	122.8140	83.1 +/- 0.8
FUSE	8.61	0.0102	0.0014	383.9	15.9	94.7	48.0648	82.9 +/- 0.8

TOTAL				2418.5	100.0			82.0
-------	--	--	--	--------	-------	--	--	------

PLATEAU AGE								83.0 +/- 0.6
-------------	--	--	--	--	--	--	--	--------------

E-40/39	E-37/39	E-36/39	TEMP
---------	---------	---------	------

.092	12.848	1.094	855
.062	9.116	3.308	940
.074	11.8	2.008	1010
.059	8.541001	2.447	1040
.054	4.109	2.875	FUSE

Temp	40Ar	37Ar	36Ar	Moles	40Ar	%Ar40	K/Ca	Age (Ma)
xC	39Ar	39Ar	39Ar	39Ar	%Total	Rad		

G-58-H

J = .003035

875	64.42	3.3273	0.1764	12.6	8.3	19.5	0.1469	67.5 +/- 7.8
925	45.89	7.0875	0.1315	9.3	6.1	16.5	0.0688	41.2 +/- 7.1
950	32.66	12.5530	0.0934	10.5	6.9	18.5	0.0387	33.1 +/- 5.0
975	25.88	15.9570	0.0683	16.0	10.5	26.9	0.0303	38.2 +/- 13.8
1000	22.57	15.0140	0.0520	21.2	14.0	37.2	0.0323	45.9 +/- 11.9
1025	20.34	13.7580	0.0424	21.8	14.4	43.7	0.0352	48.5 +/- 2.5
1075	18.95	13.8770	0.0374	15.0	9.9	47.4	0.0349	49.0 +/- 2.9
FUSE	13.09	14.4120	0.0189	45.1	29.8	65.9	0.0336	47.1 +/- 0.6
TOTAL				151.5	100.0			46.8
PLATEAU AGE								48.2 +/- 2.2

E-40/39

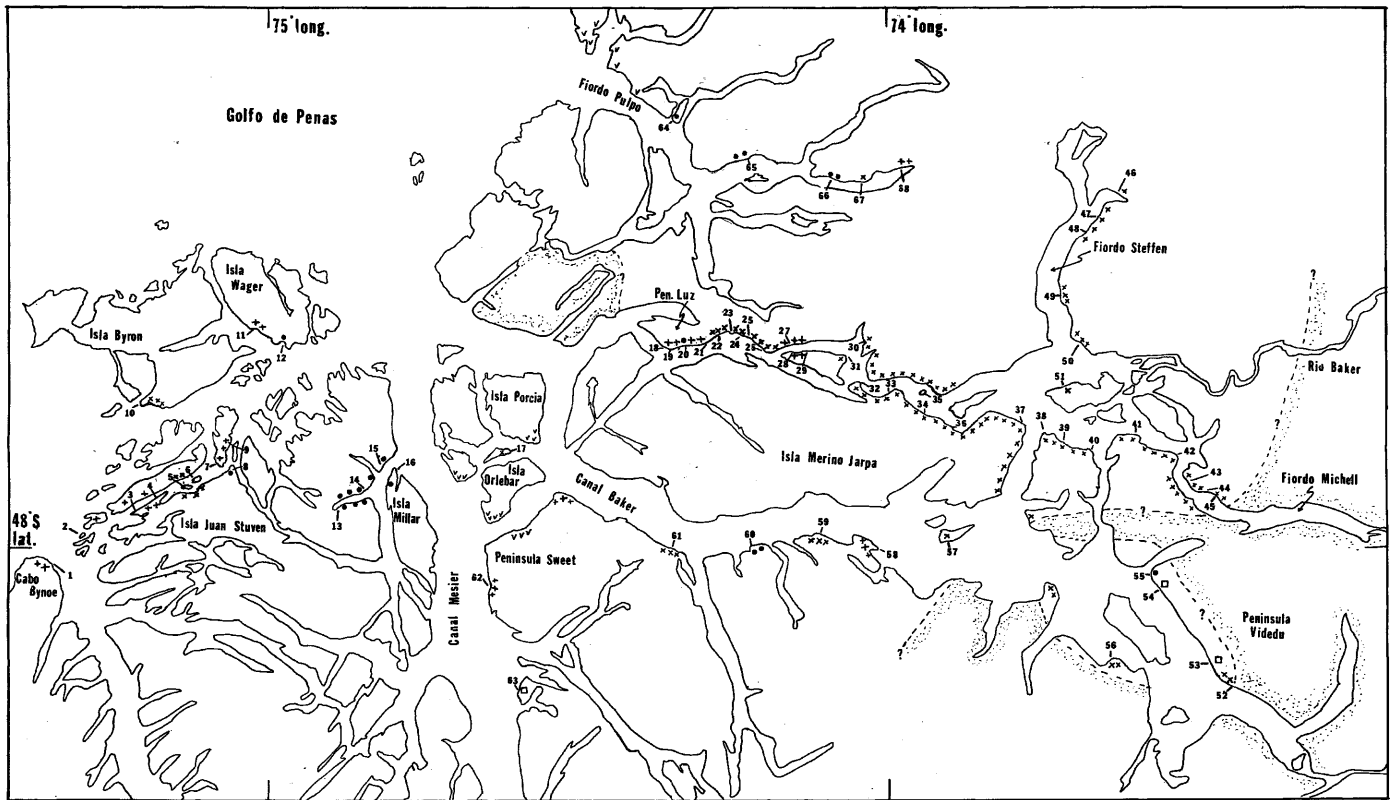
E-37/39

E-36/39

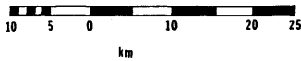
TEMP

.28	.41	1.38	875
.17	.24	1.69	925
.77	.83	1.41	950
.17	.25	6.39	975
.59	.68	7.21	1000
.12	.13	1.84	1025
.13	.14	2.39	1075
.04	.06	.72	FUSE

Plate A-1 Patagonian batholith sample locations



Scale
1 : 250,000



batholith - basement
contact



sample location



gabbro



tonalite, quartz diorite



granite, granodiorite



2-mica granite



volcanics



basement

